SORPTIVITY OF WATER IN SOUND AND DEMINERALISED ENAMEL

GAN SIEW CHEN

FACULTY OF DENTISTRY
UNIVERSITY OF MALAYA
KUALA LUMPUR

2019

SORPTIVITY OF WATER IN SOUND AND DEMINERALISED ENAMEL

GAN SIEW CHEN

THESIS SUBMITTED IN FULFILMENT OF THE REQUIREMENTS FOR THE DEGREE OF MASTER OF DENTAL SCIENCE

FACULTY OF DENTISTRY
UNIVERSITY OF MALAYA
KUALA LUMPUR

2019

UNIVERSITY OF MALAYA

ORIGINAL LITERARY WORK DECLARATION

Name of Candidate: Gan Siew Chen

Matric No: DGC150001

Name of Degree: Master of Dental Science

Title of Project Paper/Research Report/Dissertation/Thesis:

Sorptivity of water in sound and demineralised enamel

Field of Study: Cariology (Dental Studies)

I do solemnly and sincerely declare that:

(1) I am the sole author/writer of this Work;
(2) This Work is original;
(3) Any use of any work in which copyright exists was done by way of fair dealing and for permitted purposes and any excerpt or extract from, or reference to or reproduction of any copyright work has been disclosed expressly and sufficiently and the title of the Work and its authorship have been acknowledged in this Work;
(4) I do not have any actual knowledge nor do I ought reasonably to know that the making of this work constitutes an infringement of any copyright work;
(5) I hereby assign all and every right in the copyright to this Work to the University of Malaya ("UM"), who henceforth shall be owner of the copyright in this Work and that any reproduction or use in any form or by any means whatsoever is prohibited without the written consent of UM having been first had and obtained;
(6) I am fully aware that if in the course of making this Work I have infringed any copyright whether intentionally or otherwise, I may be subject to legal action or any other action as may be determined by UM.

Date:4th February 2019

Subscribed and solemnly declared before,

Date: 4th February 2019

Name: Dr Prema Sukumaran

Designation: Senior Lecturer DUG 54
Department of Restorative Dentistry
Faculty of Restorative Dentistry
University of Malaya

ABSTRACT

Initial caries which present clinically as white spot lesions typically start with demineralisation of the enamel surface which causes an increase in surface porosity. At the same time, non-porous highly mineralised surface layer which is commonly known as “surface layer” progressively forms on the enamel. If demineralisation continues, the surface layer breaks down and the enamel surface becomes porous again. The intermittent presence of the surface layer in the cycle of remineralisation and demineralisation could be the reason for the lack of conclusive evidence of success in remineralisation therapies. Remineralisation materials may not be penetrating the surface efficiently when the surface layer is present. There are currently no clinical methods to determine the porosity of the enamel surface. If porosity and presence of the highly mineralised surface layer on white spot lesions can be determined, the success of remineralisation therapy can be improved. In this research, it is hypothesised that the measured rate of absorption using sorptivity on sound and demineralised enamel surface can be used to determine the level of porosity and presence of a surface layer on the enamel surface. The aim of this thesis is to determine the association between sorptivity of water and the state of mineralisation of surface enamel by first, exploring the viability of sorptivity as a tool to measure surface absorption rate on sound and demineralised enamel. Secondly, is to explore the associations between sorptivity with mineral density on sound and demineralised enamel surface. A 0.7 microliter droplet of water was placed with a micropipette on the exposed enamel of 96 teeth (192 test sites) which had undergone various duration of pH cycling (GS- group of specimens that did not undergo pH cycling, G7- group of specimens that underwent 7 days pH cycling, G14- group of specimens that underwent 14 days pH cycling, G21- group of specimens that underwent 21 days pH cycling, G28- group of specimens that underwent 28 days pH cycling and G35- group of specimens that

underwent 35 days pH cycling). Thorlabs Swept-Source OCT system (OCS 1300SS) was used to measure the height of the drop every 10 seconds for 2 minutes. Sorptivity of each test site was then computed after accounting for evaporation. Total Delta Z of grey scale value from 10µm (TDZ10) to 50µm (TDZ50) was calculated using images taken with microcomputed tomography (Micro- CT). Integrated reflectivity is measured from 10 µm (IR10) to 50 µm (IR500 using images taken with OCT1300SS. SEM, Micro-CT, photography and stereo microscope images were taken to provide qualitative analysis. SPSS 25 (IBM) with One-way ANOVA, post-hoc Tukey and Dunnett's T3 was used to compare means and Bivariate (Pearson) Correlations was used to compare 2 variables. Results show that mean sorptivity increased from GS to G14 and from G21 to G35, juxtaposed by a decline between G14 and G21. One-Way ANOVA showed significant difference of mean sorptivity between groups ($p<0.0$). Mean TDZ10 and mean IR10 seem to project the same relationship between groups. This appears to confirm the cycle of remineralisation and demineralisation and the presence of a surface layer in G21. The most significant correlation was found between sorptivity and TDZ10 with Pearson Correlation coefficient of 0.461. IR10 show significant correlations with sorptivity when results from GS, G7, G14 and G21 were chosen with Pearson correlation coefficient of 0.275. Qualitatively, the presence of a surface layer in many test sites in G21 explains the reason for low mean sorptivity value for this group. In conclusion, these tests have shown for the first time that sorptivity of water is linearly and inversely correlated with the state of mineralisation at the surface of enamel. Sorptivity can be used to determine the presence of a surface layer.

Keywords: Sorptivity, absorption rate, surface layer, demineralisation, optical coherence tomography.

Tajuk : Sorptivity Air untuk Enamel Sihat dan Enamel Demineralisasi

Abstrak

Karies awal (white spot lesion) biasanya bermula dengan demineralisasi permukaan enamel yang menyebabkan peningkatan dalam porositi permukaan. Pada masa yang sama, lapisan permukaan yang mempunyai mineralisasi yang tinggi dan tidak porous (yang biasa dikenali sebagai "surface layer"), membentuk secara progresif pada permukaan enamel untuk mencegah kerosakan yang lebih lanjut. Sekiranya demineralisasi selanjutnya berlaku, permukaan 'surface layer' ini akan musnah dan permukaan menjadi porous semula. Kehadiran 'surface layer' dalam kitaran remineralisasi dan demineralisasi mungkin menjadi salah satu sebab kekurangan bukti konkrit mengenai kejayaan terapi remineralisasi pada white spot lesion. Bahan remineralisasi mungkin tidak dapat menembusi permukaan dengan cekap apabila surface layer tersebut wujud pada permukaan enamel. Pada masa ini tiada kaedah klinikal untuk menentukan porositi permukaan enamel white spot lesion. Jika porositi dan kewujudan surface layer pada white spot lesion boleh ditentukan, kejayaan terapi remineralisasi dapat ditingkatkan. Hipotesis penyelidikan tersebut adalah kadar penyerapan yang diukur dengan menggunakan sorptivity pada permukaan enamel sihat dan demineralisasi boleh digunakan untuk menentukan tahap porositi dan kewujudan surface layer pada permukaan enamel. Tujuan tesis ini adalah untuk menentukan perhubungan antara sorptivity dan tahap mineralisasi enamel permukaan dengan terlebih dahulu, menerokai keberkesanan sorptivity sebagai alat untuk mengukur kadar penyerapan permukaan pada enamel. Kedua, adalah untuk menerokai perhubungan antara porositi pada permukaan enamel sihat dan demineralisasi. Titisan air 0.7 mikroliter diletakkan dengan mikropipet pada enamel terdedah 96 gigi (192 tapak ujian) yang telah melalui jangakamasa pH cycling yand berbeza (GS- kumpulan specimen yang tidak melalui pH cycling, G7- kumpulan specimen yang melalui 7 hari pH cycling, G14- kumpulan specimen yang

melalui 14 hari pH cycling, G21- kumpulan specimen yang melalui 21 hari pH cycling, G28- kumpulan specimen yang melalui 28 hari pH cycling dan G35- kumpulan specimen yang melalui 35 hari pH cycling). Sistem OCT Thorlabs Swept-Source (OCS 1300SS) digunakan untuk mengukur ketinggian titisan air setiap 10 saat selama 2 minit. Sorptiviti setiap tapak ujian dikira selepas menolak isipadu yang hilang akibat penyejatan. Jumlah Delta Z grey scale value dihitung untuk kedalaman setiap 10 mikron dari 10μm (TDZ10) hingga 50μm (TDZ50) dari imej yang diambil dengan tomografi mikrokomputer (Mikro-CT). Integrated Reflectivity diukur untuk 10 μm (IR10) hingga 50 μm (IR50) dari imej yang diambil dengan OCT1300SS. Imej SEM, Mikro-CT, fotografi dan mikroskop stereo telah diambil untuk memberikan analisis kualitatif. SPSS 25 (IBM) dengan One- way ANOVA, post-hoc Tukey dan Dunnett's T3 digunakan untuk membandingkan korelasi min dan korelasi Bivariate (Pearson) digunakan untuk membandingkan 2 pembolehubah. Dalam keputusan penyelidikan, min sorptivity meningkat dari GS ke G14 dan dari G21 hingga G35, disambung oleh penurunan antara G14 dan G21. One-way ANOVA menunjukkan perbezaan ketara antara kumpulan ($p < 0.05$). Min TDZ10 dan min IR10 menunjukkan hubungan yang sama antara kumpulan. Ini mengesahkan wujudnya kitaran remineralisasi dan demineralisasi dan kehadiran surface layer dalam G21. Korelasi linear yang paling ketara adalah antara sorptivity dan TDZ10 dengan Pearson Correlation coefficient sebanyak 0.461. IR10 mempunyai korelasi yang ketara dengan sorptivity apabila keputusan dari GS, G7, G14 dan G21 digunakan dengan Pearson Correlation coefficient sebanyak 0.275. Secara kualitatif, imej SEM, Mikro-CT, fotografi dan mikroskop stereo memperkukuhkan bukti dengan menunjukkan kehadiran surface layer di tapak ujian di G21 yang menyebabkan min sorptivity yang rendah bagi kumpulan ini. Sebagai kesimpulan, ujikaji ini telah menunjukkan untuk pertama kalinya bahawa sorptivity mempunyai korelasi yang linear secara inverse dan berkait rapat dengan

keadaan mineralisasi pada permukaan enamel. Sorptivity boleh digunakan untuk menentukan kehadiran surface layer.

Kata Kunci: Sorptivity, kadar penyerapan, surface layer, demineralisasi, optical coherence tomography

ACKNOWLEDGEMENTS

My warmest gratitude to my supervisors, Assoc. Professor Dr Chew Hooi Pin, for her relentless support and guidance as well as Professor Alex Fok for being the math genius, and for the inspiration and ideas. Also, many thanks to Dr Prema A/P Sukumaran for stepping in as a supervisor towards the end of the project.

I would like to thank the staff in Biomaterials Lab at Faculty of Dentistry University of Malaya and Minnesota Dental Research Center for Biomaterials and Biomechanics, University of Minnesota, namely Hassan, Helen, Zarina, Bonnie and Dr. Rana Redsky for their support throughout the research project. Thank you very much Yen Ting for assisting with calculations done for integrated reflectivity portion. Many thanks to colleagues and friends who have assisted in collecting extracted human teeth.

Puan Aishah, assistant to Dr Chew, thank you so much for all your help. You have been such a wonderful person and have been such a great help to me. Puan Zuraidah (Aida), you are such a great help to me in matters concerning procedures and step by step in completing this masters' project. I would also like to thank Professor Chee Chin Fei of Chemistry Department University Malaya for his assistance with the demineralisation and remineralisation solutions.

To friends and family who have stood by me throughout this period, I would like to say to you, I am back!! Dr Veena Roberts for being the best friend that you are- thank you for all your input and suggestions. Ru, thanks for pushing me hard when the going got tough and laziness began to set in. Mum and family for just being there and being patient with me- thank you very much.

Last but certainly not the least, to my Lord and Saviour Jesus Christ, for without Him, I'm nothing. Thank you for providing me the strength that I need to accomplish this task. My future is in Your hands and I look forward to it.

TABLE OF CONTENTS

Abstract iii

Acknowledgements viii

Table of Contents ix

List of Figures xv

List of Tables xx

List of Symbols and Abbreviations xxi

List of Appendices xxii

CHAPTER 1: INTRODUCTION 1

CHAPTER 2: LITERATURE REVIEW 6

2.1 Anatomy of the enamel and composition 6

2.2 Initial Caries 8

2.2.1 Aetiology 8

2.2.2 Diagnosis of initial caries lesions 11

2.2.3 Surface layer 12

2.2.4 Success of remineralisation therapy 14

2.2.5 Quantifying demineralisation and remineralisation 14

2.3 Permeability of water on enamel and dentine for sound and carious teeth 16

2.3.1 Dentine Permeability 16

2.3.2 Enamel Porosity and Permeability 17

2.3.3 Rate of permeability and/or rate of sorption studies on enamel 19

2.4 Sorptivity 20

2.4.1 Introduction 20

2.4.2 Calculations in Sorptivity 21

2.4.3 Sorptivity in Dentistry 22

2.4.4 Why Sorptivity? 22
2.5 Verification of Correlations between Sorptivity with Surface Porosity 23
2.5.1 Total Delta Z with Microcomputed Tomography (Micro-CT) 23
2.5.2 Integrated Reflectivity with Optical Coherence Tomography (OCT) 25
2.5.2.1 Integrated reflectivity 26
2.5.2.2 OCT and Sorptivity 27
2.5.3 Qualitative Analysis 28
2.6 Correlation of pH cycling models and enamel density 28
CHAPTER 3: METHODS AND MATERIALS 29
3.1 Sorptivity 29
3.1.1 Feasibility of OCT as a measuring device 29
3.1.2 Pilot study to measure Sorptivity 32
3.1.2.1 Preparation of the specimens 32
3.1.2.2 pH cycling process was done as follows: 34
3.1.2.3 Experiment 35
3.1.2.4 Flow chart (for pilot study) 39
3.1.2.5 Calculations 40
3.1.2.6 Results from Pilot 46
3.1.2.7 Learnings from pilot 49
3.1.3 Materials and methods 50
3.1.3.1 Preparations 50
3.1.3.2 Demineralisation and Remineralisation solutions 53
3.1.3.3 pH-cycling process 55
3.1.3.4 Scanning using OCT 58
3.1.3.5 Flow chart of experiment 64

3.1.3.6 Calculations 65
3.2 Micro-CT Scanning, Image Processing and Data analysis 65
3.2.1 Calculations 67
3.3 Integrated reflectivity from OCT 70
3.3.1 Calculations 73
3.4 Scanning Electron Microscope (SEM) 74
Qualitative assessment of 75
3.5 Micro-CT Images 75
3.6 Photographic Images 75
3.7 Stereo microscope Images 75
3.8 Statistics 76
CHAPTER 4: RESULTS 78
4.1 Sorptivity 78
4.2 Total Delta Z (TDZ) 88
4.2.1 TDZ10 93
4.2.2 TDZ20 94
4.2.3 TDZ30 95
4.2.4 TDZ40 96
4.2.5 TDZ50 96
4.2.6 Correlations 97
4.3 Integrated reflectivity (IR) 97
4.3.1 IR10 102
4.3.2 IR20 103
4.3.3 IR30 104
4.3.4 IR40 104

4.3.5 IR50 105
4.3.6 Correlations 105
4.4 Qualitative Analysis 106
4.4.1 SEM Images 106
4.4.2 Micro CT Images 110
4.4.3 Photographic images 112
4.4.4 Stereo microscope images 115
CHAPTER 5: DISCUSSION 119
5.1 Sorptivity 119
5.2 TDZ…. 122
5.3 IR……. 126
5.4 Qualitative Analysis 129
5.5 Confounding factors 131
CHAPTER 6: CONCLUSION 132
6.1 Recommendations 132
References 134
Appendix 143
Appendix A… 143
Appendix B… 145
Statistical Analysis for Sorptivity 145
Test of Normality 145
Q-Q plots……. 145
Box Plot……. 146
Levene's test of Homogeneity of variance 146
One-way ANOVA 147

Post-hoc Tukey 147
Appendix C… 149
Statistical Analysis for Total Delta Z (TDZ) 149
Total Delta Z 10 Microns (TDZ10) 149
Total Delta Z 20 Microns (TDZ20) 152
Total Delta Z 30 Microns (TDZ30) 154
Total Delta Z 40 Microns (TDZ40) 157
Total Delta Z 50 Microns (TDZ50) 161
Appendix D… 164
Statistical Analysis for Integrated Reflectivity (IR) 164
IR10…….. 164
IR20…… 166
IR30…….. 169
IR40…….. 172
IR50…….. 175
Appendix E… 179
SEM Images 179
GS……. 179
G7……. 181
G14…… 182
G21…… 184
G28…… 186
G35…… 188
Appendix F…. 191
Micro-CT Images 191

GS……191
G7……192
G14……193
G21……194
G28……195
G35……196
Appendix G…197
Photographic Images 197
GS……197
G7……198
G14……198
G21……199
G28……200
G35……200
Appendix H…201
Stereo microscope Images 201
GS……201
G7……202
G14……204
G21……206
G28……207
G35……209

LIST OF FIGURES

Figure 2.1: SEM image of the cross section of enamel.....6

Figure 2.2: SEM image of the longitudinal section of the enamel.....7

Figure 2.3: Cross section of an enamel caries.....9

Figure 2.4: Graph of grey value versus mineral density (Huang et al., 2007).....24

Figure 3.1: OCT image of non-carious enamel surface and subsurface region.....29

Figure 3.2: OCT image of non-carious enamel surface with a droplet of water.....30

Figure 3.3: OCT image of non-carious enamel surface after a few minutes 30

Figure 3.4: Subsequent image taken with OCT of non-carious enamel surface.....30

Figure 3.5: OCT image before drop of water is placed.....31

Figure 3.6: OCT image after a drop of water is placed.....31

Figure 3.7: Tooth mounted on resin.....32

Figure 3.8: Varnish on tooth with exposed enamel surface.....33

Figure 3.9: Illustration of the round window of exposure on enamel surface of tooth...33

Figure 3.10: Thorlabs Swept Source OCT system (OCS 1300SS).....36

Figure 3.11: Desktop screen of image taken with OCT.....37

Figure 3.12: Desktop screen showing image taken with OCT 38

Figure 3.13: Illustration of droplet of water for calculation.....40

Figure 3.14: Graph of Initial Sorptivity 41

Figure 3.15:Illustration showing spherical cap where evaporation occurs.....43

Figure 3.16: Example of height of droplet measured versus time for plastic surface.....45

Figure 3.17: Graph of sorptivity for pilot study.....47

Figure 3.18: Graph of mean sorptivity in pilot study.....48

Figure 3.19: Specimen (crown of tooth) mounted on resin 50

Figure 3.20: Specimen with varnish and 2 test sites of exposed enamel surface..... 51

Figure 3.21: Image taken with OCT of sound enamel surface 52

Figure 3.22: Image taken with OCT of demineralised enamel surface..... 52

Figure 3.23: Materials for demineralisation and remineralisation solutions..... 53

Figure 3.24: 2-liter glass bottle 54

Figure 3.25: Specimen jar 54

Figure 3.26: Image of specimens in jars containing remineralising solution 56

Figure 3.27: Image of specimen jar containing demineralising solution 56

Figure 3.28: Specimens being placed carefully in the jar 57

Figure 3.29: Imaging Probe in Probe Adapter Stand 58

Figure 3.30: ThorLab software screen 59

Figure 3.31: Image taken with OCT before droplet of water is placed..... 59

Figure 3.32: Image taken with OCT during the placement of droplet of water..... 60

Figure 3.33: Image taken with OCT at 0 second 60

Figure 3.34: Image taken with OCT of droplet of water at 30 seconds 60

Figure 3.35: Parameters for measurement of diameter of base of test site 61

Figure 3.36: Parameters for measurement of diameter of base of drop 62

Figure 3.37: Parameters for measurement of height of varnish at left border 62

Figure 3.38: Parameters for measurement of height of varnish at right border 63

Figure 3.39: Parameters for measurement of height of droplet of water 63

Figure 3.40: Illustration of measurements taken of the droplet 65

Figure 3.41: Microcomputed tomography equipment 66

Figure 3.42: Schematic diagram of collection of data points and plot profiles 67

Figure 3.43: Plot profile of grey scale value for calculation of AUC 68

Figure 3.44: Plot profile of grey scale value for calculation of DZ10 69

Figure 3.45: Plot profile of grey scale value for calculation of TDZ50 70

Figure 3.46: Top view of a test site generated using Matlab 71

Figure 3.47: Screenshot of 2D analytics 72

Figure 3.48: Details in screenshot of 2D analytics 73

Figure 3.49: Graph showing backscatter intensity 74

Figure 3.50: SEM Equipment 75

Figure 3.51: Stereo microscope equipment 76

Figure 4.1: Example of a graph plotted with volume over area (V_{st}/A) as a function of square root of time, t, for a test site 79

Figure 4.2: Graph of volume over area (V_{st}/A) as a function of square root of time, t, for GS 80

Figure 4.3: Graph of volume over area (V_{st}/A) as a function of square root of time, t, for G7 81

Figure 4.4: Graph of volume over area (V_{st}/A) as a function of square root of time, t, for G14 82

Figure 4.5: Graph of volume over area (V_{st}/A) as a function of square root of time, t, for G21 83

Figure 4.6: Graph of volume over area (V_{st}/A) as a function of square root of time, t, for G28 84

Figure 4.7: Graph of volume over area (V_{st}/A) as a function of square root of time, t, for G35 85

Figure 4.8: Graph of mean sorptivity by group 86

Figure 4.9: Image taken with Micro-CT (Test site E8.2 from G28) 88

Figure 4.10: Profile of grey scale value at 1 location of test site E8.2 (G28) 89

Figure 4.11: Graph of mean Total Delta Z (TDZ) by group 90

Figure 4.12: Graph of mean TDZ10 by group 91

Figure 4.13: Mean TDZ20 by group 91

Figure 4.14: Mean TDZ30 by group 92

Figure 4.15: Mean TDZ40 by group 92

Figure 4.16: Mean TDZ 50 by group 93

Figure 4.17: Mean A-scan by group 99

Figure 4.18: Mean IR10 by group 100

Figure 4.19: Mean IR20 by group 100

Figure 4.20: Mean IR30 by group 101

Figure 4.21: Mean IR 40 by group 101

Figure 4.22: Mean IR50 by group 102

Figure 4.23: SEM image at 500x of test site B15.2 from G7 106

Figure 4.24: SEM image at 1000x of test site C3.2 from G14 107

Figure 4.25: SEM image at 2000x of test site B14.2 from G7 107

Figure 4.26: SEM image at 2000x of test site D9.1 from G21 108

Figure 4.27: Micro-CT scan of A12.2 test site from GS 110

Figure 4.28: Micro-CT scan of D7.1 test site from G21 111

Figure 4.29: Micro-CT scan of D10.2 test site from G21 111

Figure 4.30: Photographic image of test sites on D3 from G21 113

Figure 4.31: Photographic image of test sites on C8 from G14 113

Figure 4.32: Photographic image of test sites on D15 from G21 114

Figure 4.33: Image taken using stereo microscope at 1.25x of test sites on B5 from G7 115

Figure 4.34: Image taken using stereo microscope at 5.6x of test site E16.1 from G28 116

Figure 4.35: Image taken using stereo microscope at 5.6x of test site D13.1 from G21 117

Figure 5.1: Graph of mean sorptivity by group 120

Figure 5.2: Graph of mean TDZ 10 by group 123

Figure 5.3: Graph of mean TDZ 20 by group 124

Figure 5.4: Graph of mean IR10 by group 127

Figure 5.5: Graph of mean IR20 by group 128

LIST OF TABLES

Table 2.1: Chart taken from the official website of the ICDAS Foundation: https://www.icdas.org/ 12

Table 2.2: Methods of quantification in remineralisation and demineralisation studies 15

Table 2.3: Methods used for study of permeability in vitro 18

Table 3.1: Content in demineralisation and remineralisation solutions (Stookey et al., 2011) 35

Table 3.2: Sorptivity values of specimens in pilot study 47

Table 3.3: Mean sorptivity by group in pilot study 48

Table 3.4: Chemical compound in demineralisation solution 55

Table 3.5: Chemical compound in remineralisation solution 55

Table 3.6: Parameters used in measurement of IR 72

Table 4.1: Descriptive statistics of sorptivity by groups 87

Table 4.2 : Mean total Delta Z by group 90

Table 4.3: Mean integrated reflectivity by group 98

Table 4.4: Qualitative analysis of SEM images by group 108

Table 4.5: Tabulation of surface enamel loss and presence of a surface layer seen on Micro-CT images 112

Table 4.6: Tabulation of presence of white spot lesions 114

Table 4.7: Tabulation of results of test site visibility at 1.25x using stereo microscope 117

Table 4.8: Tabulation of results of presence of striae and/or a surface layer on test sites at 5.6x using stereo microscope 118

LIST OF SYMBOLS AND ABBREVIATIONS

GS	:	Group of specimens that did not undergo pH cycling
G7	:	Group of specimens that underwent 7 days of pH cycling
G14	:	Group of specimens that underwent 14 days of pH cycling
G21	:	Group of specimens that underwent 21 days of pH cycling
G28	:	Group of specimens that underwent 28 days of pH cycling
G35	:	Group of specimens that underwent 35 days of pH cycling
IR	:	Integrated reflectivity values
IR10	:	Integrated reflectivity values at surface of enamel to 10μm depth
IR20	:	Integrated reflectivity values at surface of enamel to 20μm depth
IR30	:	Integrated reflectivity values at surface of enamel to 30μm depth
IR40	:	Integrated reflectivity values at surface of enamel to 40μm depth
IR50	:	Integrated reflectivity values at surface of enamel to 50μm depth
TDZ	:	Total Delta Z values
TDZ10	:	Total Delta Z values at surface of enamel to 10μm depth
TDZ20	:	Total Delta Z values at surface of enamel to 20μm depth
TDZ30	:	Total Delta Z values at surface of enamel to 30μm depth
TDZ40	:	Total Delta Z values at surface of enamel to 40μm depth
TDZ50	:	Total Delta Z values at surface of enamel to 50μm depth

LIST OF APPENDICES

Appendix A …….....143

Appendix B……145

Appendix C……149

Appendix D……164

Appendix E……179

Appendix F……191

Appendix G……197

Appendix H……201

CHAPTER 1: INTRODUCTION

On an anatomically well-formed tooth, the formation of caries which is a bacterial disease typically starts with demineralisation of surface enamel. If left unchecked, these demineralised surface start to breakdown and form initial caries or early caries lesions which is clinically seen as white spot lesions. Eventually frank caries is formed (Ole Kejerskov, 2008; Thylstrup A, 1994).

The typical way of diagnosing caries is by clinical approach combining patient complaints, clinical observations, radiographic assessment and tactile or probing of lesion. Dentists are also trained to use various caries classifications such as Black's classification system, Mount and Hume classification system, World Health Organization (WHO) visual tactile classification of carious lesions (Decayed-Missing-Filled Surface – DMFS) and International Caries Detection and Assessment System (ICDAS^{TM}) (Chu CH, 2013; E. K. Pitts NB, 2013; Z. D. Pitts NB, Marsh PD, Ekstrand K, Weintraub JA, Ramos-Gomez F, Tagami J, Twetman S, Tsakos G, Ismail A, , 2017) which also include classification for initial caries. These classifications provide a structure for diagnosis of the caries disease which then can be used to deliver a comprehensive treatment plan. This way of diagnosing early caries, while affordable and easy, does not provide a quantitative analysis of the quality of the enamel surface.

Apart from clinical diagnostic tools mentioned above newer technologies such as DIAGNOdent, Quantitative Light-induced Fluorescence, Optical Coherence Tomography, Electrical Conductance Cone Beam Computed Tomography have recently emerged. These are non-invasive tools which uses various types of technologies aim to provide a more comprehensive diagnosis (Gomez, 2015; Z. D. Pitts NB, Marsh PD, Ekstrand K, Weintraub JA, Ramos-Gomez F, Tagami J, Twetman S, Tsakos G, Ismail A, , 2017) . With the use of radiography and microcomputed tomography (micro-CT) (Swain

& Xue, 2009), one can also determine the presence of demineralisation both qualitatively and quantitatively. While these methods are good, there are currently no specific methods looking at the level of porosity of the surface enamel.

Many studies have been done to look at various ways to diagnose and classify early caries lesions as well as treat these lesions because it is known that early caries is reversible if treatment is provided early to arrest its progress (Amaechi, 2015). When diagnosing an early caries lesion, a clinician may be able to detect it based on surface texture and colour (i.e. white spot lesion) but one cannot tell the difference between an active lesion which is typically more porous and an arrested lesion which has a protective surface layer that reduces porosity of surface enamel.

There is a wide array of treatment options with various delivery systems for management of early caries lesions. Deliveries in form of gel, toothpaste and mouth rinses which deliver a wide choice of materials including various types of fluoride and calcium in various concentrations are all aimed at ensuring success in treatment provided (Ekambaram M, 2017; NakataT, 2018). Protocols typically accompany these materials including in office treatment, take-home therapies and a combination of the two. However, there has been a lack of evidence to conclusively support the success of various techniques and materials to produce satisfactory remineralisation results (Paula et al., 2017; Sonesson, Bergstrand, Gizani, & Twetman, 2017). One possible factor could be the ability of materials to penetrate to the subsurface region due to the presence of a surface layer which can affect the success of remineralisation.

One of the ways of looking at surface porosity is by looking at the rate of absorption of water on the enamel surface. If the rate of absorption can be used to determine and diagnose the level of porosity and the presence of a highly mineralized surface layer, then a definitive therapy including protocol, type of material and its concentration can be

provided. At the same time, absorption rate before and after therapy can also provide information for the next course of action in the treatment process. Also, if rate of absorption of therapeutic substances can be an indicator of the efficacy of the material on lesions undergoing treatment, then, therapies provided will be highly efficacious.

One of the ways of looking at the porosity of enamel is the study on permeability. Permeability studies for dentine is well researched on and well understood probably due to the complexities of this layer. The need to understand dentine hypersensitivity as well as the importance of ensuring proper adhesion of dental materials to this surface is important in dental treatment. On the other hand, permeability studies in enamel is much less researched on though much has been done to measure porosity which is then translated to surface hardness measurements (Schlueter, Hara, Shellis, & Ganss, 2011). There are studies done to relate porosity to pore volume as well (Brudevold, Tehrani, & Cruz, 1982). While many studies were done to measure depth of permeability of materials into enamel either for diagnosing early caries or to look at permeability of test materials on the enamel surface, none were done on the rate of the absorption of liquid on the surface of sound and demineralised teeth in order to quantify the level of porosity of lesions.

Sorptivity is defined as the measurement used to quantify the rate of which liquid is absorbed or desorbed on a medium or surface by means of capillarity (Philip, 1957) . It is widely used in characterizing soils and porous construction materials such as brick, stone and concrete (Hall, 2012). Sorptivity has not been used before in the field of Dentistry to look at absorption rate on enamel surface to determine level of porosity.

The research hypothesis is that the measured rate of absorption using sorptivity on sound and demineralised enamel surface can be used to determine the level of porosity and presence of a surface layer on the enamel surface.

The aim of this research is to determine the association between sorptivity of water and the state of mineralisation of surface enamel and the objectives are as follows:

i. To explore the use of sorptivity as a tool to measure absorption rate of sound enamel and artificially induced carious enamel of different stages of demineralisation.

ii. To explore the associations between sorptivity of sound and artificially induced carious enamel with the mineral density on the enamel surface of various depths using results obtained from Micro-CT images.

iii. To explore the association between sorptivity of sound and artificially induced carious enamel with the total attenuated coefficient of integrated reflectivity of images taken with OCT on the enamel surface at various depths.

For the scope of this research, extracted teeth were used and experiments were done in vitro to ensure a more controlled environment. A cross sectional study instead of a longitudinal one was done for the groups of specimens with different stages of demineralisation due to the limitations of the facilities in the lab. For scanning using computed tomography (Micro-CT), the specimens had to be sent to University of Minnesota. It was not feasible to carry out a longitudinal study as specimens will need to be sent back and forth repeatedly. If this was done, the risk of damage on the enamel surface on specimens will increase thereby reducing the accuracy of the results.

Structure of this thesis follows the recommended guidelines provided by the university as below:

Chapter 1: Introduction

Chapter 2: Literature Review

Chapter 3: Methods and Materials

Chapter 4: Results

Chapter 5: Discussion

Chapter 6: Conclusion

References

Appendix

CHAPTER 2: LITERATURE REVIEW

2.1 Anatomy of the enamel and composition

Enamel is the outer most layer of the tooth and is the substance that has the highest percentage of mineral in the body. Hydroxyapatite (HAP, $Ca_{10}(PO_4)_6(OH)_2$), a calcium phosphate compound, makes up to almost 96% of the enamel while the remaining components are water and protein (amelogenins and enamelins). The thickness of the enamel is typically below 2.5 mm varying from site to site on a tooth surface as well as from one tooth to the other.

Hydroxyapatite crystals are tightly bound together in an orderly pattern to form enamel rods and inter-rod of the enamel layer. Figure 2.1 is a scanning electron microscope (SEM) image of the cross section of the enamel whereby the enamel rods (R) can be seen surrounded by inter-rod enamel (IR).

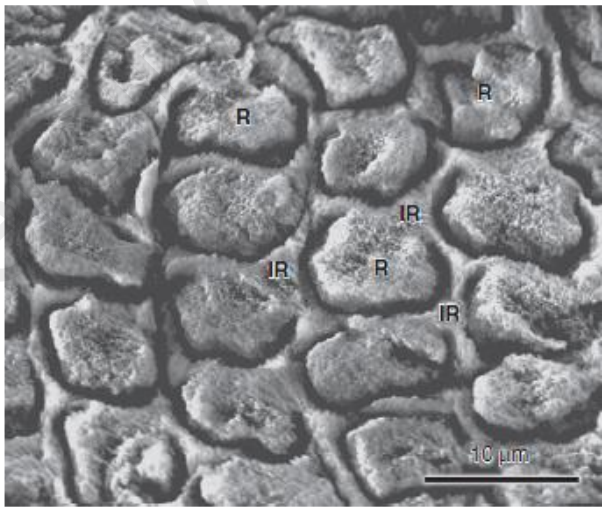

Figure 2.1: SEM image of the cross section of enamel

In this image, R marks the enamel rods and IR, the inter-rod enamel

The closely bound hydroxyapatite crystals which form the enamel rods can measure up to 70nm and is 25-30nm in thickness. Figure 2.2 is the SEM image of the longitudinal

section of the enamel. The hydroxyapatite crystals can be seen tightly bound together but not in the same direction in the enamel rod and the inter-rod enamel (Nanci, 2012)

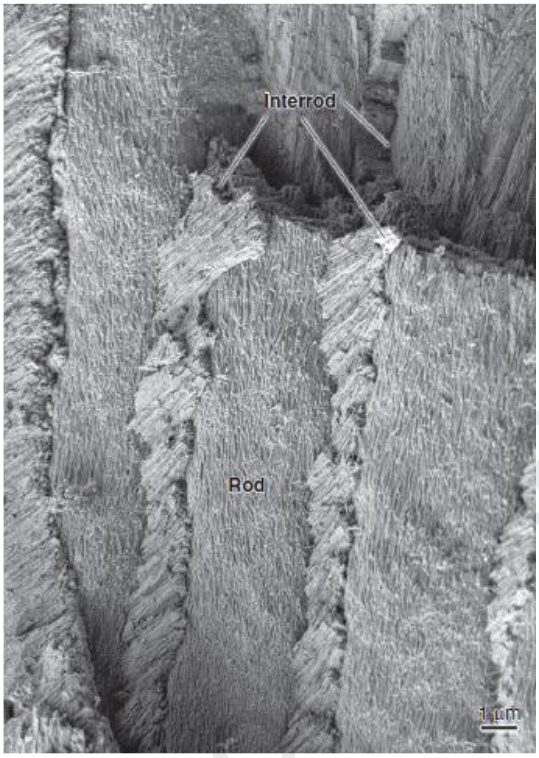

Figure 2.2: SEM image of the longitudinal section of the enamel

In this image, the direction of the hydroxyapatite crystals is seen to be in a different direction in the enamel rod than that of the inter-rod region.

The enamel layer which acts as a protective layer is more resistant to acid and bacterial degradation than the underlying dentine layer due to its high mineral content. The high mineral content in the enamel also contributes to the microhardness of the layer with a Knoop's hardness of 270-440 KHN while the range for dentine is only 50-70 KHN (Meredith N, 1996).

2.2 Initial Caries

2.2.1 Aetiology

As mentioned, enamel, being the protective layer of the tooth, is the layer that is exposed to the oral environment and is the first line of defence against bacterial degradation. In essence, dental caries is the sign and symptom of a progressive uncontrolled demineralisation on any surface of the tooth. The biofilm or dental plaque plays a role in maintaining the health of the surface of the tooth. On the surface of a healthy tooth, the presence of biofilm does not cause caries. However, when the biofilm is present on that surface for a long period of time and is allowed to mature, the metabolic activity and ecology in the film cause an imbalance in mineral equilibrium between the tooth and the biofilm thereby causing pH fluctuation to happen. This imbalance cause demineralisation to happen and without intervention will further progress to form caries.

Many factors can influence the metabolic activity in the biofilm such as thickness of biofilm, mineral composition and fluoride concentration in saliva, saliva flow rate and buffering capacity, diet, oral hygiene and genetic predisposition (Kidd EA, 2004). The presence of fermentable carbohydrates can dramatically shift this balance as well by decreasing the pH level thereby encouraging the growth of more aciduric species of bacteria. At the same time, certain microorganisms are capable of storing carbohydrates which can later be metabolized to acid thereby contributing to the risk of caries formation. Microbial colonization includes S. sanguinis, S. oralis, S. mitis biovar 1, S mutans, S sobrinus, Lactobacilli, Actinomyces species and Gram-negative bacteria such as Haemophilus and Neisseria species (Ole Kejerskov, 2008).

Initial caries is defined as the start of demineralisation on the surface of the teeth forming early caries lesions of which the result is clinically noticeable by visual inspection. When demineralisation happens, hydroxyapatite is dissolved by acid in the

oral environment and gaps start to form in the enamel rods. Loss of minerals on the enamel surface causes microporosity to occur which clinically will appear chalky either with or without air drying of the surface. These lesions are clinically diagnosed as white spot lesions.

Histologically, there are 4 areas in enamel caries: translucent zone, dark zone, body of lesion and surface zone as seen in Figure 2.3. As demineralisation progresses further, enamel rods as well as the striae of Retzius start to become more prominent and visible (Ole Kejerskov, 2008; Thylstrup A, 1994).

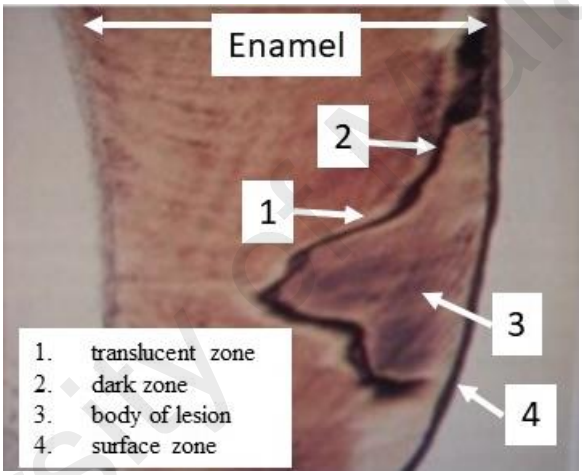

Figure 2.3: Cross section of an enamel caries

This cross section of the enamel shows the 4 zones of demineralisation

Initial caries caused by demineralisation from acid attack form microporous surface with etch patterns similar to the patterns seen when enamel surface is etched. (J. W. Arends J, Ogaard B, Rölla G, 1987; E.I.F. Pearce, 1989). Etching of enamel with inorganic acid is commonly done in Dentistry to increase surface contact of enamel to bonding agents used in composite restorations. Typically, etching is done with the use of phosphoric acid (37%) and this procedure increases the bond strength significantly (Nanci, 2012). When enamel is being etched, there are 5 types of acid etched pattern on enamel. Type I, with etching effects predominantly on prism core shows honey comb

pattern. Type II is the opposite of Type I with etching effect mostly seen on the side of the prisms, with cobblestone like appearance. Type III is a mix of both Type I and Type II (Silverstone L.M., 1975). Type IV which shows uneven surface and Type V, flat and smooth demineralised surface, are surface appearances of a more advanced etch surface morphology (Galil KA, 1979).

Remineralisation, a process to reverse the effects of demineralisation, occurs with the presence of saliva on the enamel surface (Hara AT, 2014). Saliva is known to be supersaturated with calcium and phosphate ions which does not precipitate on the surface on the enamel due to the presence of statherin, the acidic proline-rich phosphoproteins (PRPs), cystatins and histatins. This supersaturated state is what causes the saliva to have the capacity to remineralise (Lenander-Lumikari & Loimaranta, 2000).

This process of demineralisation and remineralisation can be rather complex and is cyclical. On the healthy enamel surface, it is a natural process of destruction and reconstruction and in a balanced scenario, no caries will form on the surface of the enamel. Initial caries on the enamel starts to form when this balance is disrupted and demineralisation occurs at a faster rate than remineralisation. However, this demineralisation of the enamel surface is reversible in its initial stages with active and aggressive remineralisation. But if the assault on the teeth continues and demineralisation action that occurs is aggressive with little or no preventive intervention done, over time, decay can progress further and frank cavitation is formed (Ole Kejerskov, 2008).

Remineralisation therapy assist in reversing the effects of demineralisation on initial caries by actively providing high concentrations of various types of fluoride or calcium or a mix of the two (Ekambaram M, 2017; NakataT, 2018). Fluoride, which is widely found in toothpastes, gels, rinses as well as in drinking water is also known to prevent caries formation by turning surface hydroxyapatite to fluorapatite which is a substance

more resistant to acid attack and therefore prevents demineralisation (Adair et al., 2001; Pizzo G, 2007; Sicca, 2016 ; Wong A, 2017). Many studies have also shown that administering low fluoride concentration at a high frequency is more effective at caries prevention and is safer (Afonso et al., 2013; JS, 1990). Calcium and phosphate compounds such as beta-tricalcium phosphate(β-TCP) and casein phosphopeptide-amorphous calcium phosphate (CPP-ACP) can also be used in the remineralisation process (Karlinsey RL, 2012; Li, Wang, Joiner, & Chang, 2014; Lynch RJ, 2012).

2.2.2 Diagnosis of initial caries lesions

Most common and widely used method in diagnosing caries is the use of visual, radiographic (if the demineralisation is high enough to be detectable) and tactile examination. Patients' complaints (for example, patients' ability to visually see the white spot lesions) is often a good starting point in diagnosing caries. Transillumination is another method used especially when trying to determine the presence of caries in the interdental space (Ole Kejerskov, 2008; Swedish Council on Health Technology, 2008).

There are other equipment used to diagnose caries such as Quantitative Light-induced Fluorescence (QLF), DIAGNOdent (DD), Fibre-optic Transillumination (FOTI) and Electrical Conductance (EC). While these equipment assist in diagnosis of early caries lesions, it is recommended that they should be used concurrently with the traditional method of visual, tactile and radiographic examinations in order to achieve a more accurate diagnosis (Gomez, 2015; Z. D. Pitts NB, Marsh PD, Ekstrand K, Weintraub JA, Ramos-Gomez F, Tagami J, Twetman S, Tsakos G, Ismail A, , 2017).

There are various methods of classification of dental caries such as Black's classification system, Mount & Hume classification system, WHO visual tactile classification of carious lesions (DMFS) and ICDAS (Chu CH, 2013; E. K. Pitts NB, 2013; Z. D. Pitts NB, Marsh PD, Ekstrand K, Weintraub JA, Ramos-Gomez F, Tagami J,

Twetman S, Tsakos G, Ismail A, , 2017). International Caries Classification and Management System (ICCMS^{TM}) is a caries risk assessments tool used to assess patients' caries risk level and used in combination with ICDAS method of classification to ensure a more thorough diagnosis of the extend of the caries disease in patients (Ismail, Pitts, & Tellez, 2015; E. K. Pitts NB, 2013).

ICDAS is arguably the most popular system currently used that includes the diagnosis of non cavitated lesions or initial caries. Diagnosis is done base on a visual, tactile and radiographic assessment of the teeth. Early caries lesion which are non cavitated is classified as ICDAS 1 and 2 (Table 2.1).

Table 2.1: Chart taken from the official website of the ICDAS Foundation: https://www.icdas.org/

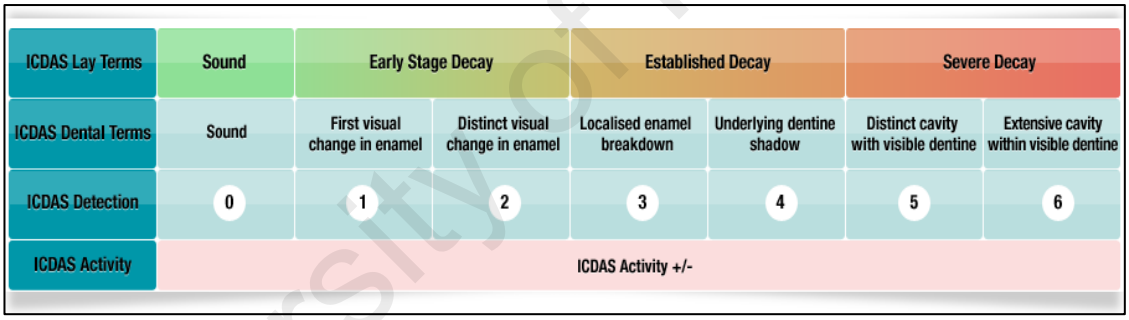

The classification of non cavitated lesions is a step forward in recognizing initial caries as a treatable disease and not just as cavitations that needs filling up. Therefore, understanding the nature of the affected tooth surface including porosity of the surface enamel is important especially during treatment planning.

2.2.3 Surface layer

During demineralisation, dissolved calcium and phosphate in the subsurface region is carried to the surface and precipitates, thus becoming part of the remineralisation process that occurs on the enamel surface. However, the species of precipitated calcium and phosphate crystal may defer from the original and may not crystalize in the original shape

and direction (Nicola X. West, 2014; Robinson C, 2000). Over time, if calcium and phosphate continue to leech to the surface, a surface layer can form on the tooth and becomes a protective layer for the weakened and hypomineralised subsurface area. Formation of a surface layer is also one of the effects of remineralisation therapy on demineralised enamel surface (Featherstone, Duncan, & Cutress, 1978). While this is a positive response, the formation of this surface layer can prevent the remineralisation of the decalcified underlying tooth structure (C. J. Arends J, 1986). Also, as mentioned earlier, the remineralisation and demineralisation cycle is complex which leaves the lesion at periods of time either in a stabilized state where the surface layer is believed to be protecting the underlying hypomineralised area or in an active state whereby the surface area is not present and the subsurface region risk being further demineralised.

The surface layer can be identified using various methods such as radiographs, scanning electron microscope (SEM) and optical coherence tomography (OCT) imaging (Espigares et al., 2015). Typically, these surface layers formed are between 35 to 60μm and have been shown to reach 130μm (Cochrane et al., 2012). Cochrane (2012) also showed that the mineral content in these surface layers can range between 75-100% of the mineral content of sound enamel. The presence of a surface layer can cause the enamel surface to be less permeable and thus, remineralisation of the subsurface region is impeded. In a study by NN Chang (2018) looking at the relationship between surface layer thickness of demineralised enamel and dehydration rate of the lesion, while the relationship was not linear, the findings from this research did suggest that just a small increase in surface layer thickness decreases surface permeability significantly (Chang, Jew, & Fried, 2018).

Chersoni S (2011) also showed that fluoride therapy done on surface of teeth can reduce permeability of the surface to water. When permeability on enamel surface is

reduced, fluid movement in the enamel happens in such a way that encourages precipitation and remineralisation on the surface as well as prevent ions fluoride diffusion in the deeper regions of the tooth. This also explains how fluoride deposits on the surface of the enamel (Chersoni et al., 2011).

Currently there is no diagnostic tools that can be used to determine the presence of a surface layer on the enamel.

2.2.4 Success of remineralisation therapy

Systematic reviews were done separately by Sonesson M (2017) and Paula (2017) on management of demineralised tooth surface clinically visible as white spot lesions. Both of them concluded that there is a lack of evidence to support the success of remineralisation with the use of various methods and mineralising materials. Sonesson also mentioned that the results from the studies showed either no significant improvement or that the studies done were biased. Both Sonesson and Paula suggested that more well controlled clinical studies needed to be done to ascertain the efficacy of current methods of remineralisation of white spot lesions (Paula et al., 2017; Sonesson et al., 2017). One of the reasons these therapies show mixed results could be due to the fact that currently, there is little understanding of the efficiency of the penetration of these mineralizing materials through the highly mineralised surface layer via the knowledge of the quality of the surface porosity and a quantitative measurement of this porosity. If a method can be developed to determine and quantify surface porosity *in vivo*, then perhaps, conclusive evidences can be gathered.

2.2.5 Quantifying demineralisation and remineralisation

In demineralisation and remineralisation studies, methods used to measure the results include the following (Table 2.2):

Table 2.2: Methods of quantification in remineralisation and demineralisation studies

Methods	Measurements
Polarized-light microscope (Rajan, Krishnan, Bhaskaran, & Kumar, 2015; Vanichvatana & Auychai, 2013)	Measurement of light
Photographic record (Robertson et al., 2011)	Determining the presence of white spot lesions
Laser fluorescence technology (DIAGNOdent) (Patil, Choudhari, Kulkarni, & Joshi, 2013; Shen et al., 2011)	Measuring remineralisation-demineralisation using data obtained with DIAGNOdent
Surface microhardness measurements (Vickers) (Shetty, Hegde, & Bopanna, 2014) and nanohardness test(Vickers) (X. Wang, Megert, Hellwig, Neuhaus, & Lussi, 2011)	Measuring surface hardness to quantify remineralisation
Field emission scanning electron microscopy (FE-SEM) (Karlinsey, Mackey, Schwandt, & Walker, 2011)	Qualitative observations of demineralisation
Backscattered electron-scanning electron microscope (BSE-SEM) (Angker, Nockolds, Swain, & Kilpatrick, 2004)	Measuring demineralisation using mineral content data
Combination of measurement of surface microhardness and 3D-profilometry (De Souza, Cury, Coutinho, Da Silva, & Tostes, 2014)	Measure demineralised enamel changes
Transverse microradiography (Shen et al., 2011)	Measuring remineralisation using mineral content data
Atomic force microscopy (AFM) (Poggio, Lombardini, Dagna, Chiesa, & Bianchi, 2009)	Measure surface mineral on enamel

Field J (2010) did a comprehensive review on methods used to measure surface hardness changes and none was mentioned about a method used to look at rate of absorption of water on tooth surface to measure surface changes (Field, Waterhouse, & German, 2010).

2.3 Permeability of water on enamel and dentine for sound and carious teeth

Demineralised enamel causes porosity and porous surfaces allow liquids to be absorbed. Similarly, enamel surface will allow liquids to flow into porous areas to fill up the spaces which have been made void due to demineralisation. When enamel surface is etched with 37% phosphoric acid, gaps form on the surface of the enamel and surface porosity is created which allows bonding agent to penetrate. The increase is contact between surface area and bonding agent increases the bond strength of enamel to resin (Nanci, 2012). Hence, it is a well-established fact that porosity allows a material or surface to be permeable to liquid. The definition of permeability, according to Oxford Dictionary is 'the ability of a substance to allow gases or liquids to go through it'.

2.3.1 Dentine Permeability

The study of dentine permeability is extensive as it is related to issues such as dentine hypersensitivity and adhesion of materials to its surface which can be both complex and challenging. Intra-pulpal pressure in the dentinal tubules which are exposed and patent is believed to the reason for fluid movement in the dentine and thus influences the permeability of the dentine. Studies on dentine permeability is not limited to fluids but also include permeability of ions, bacteria and more recently, with the availability of materials containing nanoparticle-based materials, permeability to nanoparticles as well. Factors governing the permeability of these materials include the area exposed, chemical and structural considerations, the thickness and condition of the tissue, as well as pressure exerted in the process (Mjör, 2009).

Dentine hypersensitivity is related to the permeability of dentine to substances and the movement of liquid in the tubules of exposed dentine. In theory, substances which penetrates through the surface of the exposed dentin into the dentinal tubules causes dentine hypersensitivity (Brannstrom, Linden, & Johnson, 1968; Orchardson & Gillam, 2006). Sharp pain and discomfort experienced due to dentine hypersensitivity can be brought about simply by the touch of an exposed dentine surface with an instrument for example a toothbrush or a probe. Cold, sweet as well as hot food and beverages can also trigger a sensation. By occluding the surface of the exposed dentine with various types of minerals and salts as well as desensitizing agents, Wang et al has shown a reduction in hypersensitivity as the exposed dentinal tubules are plugged with these materials and rendered these tubules impermeable (Z. Wang et al., 2010).

2.3.2 Enamel Porosity and Permeability

In general, the purpose of measuring enamel permeability and porosity is often associated with the study of surface morphology, the ability of certain substances to penetrate the enamel surface and its effects on the enamel as well as the efficiency of materials to prevent penetration of unwanted elements.

Some of the methods used in the laboratory for study of permeability of liquid into porous enamel are as follows (Table 2.3):

Table 2.3: Methods used for study of permeability in vitro

Methods	Measurements
Confocal micrography, transversal micrography (Meyer-Lueckel, Paris, & Kielbassa, 2007), electron paramagnetic resonance and a two-chamber diffusion cell (Kuhar, Cevc, Schara, & Funduk, 1997)	Permeability of etched enamel to water
Orientation-independent polarizing microscopy (Meira, de Mattos Brito, & de Sousa, 2015)	2D mapping of real time capillary flow of aqueous solutions of mercuric and potassium iodide on surface of carious enamel
Laser scanning confocal microscope (LSCM) in dual fluorescence mode (Neuhaus, Schlafer, Lussi, & Nyvad, 2013; Paris, Soviero, Chatzidakis, & Meyer-Lueckel, 2012)	Penetration of resin and experimental infiltrates on non cavitated enamel lesions
Conductivity experiments (Ren, Baig, & Li, 2014)	Electrical and barrier properties of enamel during transport of fluoride either passively or via iontophoretic transport
Electrochemical method (Hoppenbrouwers, Scholberg, & Borggreven, 1986).	Electrical resistance looking at enamel permeability at varying depths of unerupted and erupted premolars
Raman and IR Spectroscopy/Spectrophotometry (Bertacci, Lucchese, Taddei, Gherlone, & Chersoni, 2014)	Carbonate compounds of enamel apatite post etching treatment
Spectrophotometer (Palo et al., 2012).	Measure optical density of blue solution that penetrated teeth which signified the degree of penetration of hydrogen peroxide
QLF, thermal and near infrared imaging (Ando, Stookey, & Zero, 2006; Lee, Darling, & Fried, 2015; Usenik, Burmen, Fidler, Pernus, & Likar, 2014; Zakian, Taylor, Ellwood, & Pretty, 2010)	Detect optical changes from loss of water on surface of tooth

Methods used currently to quantify porosity on enamel surface as well as mineral density are rather invasive and samples tested are destroyed in the process. These studies are typically done in the lab to look at loss or increase in mineral content when enamel undergoes a certain demineralisation or remineralisation process. Methods used include polarized light microscopy, electrophoresis, surface microhardness tests (Vicker's and Knoop's), profilometry, microscopy, microradiography, atom force microscopy and iodide permeability test (Attin T, 2014 ; F. R. White DJ, Bowman WD., 1992). One of the methods of measuring porosity for measurement of pore volume on tooth surface looks at the use of iodide permeability test. While all these methods employed are accurate in providing information regarding the chemistry, histology and mechanical properties, they are not or yet to be suitable for use in-office for diagnosis intraorally.

Methods which are non-invasive and do not require the destruction of samples in the lab such as microcomputed tomography (Micro-CT) is reliable and widely used in vitro research setting (Swain & Xue, 2009). Currently there are some studies done to further understand the use of optical coherence tomography (OCT) in caries diagnostics. It uses low levels of infrared light spectrum and safe to use intraorally (Clarkson, 2014). However, these methods are not viable to be used clinically yet.

2.3.3 Rate of permeability and/or rate of sorption studies on enamel

There are very few studies done to look at correlating rate of permeability and sorption to degree of porosity of enamel surface. Bakhos and Brudevold (1982) looked at correlating demineralisation with permeability of enamel by looking at rate of permeability using iodide. The result suggests that water does not pass through in a straight forward manner like through a porous medium (Bakhos & Brudevold, 1982).

Currently, no study has been done to correlate the rate of water absorption to the degree of porosity of the enamel surface to water and whether it can be used to determine the presence of the highly mineralised surface layer on the enamel. There are also no study done to correlate the absorption rate of mineralising solutions on enamel surface to the efficacy of the materials**.** Clinically, if classification of initial caries includes the diagnosis of the degree of porosity of the enamel surface as well as the presence of a surface layer, then remineralisation therapy can be customized. Also, looking at the rate of absorption of remineralisation solutions can assist in determining the types of materials which are feasible to be used to provide a deeper and more effective remineralisation. Pre- and post-remineralisation comparison of rate of absorption can be used to determine success of therapy as well.

2.4 Sorptivity

2.4.1 Introduction

Enamel which consists of enamel prisms, when demineralised, forms 'finger-like extensions on the surface' which also appears like pores on the surface (Featherstone JD, 1979). Hence, liquid substance placed on its dried surface will be absorbed into the tooth surface naturally by means of capillary action. Capillary action is the ability for liquid substances to flow though narrow areas with the existence of intermolecular forces between the liquid and the surface area. This force is even strong enough to resist gravitational pull (Washburn, 1921).

Sorptivity is defined as the measurement used to quantify the rate at which liquid is absorbed or desorbed on a medium or surface by means of capillarity (Philip, 1957). Sorptivity is widely used in characterizing soils and porous construction materials such as brick, stone and concrete (Hall, 2012).

2.4.2 Calculations in Sorptivity

In 1969, John R Philips showed that sorptivity can be calculated when water flowing through a substance is mostly done though capillary action (Philip, 1957). The mathematical equation is as follows:

$$L = S\sqrt{t}$$

where S is sorptivity, L is the accumulated length of infiltration (m) and t is the time (s) it takes for this to occur. Its associated SI unit is $ms^{-1/2}$. When liquid is absorbed into a material, absorption happens at a rate that will decrease over time. The material comes into contact with water where surface contact area with the liquid is measured (A) and the amount absorbed is the accumulative volume (V). L is then calculated as below:

$$L = \frac{V}{A}$$

Therefore,

$$V = AS\sqrt{t}$$

Hence,

$$S = \frac{V}{A\sqrt{t}}$$

Another equation that calculates absorption rate by means of capillarity of a bundle of parallel cylindrical tubes is the Washburn's equation (Washburn, 1921). The equation is as follows:

$$L^2 = \frac{\gamma D t}{4\eta}$$

where t is the time for a liquid of dynamic viscosity η and surface tension γ penetrates an accumulative distance of L with accumulative pore diameter of D. In this particular equation, it also factors in temperature which is related to surface tension γ.

Therefore, putting the sorptivity and Washburn equations together,

$$S = \sqrt{\frac{\gamma D}{4\eta}}$$

Pore diameter is therefore related to sorptivity which establishes a relationship between porosity and sorptivity.

2.4.3 Sorptivity in Dentistry

Sorptivity studies are mostly done in geo-analysis. There is no study done looking at sorptivity on enamel surface and the correlation between sorptivity and porosity of enamel surface.

2.4.4 Why Sorptivity?

As discussed earlier, dentine permeability and the path to which liquid is transported has been explained through various investigations but few studies explain how enamel (sound or carious) can absorb liquids. Absorption through the enamel could be due to capillary action of liquid on enamel surface particularly when there is demineralisation on enamel surface producing finger-like extensions. In this research, attempts will be made to show that rate of absorption of water on both sound and induced non cavitated initial caries is associated with sorptivity, and to quantify its relationship with porosity of the enamel surface.

2.5 Verification of Correlations between Sorptivity with Surface Porosity

There are many ways to quantify surface porosity or density, some of which are mentioned earlier in porosity and permeability studies. In this research, 3 methods were used to correlate sorptivity measurements and surface mineral density.

2.5.1 Total Delta Z with Microcomputed Tomography (Micro-CT)

Micro-CT is used in Dentistry to provide three-dimensional (3D) view using spatial distribution maps of material density taken at different angles of teeth. It is considered a non-invasive method to calculate mineral density as the samples are not destroyed in the process of gathering information. Calculations done on the intensity of grey scale value of the images taken with micro-CT can be converted to mineral density values (Swain & Xue, 2009).

Huang (2007) used 5 hydroxyapatite (HAP) phantoms with density of 1.52, 1.63, 1.85, 2.08, 3.14 g/cm^3 and measured the grey scale value of images produced by Micro-CT for the phantoms. A linear relationship is seen between mineral density and grey scale value in Figure 2.4 (Huang, Jones, He, Darendeliler, & Swain, 2007).

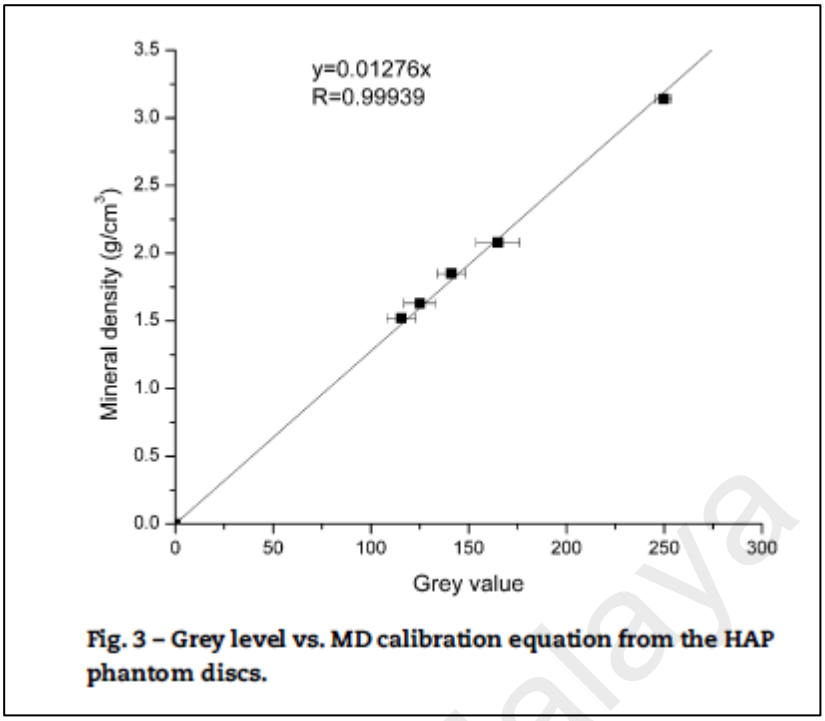

Fig. 3 – Grey level vs. MD calibration equation from the HAP phantom discs.

Figure 2.4: Graph of grey value versus mineral density (Huang et al., 2007)

This graph shows that grey scale value is linearly correlated with mineral density.

Subsequently, mineral density of white spot lesions was measured based on this graph above. The mineral density of sound enamel, apparent intact surface layer of white spot lesion (WSL) and lowest level of WSL was found to be 2.65–2.89 g/cm^3, 2.23–2.58 g/cm^3 and 1.48–2.03 g/cm^3 respectively.

In regards to mineral density in dentin, Inoue (2013) showed that the mineral density of coronal dentine quantified using micro-CT was 1,628±34.0 mg/cm^3 and radicular dentine was 1,406 ±38.7 mg/cm^3 respectively (Toshiko Inoue, Saito, Yamamoto, Nishimura, & Miyazaki, 2013). In another paper, Inoue also showed that coronal dentine had a higher nanohardness level compared to radicular area with hardness measurements of coronal dentine was 0.8GPa and radicular dentine was 0.6 GPa respectively (T. Inoue et al., 2009). In the same study, he noticed that Young's modulus was higher at the coronal region with value of 26.6GPa as compared to 20.9GPa at radicular dentine area.

Combining the results from these 2 papers, one can conclude that higher mineral density in coronal dentine contributes to higher nanohardness and Young's modulus.

The use of Micro-CT and measurement of intensity of grey scale value to quantify mineral density of a certain ROI has shown to be both reliable and accurate. It is widely used as a measurement of mineral density, microhardness and nanohardness of both enamel and dentine (He, Huang, Jing, & Hao, 2010; Neves Ade, Coutinho, Vivan Cardoso, Jaecques, & Van Meerbeek, 2010; Schwass, Swain, Purton, & Leichter, 2009).

Calculations for mineral loss (Delta Z) using microradiography has also been widely used in demineralisation studies as well (Zhou, 2015). The calculation done is based on the change in grey scale value which is measured over a certain area and depth. When done with transverse micrography, an aluminium step wedge is used for calibration for calculation of mineral density and the unit used is volume % μm.

2.5.2 Integrated Reflectivity with Optical Coherence Tomography (OCT)

Optical coherence tomography (OCT) uses low-coherence interferometry and near-infrared light to capture three-dimensional images of human tissues which allows a subsurface view of the image captured at micro meter resolution (Fercher, Drexler, Hitzenberger, & Lasser, 2003).

Initially, OCT was divided into 2 types based on the methods of obtaining images- the time domain optical coherence tomography (TdOCT) and Fourier domain optical coherence tomography (FdOCT). In recent development, 2 more commonly used systems are the spectral optical coherence tomography (SOCT) and the Swept-Source OCT (SS-OCT) or Optical Fourier domain imaging (OFDI) (Machoy et al., 2017).

OCT has been widely used in the field of medical science namely, Ocular, Vascular and Cardiology as well as Gastroenterology (Regar, Schaar, Mont, Virmani, & Serruys,

2003; Ripandelli, Coppé, Capaldo, & Stirpe, 1998; Testoni, 2007). In the field of Dentistry, its use is still fairly new and untapped. Its ability to view subsurface of the tooth up to 3mm in hard tissue and 1.5mm in soft tissue (Colston et al., 1998) enables its potential use in diagnosis for Periodontal disease (Mota, Fernandes, Cimoes, & Gomes, 2015; Xiang et al., 2010), pulpal health in Endodontics (Mortman, 2011), progression of caries lesion and remineralisation (Clarkson, 2014), integrity of resin restorations (Lin, Kuo, Chang, Yu, & Lin, 2014; Turkistani, Nakashima, Shimada, Tagami, & Sadr, 2015; Turkistani et al., 2014), outcome of oral rehabilitation in dental implants (Benic, Elmasry, & Hammerle, 2015) and diagnosis of cracks in teeth (Shimada, Sadr, Sumi, & Tagami, 2015). OCT has also been widely used in enamel studies in Dentistry to look at tissue characteristics (Mahdian, Salehi, Lurie, Yadav, & Tadinada, 2016), thickness of enamel (Algarni, Kang, Fried, Eckert, & Hara, 2016), the role of enamel thickness and refractive index on human tooth colour (Oguro et al., 2016), resin infiltration on enamel surface (Min, Inaba, Kwon, Chung, & Kim, 2015) and monitoring cariogenic lesion formation at the enamel-composite interface (Horie et al., 2016). Prototypes of hand-held OCT for use on patients in clinics have also been developed (Demian et al., 2014).

2.5.2.1 Integrated reflectivity

Integrated reflectivity of images measured using OCT has been used in various studies to define the severity of demineralised lesions (Chan et al., 2015; Le, Darling, & Fried, 2010; Nee et al., 2014)

KH Chan (2013) demonstrated the use of 2D images of depth of lesion captured using cross-polarization OCT (CP-OCT) and integrated reflectivity to show the severity of the demineralisation. Value of mean reflectivity per pixel was calculated by dividing the sum of each A-scan in linear intensity units (IU) by the number of pixels. The integrated reflectivity over a fixed depth was then calculated followed by the calculation of

integrated reflectivity of lesion depth (in microns). There are many other studies done to correlate the state of demineralisation with integrated reflectivity.

The area under curve (AUC) for A-scans have also been measured by AC Cara (2014) against the degree of demineralisation with microhardness tests and the outcome suggests a linear correlation of the two between 25-120μm depth (Cara, Zezell, Ana, Maldonado, & Freitas, 2014). Sowa (2011) also measured the AUC of A-scans for a certain area of ROI (Region of Interest) in the enamel. From his study, he suggested that direct analysis from the A-scans, the intensity histogram or the attenuation coefficient measurements obtained from the descending slope of the OCT A-scan can be used to differentiate sound and carious enamel (Sowa, Popescu, Friesen, Hewko, & Choo-Smith, 2011). OCT has also been shown to be a reliable equipment to diagnose the presence of highly mineralized layer as well as subsurface caries lesions in remineralisation/demineralisation studies in which the highly mineralized surface layer under the OCT appears to be similar to that of sound enamel (Espigares et al., 2015).

2.5.2.2 OCT and Sorptivity

OCT as tool for measuring absorption of water has not been used before in Dentistry. It is a good tool to use because this equipment captures details at air to water and air to tooth interface. Thorlabs OCS 1300SS Swept Source OCT which was used in this study has an axial resolution of 12μm in air and 9μm in water as well as transverse resolution of 25 μm. This instrument was able to capture the information needed for calculation of water lost due to sorptivity during the experiments. So far, no research papers have been published showing the use of OCT to look at sorptivity of water or liquid into the surface of enamel and dentine.

2.5.3 Qualitative Analysis

Scanning electron microscope (SEM) has been widely used to view surface topography and to provide a microscopic view and a qualitative analysis of regions of interest (Attin T, 2014 ; Frank, 1990). Together with SEM, images from Micro-CT, photography and stereo microscope will be able to provide a comprehensive overview and qualitative analysis of the enamel surface in this study.

2.6 Correlation of pH cycling models and enamel density

The use of pH cycling models has been widely accepted in the field of cariology looking at demineralisation and remineralisation process in enamel (Featherstone JD, 1979; Featherstone, Stookey, Kaminski, & Faller, 2011; Stookey et al., 2011; ten Cate JM, 1982). However, no research has been done previously to compare the sorptivity (or permeability) of pH cycling models of different durations of cycle.

CHAPTER 3: METHODS AND MATERIALS

3.1 Sorptivity

A simple test was firstly done to look at OCT as an equipment that was to be used to measure height of drop of water on enamel surface followed by a pilot study to look at the feasibility of the methods used and to provide some preliminary findings (all the images on print which may be unclear can be seen clearly in the soft copy of the thesis).

3.1.1 Feasibility of OCT as a measuring device

The first test was done to look at the feasibility of using OCT to look at absorption of water on enamel surface. A drop of water which has been mixed with methylene blue dye was dropped unto sound enamel surface. Below were the images taken at intervals showing quite clearly, the level of water on a non-carious enamel surface reducing over time (Figures 3.1-3.4).

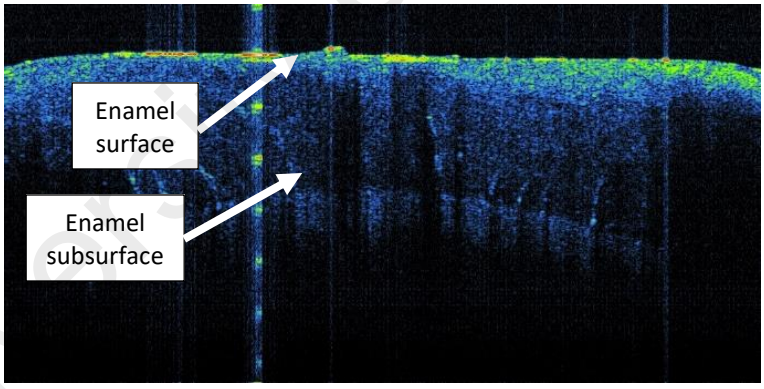

Figure 3.1: OCT image of non-carious enamel surface and subsurface region

Before water droplet was placed on surface.

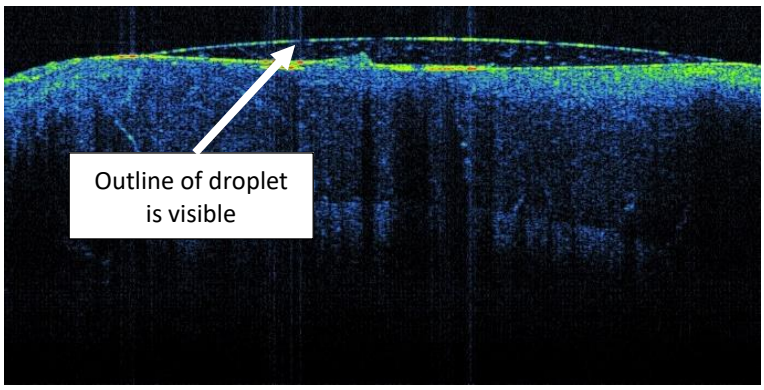

Figure 3.2: OCT image of non-carious enamel surface with a droplet of water

Water droplet placed on enamel surface and level of water is seen clearly

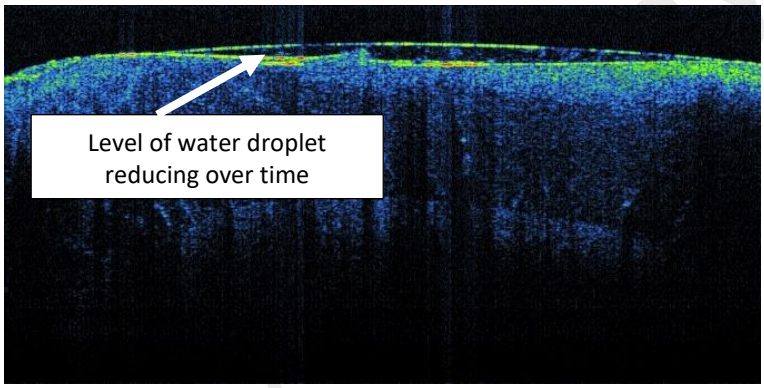

Figure 3.3: OCT image of non-carious enamel surface after a few minutes

This image shows reduction of height of water droplet over a period of time

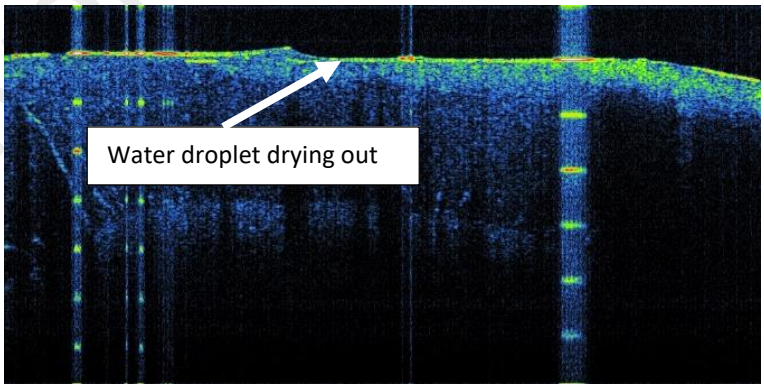

Figure 3.4: Subsequent image taken with OCT of non-carious enamel surface

This image shows water droplet on enamel surface drying out

In this preliminary study on use of OCT, though methylene dye was added to the water in the experiment done, it was later not added to water in the pilot as well as the study

done to reduce the possibility of the molecules of the dye being a confounding factor in water absorption rate during the experiment. Use of specular reflection on surface was then used as seen in Figure 3.6. This method provided a more accurate way of determining the highest spot of the drop and to measure the level at every time point with much more accuracy. Figure 3.5 show a screen shot of the image generated by the OCT before the drop of water is placed.

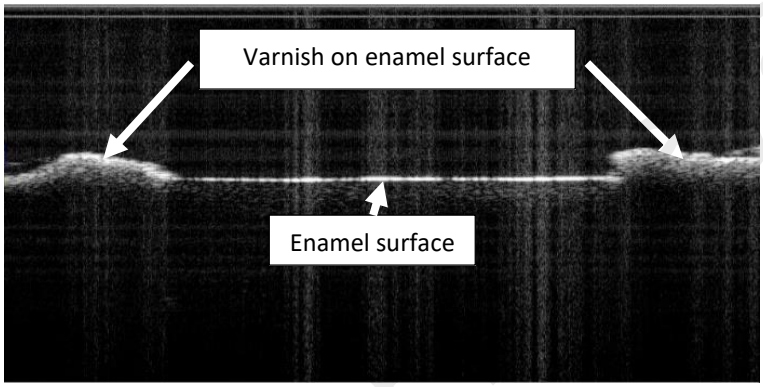

Figure 3.5: OCT image before drop of water is placed

No droplet of water on surface

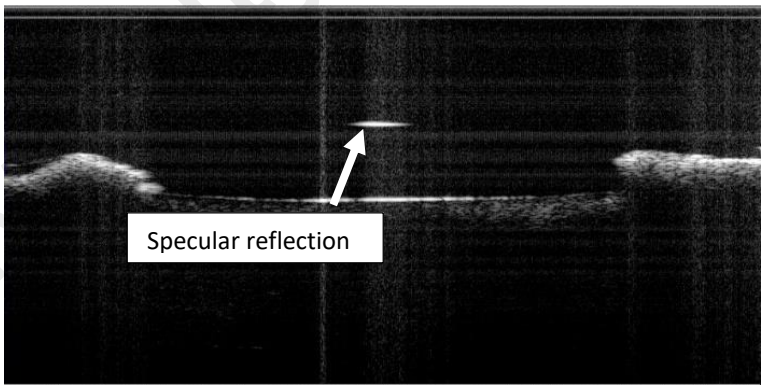

Figure 3.6: OCT image after a drop of water is placed

Droplet of water is seen on enamel surface with specular reflection seen at the highest point of the drop

3.1.2 Pilot study to measure Sorptivity

3.1.2.1 Preparation of the specimens

12 extracted teeth with caries free surfaces were cleaned with water and mounted on resin base (Figure 3.7).

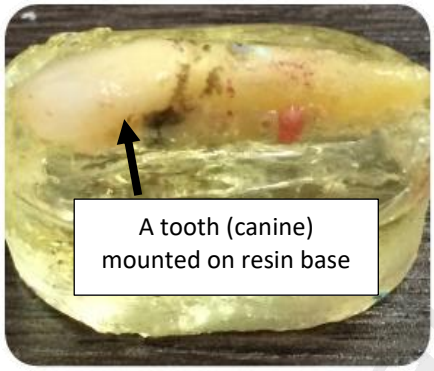

Figure 3.7: Tooth mounted on resin

For the pilot study, teeth were mounted on a resin base for ease of placement on OCT platform

Nail varnish (Tevez, US) was painted on the surfaces of all the mounted teeth and was left to dry. A portion of the varnish was gently removed using a probe providing a round shaped window of exposed enamel surface with a diameter between 1.0 to 2.4mm (Figure 3.8) which is the test site. Figure 3.9 is the illustration. All specimens were placed in 40ml of reverse osmosis (R.O) water (2 per glass jar) till the start of pH cycling.

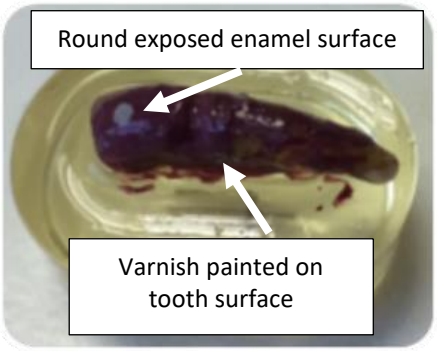

Figure 3.8: Varnish on tooth with exposed enamel surface

After mounting teeth on resin base, varnish was applied leaving a round window of exposed enamel surface and its diameter is measured.

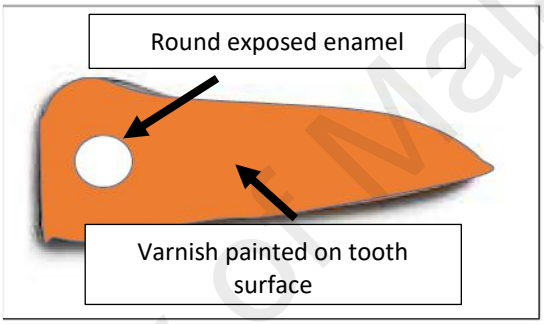

Figure 3.9: Illustration of the round window of exposure on enamel surface of tooth

This is an illustration of a round window of exposed enamel surface to be the area for testing.

2 specimens (teeth) were prepared per duration of pH cycling of 7, 14, 21, 28 and 35 days. 2 specimens were used as control and did not undergo pH cycling. pH cycling was done on the specimens using the modified Featherstone technique which is a widely excepted technique in the field of Dentistry to produce demineralised caries lesions. This technique is able to produce lesions that are similar to naturally occurring lesions (Featherstone JD, 1979; Featherstone et al., 2011; Stookey et al., 2011; ten Cate JM, 1982; F. J. White DJ, 1987).

3.1.2.2 pH cycling process was done as follows:

i. Glass jars containing 40ml of demineralisation solutions (composition of the solution in the Table 3.1(Stookey et al., 2011)) were prepared. 2 specimens were placed in each glass jar. These glass jars were then placed in the incubator (37°Celsius) for 6 hours.

ii. After 6 hours, the specimens were rinsed with R.O water and then dabbed dry. Specimens were place in glass jars containing 20 ml of remineralising solutions, 2 specimens per glass jar. These specimens were then placed in the incubator (37° Celsius) for 17.5 hours. It is not 18 hours, taking into account the time it takes to process the specimens after each demineralisation cycle.

iii. This process of remineralisation and demineralisation of the specimens were done daily except on weekends when it is soaked in glass jars containing 20mls of remineralisation solution (2 specimens in each jar) placed in the incubator.

iv. This daily cycle of demineralisation and remineralisation were carried out for 7, 14, 21, 28, 35 days for respective sets of specimens with solutions regularly changed to avoid saturation which reduces the efficacy of the solutions.

Table 3.1: Content in demineralisation and remineralisation solutions (Stookey et al., 2011)

Demineralising solution*				
Material name	**Molarity**	**Chemistry**	**Molecular weight**	**g/L**
Calcium Nitrate Tetrahydrate	Calcium 2.0 mmol/L	Ca(NO3)2•4H2O	mwt = 236.16	0.4723 g/L
Monopotassium Phosphate	Phosphate 2.0 mmol/L	KH2PO4	mwt = 136.09	0.2722 g/L
Acetic Acid	Acetic acid 75.0 mmol/L	CH3COOH	mwt = 60.05	4.5083 g/L
Sodium Hydroxide 50% w/v	Sodium Hydroxide	NAOH	39.9971 g/mol	
* Adjusted to appropriate pH with 50% NaOH after all ingredients were dissolved completely.				
Remineralising solution+				
Material name	**Molarity**	**Chemistry**	**Molecular weight**	**g/L**
Calcium Nitrate Tetrahydrate	Calcium 1.5 mmol/L	Ca ((NO3)2•4H2O	mwt = 236.16	0.3542 g/L
Monopotassium Phosphate	Phosphate 0.9 mmol/L	KH2PO4	mwt = 136.09	0.1225 g/L
Potassium Chloride	KCl 130.0 mmol/L	KCl	mwt = 74.55	9.6915 g/L
Sodium Cacodylate	Sodium cacodylate 20.0 mmol/L	NaC2H6AsO2•3H2O	mwt = 214	4.28 g/L
Hydrochloric Acid	HCL	HCL	36.458 g/mol	
+ Standard volume prepared in 4L glass beaker. Adjusted to pH 7.0 with concentrated HCl. Shelf life – no more than 7 days.				

At the end of the pH cycling process based on the duration needed, specimens were then soaked in R.O. water (40mls) in a glass jar (2 teeth per glass jar and both specimens with the same duration of pH cycling) and placed in the incubator (37° Celsius) until the time the experiment would be carried out.

3.1.2.3 Experiment

Specimens were removed from the incubator and dried (air dry for 30 seconds using a hand air blower after blot-dry of surface with a dry paper towel) just before the testing is done. Specimens were mounted unto the platform used with the Thorlabs Swept Source OCT system (OCS 1300SS) (Figure 3.10).

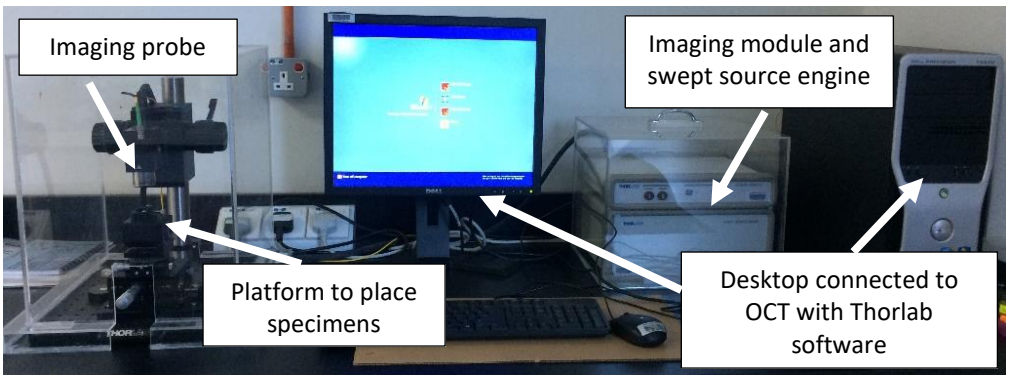

Figure 3.10: Thorlabs Swept Source OCT system (OCS 1300SS)

This is a picture of the OCS 1300SS which is used in this research. The labels in the picture indicate the parts of the equipment.

Adjustments of the position of the specimens were done to ensure that the surface which had undergone testing was as horizontal as possible and the scanning was done at the centre of the test site. To ensure that the specular reflection can be clearly seen, adjustments to the brightness and contrast were done.

A 10µL pipette (Eppendorf Research Plus pipette) which delivers 1.5µL of R.O. water was used (temperature was taken every time the experiment was done). The drop is placed on the exposed tooth surface.

Using the OCT system, a B-scan of each specimen was taken at every 10s interval for a period of 2 minutes at the centre of the test site where the diameter was maximum (screen size used on OCT were 2.5mm for X-axis (1024 pixels) and 2mm for Y-axis (512 pixels). Measurement of the height was taken at intervals of 10s using the Thorlab software which provides an electronic ruler for accurate measurement.

Recordings were taken before the drops were placed to determine the actual height of the floor of the tested area. Distortion in image caused by refraction of light happens when a drop of water is placed on the surface of the test site. In Figure 3.11 and 3.12, one can clearly see that the floor of the test site before and after a drop of water is placed. Height

of the drop is then measured from the base height before the drop was placed. Tests were repeated 3 times for every specimen. An average volume was calculated from the 3 for every interval. The diameter of the base of the drop for each specimen is determined using the same method and software.

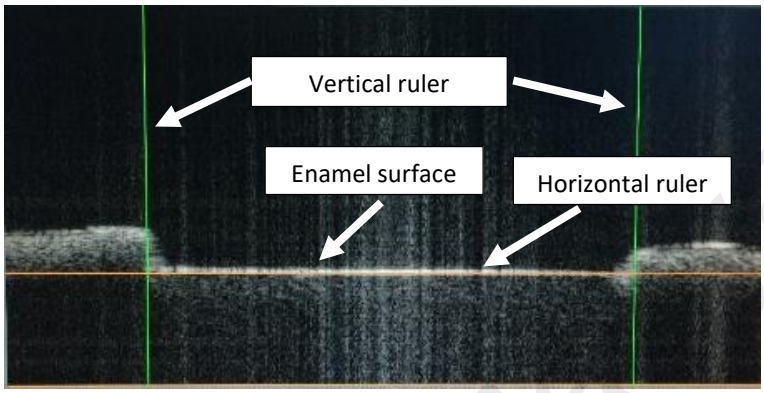

Figure 3.11: Desktop screen of image taken with OCT

This is an image of the screen of ThorLab software showing the enamel surface before the droplet is placed. Note that the enamel surface is at the same level as the yellow line. Also seen are the rulers available for measuring either horizontal or vertical width on screen.

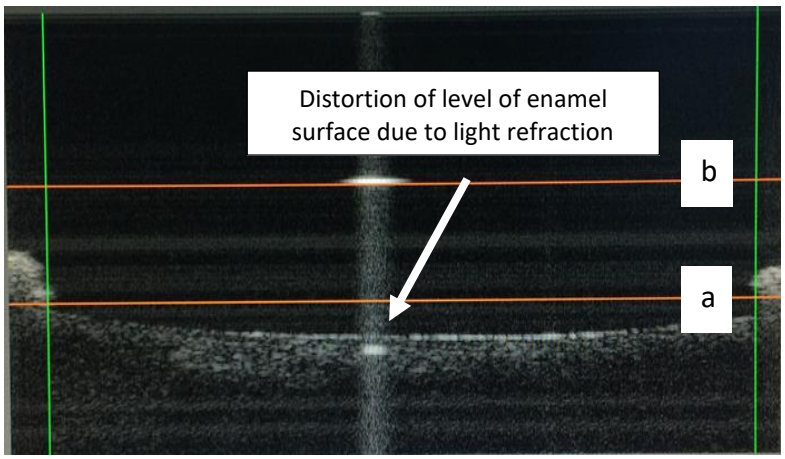

Figure 3.12: Desktop screen showing image taken with OCT

After droplet is placed, the initial height of enamel surface has moved as indicated by the white arrow. The yellow horizontal line near the base (a) is where the initial enamel surface was seen. This distortion is due to refraction of light. The length between the 2 yellow lines, a and b, is the measurement taken for the height of the droplet.

3.1.2.4 Flow chart (for pilot study)

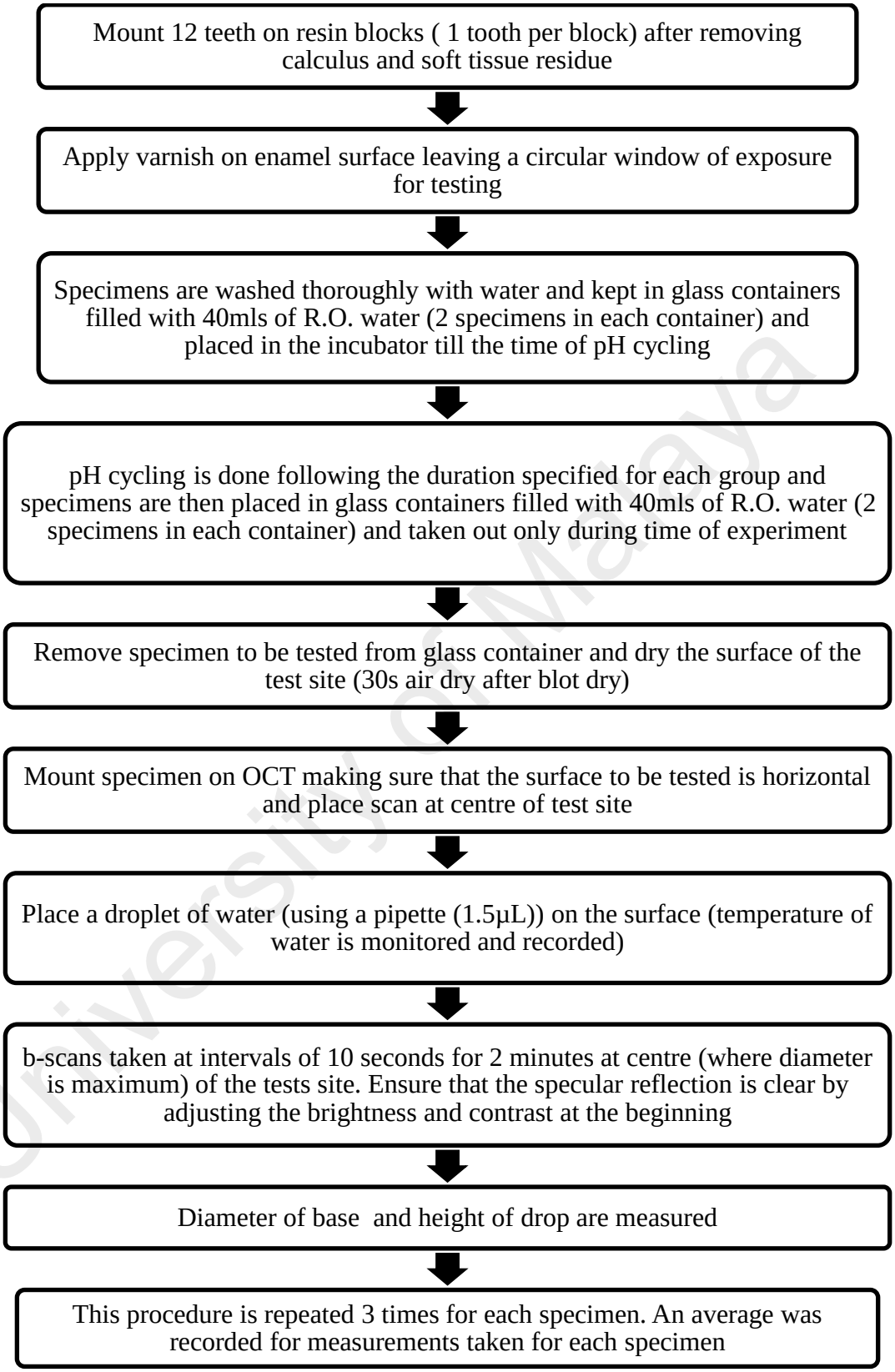

This flow chart shows the step by step of the experiment done in the pilot study.

3.1.2.5 Calculations

(a) ***Volume of droplet and Volume loss***

Volume of the drop at t seconds was calculated using this equation illustrated in Figure 3.13,

$$Vt = \frac{\pi h}{6}(3b^2 + h^2)$$ (Polyanin, 2006)

And, Vloss = V_0- V_t

Vloss= Volume loss at t seconds

V_t= Volume of drop at t seconds (interval for t is 10 seconds)

V_0= Volume of drop at the start

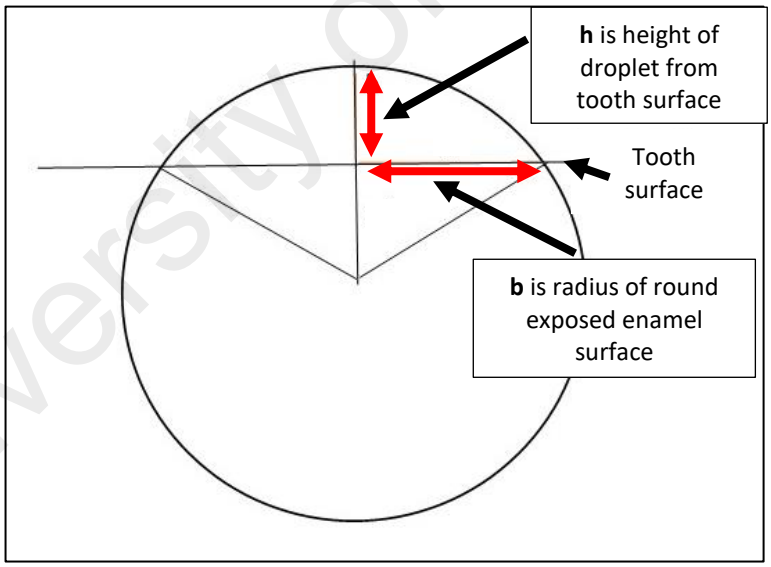

Figure 3.13: Illustration of droplet of water for calculation

This diagram is an illustration of the droplet of water on the surface of the enamel in a cross-sectional view with a full circle drawn to explain the calculation for sorptivity

(b) ***Sorptivity***

$$St = \frac{Vloss}{A\sqrt{t}}$$

St is Sorptivity at t seconds

Vloss is total volume loss at t seconds

A is Area of which the absorption occurs, A = πb^2

t is the duration of which the volume loss occurs

Unit used is mm/$s^{1/2}$

(c) ***Initial results***

In Figure 3.14 below, showing the Sorptivity curve of all the specimens, X-axis is the square root of time ($\sqrt{t}$) and Y-axis represent Volume (V) over Area (A).

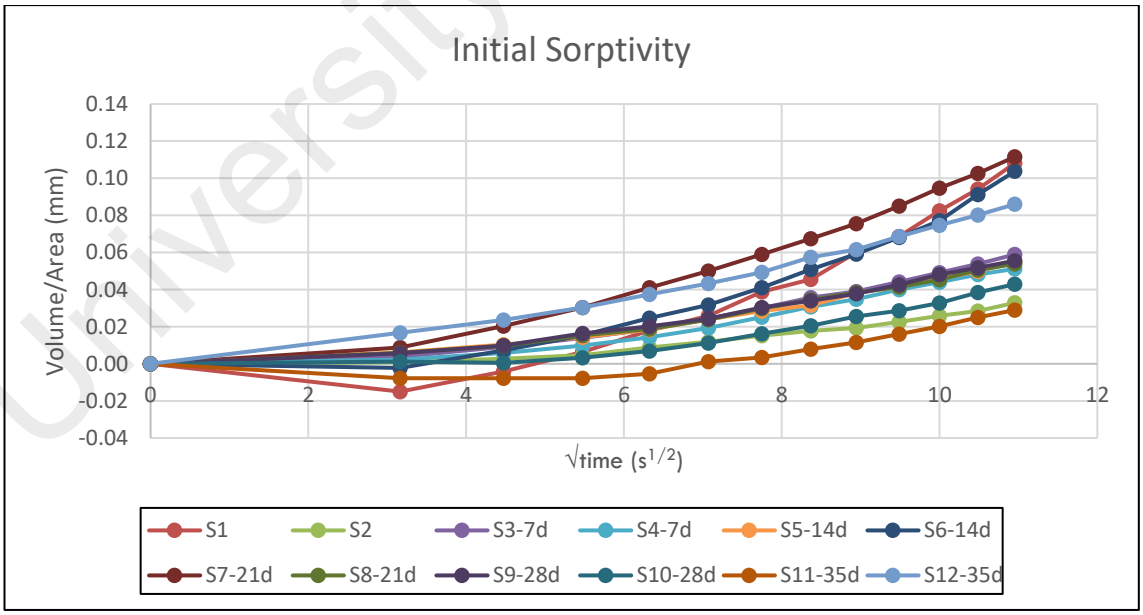

Figure 3.14: Graph of Initial Sorptivity

This graph shows that sorptivity was not constant in all the specimens and the correlation between V/A to $\sqrt{t}$ was not linear

From this graph, it was noticed that the sorptivity rate varies from one specimen to the other. Except for 1 specimen, most of the specimens show a polynomial upward trend instead of a linear upward trend. It became apparent that the reason for this phenomenon was that volume lost from evaporation of the drop was not accounted for and hence confounded the results. Volume loss due to evaporation had to be removed from the total volume loss. The remaining lost in volume will be due to absorption into the surface of the specimen.

(d) ***Evaporation***

A flat plastic surface with no absorption capabilities was used for the experiment to calculate the volume loss due to evaporation for all the specimens. The surface was painted with varnish leaving a small circular window similar to the preparations done for the specimens. Also similar to the specimens, the flat surface underwent the procedure 3 times and an average height of drop, h, was calculated at t seconds. As the diameter of the base of the circular test area defers one to another, the calculation for volume loss due to evaporation Vet at t seconds is done as follows:

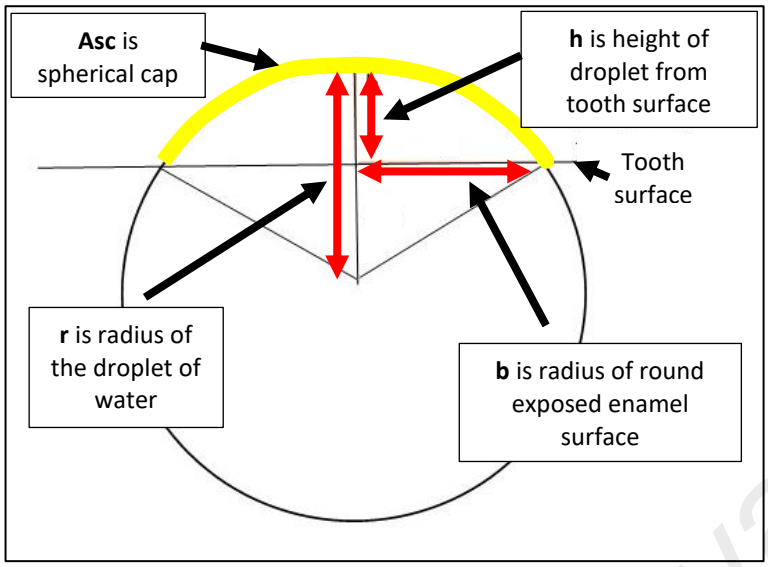

Figure 3.15:Illustration showing spherical cap where evaporation occurs

This diagram illustrates where the r (radius) is measured from. r is used in calculation of the spherical cap which is the area where evaporation takes place.

The equation for the area of which the evaporation take place, which is the spherical cap (Asc) as highlighted in Figure 3.15,

$$Asc = 2\pi rh$$

(at every time point) of which r, the radius of the droplet is calculated from this equation below (Polyanin, 2006),

$$r = \frac{(b^2 + h^2)}{2h}$$

Therefore,

$$Asc = \pi(b^2 + h^2)$$

Asc is then used to calculate volume loss due to evaporation for every 10 seconds, dVe. Assuming that rate of volume loss due to evaporation is proportional to surface of spherical cap where evaporation occurs,

$$\frac{dVe}{dt} = -kAsc$$

Therefore,

$$dVe = -kAscdt$$

dVe is Volume loss through evaporation over dt which is the duration of which the evaporation occurs. In this scenario, the measurements were done at every 10 seconds. Therefore, dt is 10s. Asc is the area of spherical cap where evaporation occurs. Volume loss due to evaporation at t seconds (Vet), will be a total of dVe calculated at every 10 seconds from 0 seconds to t seconds.

K was derived as follows:

Volume of droplet where evaporation occurs,

$$V = \frac{\pi h}{6}(3b^2 + h^2)$$

Therefore,

$$\frac{dV}{dt} = \frac{\pi}{2}(b^2 + h^2)\frac{dh}{dt}$$

At the same time (as mentioned earlier), $Asc = \pi(b^2 + h^2)$ and $\frac{dV}{dt} = -kAsc$

Therefore,

$$\frac{dh}{dt} = -2k$$

and

$$ht = h(t - 10) - 2kt$$

k is constant

ht is height of droplet at t seconds and h(t-10) is height of droplet at previous time point which is t- 10 seconds (minimum t is 0)

t is time it takes for h(t-10) to reach ht

In this equation, the height of the drop at any given time point is inversely and linearly correlated to time. An average for k was then derived from k of every time point for every test site.

This equation was verified when an initial test was done whereby the height of droplet was measured against time on plastic surface. The reduction in height of droplet is inversely and linearly related to time as seen here in the graph below (Figure 3.16).

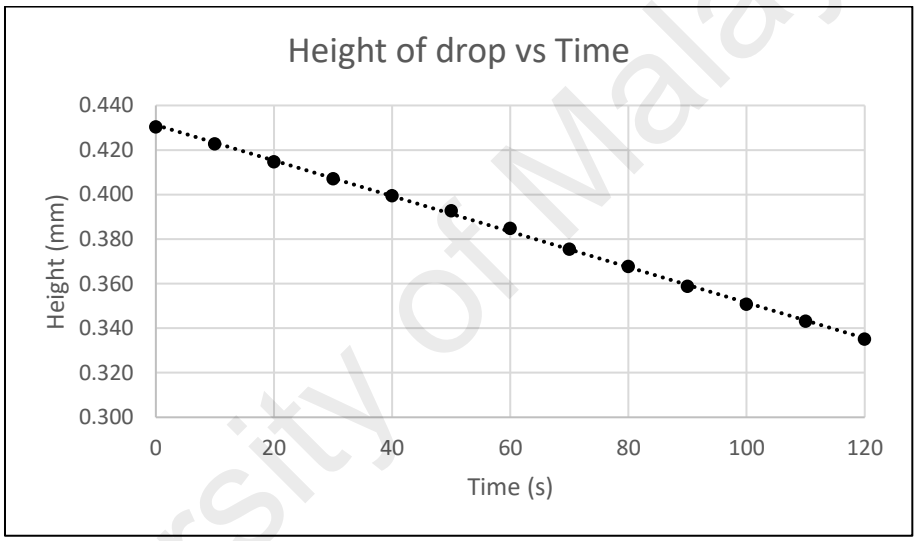

Figure 3.16: Example of height of droplet measured versus time for plastic surface

This graph shows that the reduction in height of droplet is inversely and linearly related to time which confirms that the equation used to measure k from height of drop is correct and that k is a constant.

(e) Calculations for Volume loss due to Sorptivity

Hence, volume loss due to sorptivity at t seconds, Vst, was calculated as below:

$$Vst = Vo - (Vt + Vet)$$

Vst is volume absorbed via sorptivity at a given time point

Vo is volume of droplet at the start

Vt is total volume of drop at t seconds

Vet is total volume loss due to evaporation at t seconds

Vst is then used to calculate sorptivity (calculation shown above).

Units used for volume is µL or mm^3.

Graphs for sorptivity ($\frac{Vst}{A}$ to $\sqrt{t}$) were plotted for all test sites and the linear correlation value (m in y=mx + c) was recorded as sorptivity value for each test site.

3.1.2.6 Results from Pilot

Volume of sorptivity was calculated by deducting volume loss from evaporation from total volume lost. As shown in the graph below for V/A to √t, the results were very encouraging. Figure 3.17 shows a much more linear increase of volume absorbed over time compared to when volume loss due to evaporation was not considered. This suggests that in the 2 minutes of the test period, the sorptivity for each specimen appears to be constant. Sorptivity ranged between 0 to 0.09 (Table 3.2). This results from the pilot study shows that sorptivity can be used as a measurement for absorption of water on enamel surface.

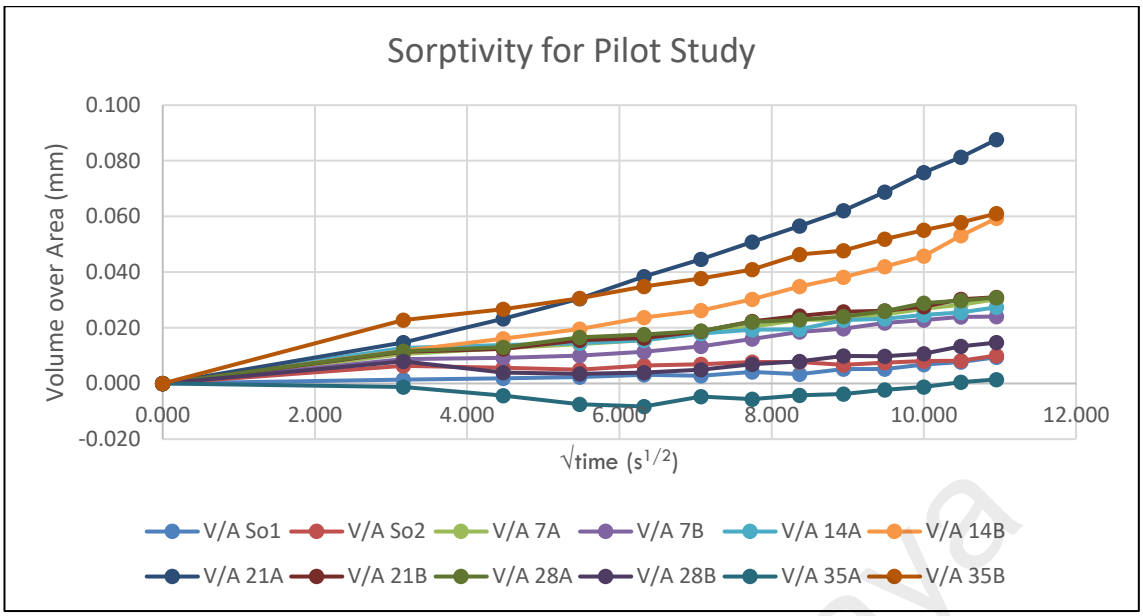

Figure 3.17: Graph of sorptivity for pilot study

After removing volume loss due to evaporation, sorptivity is now seen as constant for all the specimens. V/A to $\sqrt{t}$ *is linearly correlated.*

Table 3.2: Sorptivity values of specimens in pilot study

Sample	Sound 1	Sound 2	7days 1	7days 2	14days 1	14day 2	21days 1	21days 2	28day 1	28days 2	35days 1	35days 2
Sorptivity	0.0008	0.0007	0.0026	0.0023	0.0022	0.0052	0.0083	0.0028	0.0027	0.0011	0.0001	0.0053

Table 3.2 shows the sorptivity calculated for each specimen. It was observed that specimens which underwent same duration of pH cycling did not produce the same or similar sorptivity rate suggesting that the rate of demineralisation and remineralisation is unique to each specimen. However, when an average was calculated, the correlation was interesting. The average sorptivity rate did not increase linearly between the different sets of specimens of different duration of pH cycling as seen in Table 3.3 and a graph plotted in Figure 3.18. In this graph, the average sorptivity rate of the 2 specimens in each group were plotted to show that from sound enamel samples to 21 days pH cycling samples, the average sorptivity was on a steady incline and then a drop in mean sorptivity of 28 days samples were observed followed by an increase of mean for 35 days samples.

The possibility is that the highly mineralised surface layer on enamel surface prevented sorptivity levels from increasing linearly following the duration of pH cycling as the presence of a surface layer impedes the absorption of water into the subsurface region.

Table 3.3: Mean sorptivity by group in pilot study

Groups	Mean Sorptivity
Sound	0.0008
7 days pH cycling	0.0025
14 days pH cycling	0.0037
21 days pH cycling	0.0056
28 days pH cycling	0.0019
35 days pH cycling	0.0027

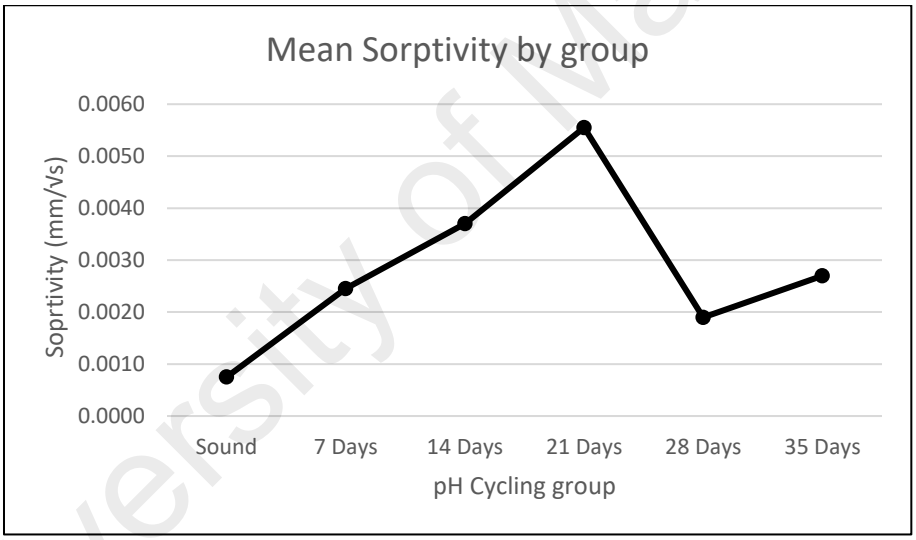

Figure 3.18: Graph of mean sorptivity in pilot study

This graph shows that sorptivity does not increase linearly with duration of pH cycling. This finding confirms the cycle of demineralisation and remineralisation and the presence of surface layer which reduces the porosity of the enamel surface significantly.

Based on the pilot study, sorptivity as a method used to quantify rate of absorption seem to be very promising. Also, a study on mean sorptivity of each pH cycling group

will be able to provide a better understanding of sorptivity and its relationship with the mineralization level of surface of the enamel.

3.1.2.7 Learnings from pilot

i. There was a need to ensure that all the specimens that were said to be sound prior to pH cycling was confirmed with proper investigations. In the experiment, OCT was used to screen, gauge and ensure that all the enamel surface tested were sound prior to pH cycling.

ii. Specimen size per pH cycling group had to be of sufficient size. Since there were no previous similar studies done before to provide a protocol, a sizable number of 16 specimens per set were chosen and for each specimen, 2 sites were prepared. A total of 32 test sites per pH cycling group were prepared.

iii. The diameter for the specimens in the pilot study was between 1mm to 2.4mm. In the experiment, given the limitations of this protocol with the use of application of nail varnish on teeth, the diameter of the circular window of enamel test sites was ensured to be in the range of 1.4±0.1mm with the use of a calliper.

iv. It was also noticed that during the pilot and subsequent tests, water drops were going beyond the test sites though still maintaining a circular base. Hence, measurements for volume loss due to evaporation used the diameter of the drop. The base of which the height of the drop was to be calculated from was the average height of the varnish on both sides of the test sites. For the calculation of sorptivity, the area calculation used the diameter of every test site which was where absorption happened.

v. While calculating volume lost due to sorptivity, volume lost due to evaporation had to be considered. Hence, for the experiment, the protocol was that at the

start of every experiment day, evaporation rate was calculated by running the tests using a plastic flat surface.

3.1.3 Materials and methods

3.1.3.1 Preparations

96 extracted teeth with caries free enamel surfaces were cleaned with water. Incisors, canines and premolars were chosen because these teeth have a relatively flat labial or buccal surface. The roots were separated from the crowns using a precision low speed saw with calculus and soft tissue residue removed and then rinsed with R.O. (Reversed Osmosis) water and air dried. These were then separately mounted on a resin base (Mirapox (Miracon MY)) using a pre-designed mould.

2 coats of nail varnish (Revlon, US) were painted on the surfaces of all specimens (mounted crown of teeth) (Figure 3.19) and left to dry. Another layer of top coat (Revlon, US) was then applied to ensure the resilience of the varnish on the surface while going through pH cycling. A portion of the varnish was gently removed using a probe and a template providing 2 circular shaped window of exposed enamel surface on the specimens with diameter of 1.4±0.1mm marked as test sites which were 2-4 mm apart (Figure 3.20). A calliper was used to ensure the diameter was within the range.

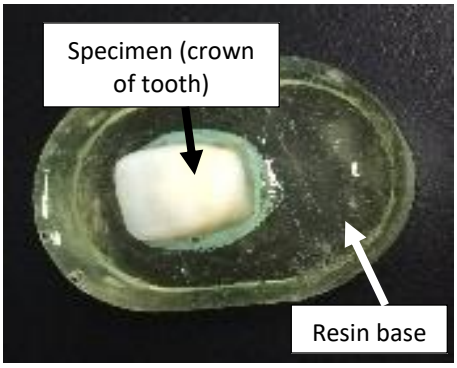

Figure 3.19: Specimen (crown of tooth) mounted on resin

The roots of teeth were removed and the specimens were mounted on resin.

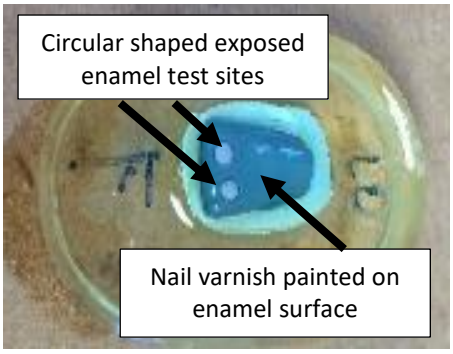

Figure 3.20: Specimen with varnish and 2 test sites of exposed enamel surface

Each specimen has 2 test sites that were 1.4±0.1mm in diameter to ensure uniformity of the test sites.

OCT was used to screen all the specimens to ensure that they were sound before pH cycling. Screen size used for tooth screening before and after pH cycling were X-axis- 1.6mm (1024 pixels), Y-axis- 2mm (512 pixels) (depth of sub surface recorded of 1.5mm), Z-axis is between 2-2.5mm for 3D screening. Figure 3.21 shows an image taken of an enamel surface for tooth screening. The beam of OCT which is near infra-red light manage to penetrate through the enamel surface capturing the details in the subsurface region. This image shows that the enamel surface is sound. Figure 3.22 is an image taken after pH cycling whereby the image shows a concentrated white area on the enamel surface because the beam is unable to penetrate through to capture details below the subsurface region. (Detailed step by step of image capturing using OCT in Appendix A). This image shows that the enamel surface is demineralised.

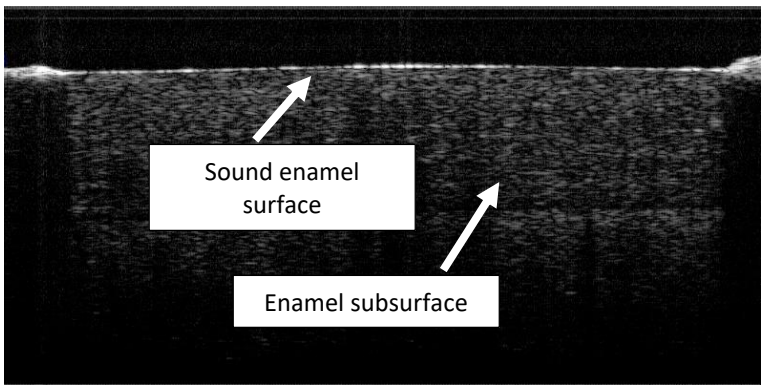

Figure 3.21: Image taken with OCT of sound enamel surface

Before pH cycling, details of subsurface of enamel is captured as the beam of near infra-red light of OCT is able to penetrate through the enamel surface which is sound. This confirms that this test site is sound.

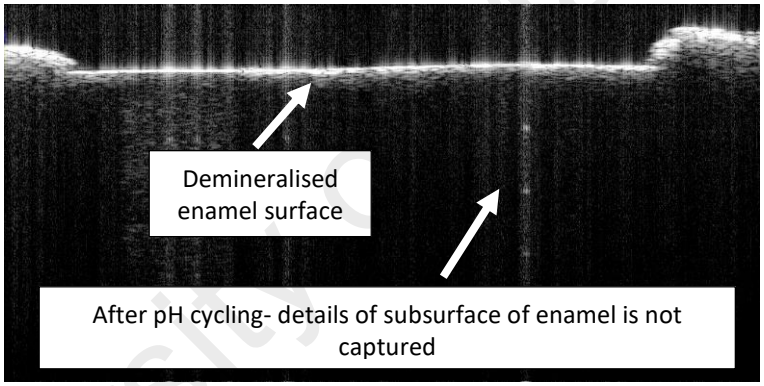

Figure 3.22: Image taken with OCT of demineralised enamel surface

After pH cycling, details in subsurface region is no longer visible as the near infra-red beam is unable to penetrate through the demineralised enamel surface.

16 specimens (2 test sites per specimen) were prepared per pH cycling duration of 7, 14, 21, 28 and 35 days which were placed in groups labelled G7, G14, G21, G28 and G35 respectively. 16 specimens were used as control (GS) and did not undergo pH cycling. Test sites were labelled A for GS, B for G7, C for G14, D for G21, E for G28 and F for G35, and tagged with specific numbers unique for every test site for identification purposes. pH cycling was done using the modified Featherstone method which was first developed by Featherstone et al (1979). This method of producing demineralised lesions

is widely accepted in the field of research in dentistry. (Featherstone JD, 1979; Featherstone et al., 2011; Stookey et al., 2011; ten Cate JM, 1982; F. J. White DJ, 1987).

3.1.3.2 Demineralisation and Remineralisation solutions

Preparation for demineralisation and remineralisation solutions were prepared based on chemical compound and concentration provided by Featherstone et al in Table 3.1.

Preparation of the solutions were done as follows:

i. Materials and equipment were obtained for the preparation of these solutions (Figure 3.23 to Figure 3.25) and the list of materials included:
    a. Chemical compounds (from Chemolab Supplies Sdn. Bhd. (668415-H))
        i. FS:C1081- Calcium Nitrate Tetrahydrate AR (500g)
        ii. FS: P5104- Potassium Dihydrogen Phosphate Anhydrous AR (500g)
        iii. FS: P5067- Potassium Chloride AR (500g)
        iv. FS: A1020- Acetic Acid Glacial AR (2.5L (P))
        v. FS: S5158- Sodium Hydroxide Pellets AR (500g)
        vi. FS:H8040- Hydrochloric Acid 37% AR (2.5L(P))
        vii. SA:C0250- Sodium Cacodylate Trihydrate 98% (100g)
        viii. FS: A7029- Buffer Solution pH 4.00 (1L)
        ix. FS A7039- Buffer Solutions pH 7.00 (1L)

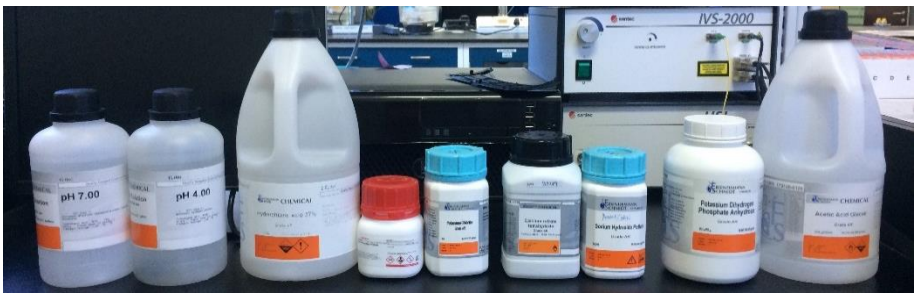

Figure 3.23: Materials for demineralisation and remineralisation solutions

b. 2-liter glass bottles (Schott Lab Bottle, Boro) with blue PPN screw cap used to store solutions (Figure 3.24)

Figure 3.24: 2-liter glass bottle

c. Specimen jar with bakelite screw cap (60ml/52mm OD x 52mmH) (Figure 3.25) to be used to store the specimens during the remineralisation and demineralisation cycle.

Figure 3.25: Specimen jar

ii. Process of producing demineralisation and remineralisation solutions:

a. Materials needed were measured for a mixture of 5L of remineralisation and demineralisation solutions for each preparation done.

b. R.O water was measured to 5L and placed in a beaker and all the materials in the recipe were added into the water and mixed thoroughly. 2 batches of 5Ls of each solution were prepared and stored for immediate use. Table 3.4 and 3.5 show the amount needed for 5L of each solution.

c. Calibrate pH meter using Buffer Solution pH 4.00 (FS: A7029) and Buffer Solutions pH 7.00 (1L) (FS A7039). pH meter is used to ensure pH is adjusted according to specifications of the solutions using Sodium Hydroxide 50% for demineralisation solution and Hydrochloric Acid 37% for remineralisation solution.

Table 3.4: Chemical compound in demineralisation solution

Demineralisation solution		
Code	Material	For 5L
FS:C1081	Calcium Nitrate Tetrahydrate AR (500g)	2.3615 g
FS: P5104	Potassium Dihydrogen Phosphate Annhydrous AR (500g)	1.361 g
FS: A1020	Acetic Acid Glacial AR (2.5L (P))	22.5415g
FS: S5158	Sodium Hydroxide Pellets AR (500g) 10g mixed to 20ml of water dilution (50% NaOH) and added to mix to adjust to pH 4.4	

Table 3.5: Chemical compound in remineralisation solution

Remineralisation Solution		
Code	Material	For 5L
FS:C1081	Calcium Nitrate Tetrahydrate AR (500g)	1.771g
FS: P5104	Potassium Dihydrogen Phosphate Annhydrous AR (500g)	0.6125g
FS: P5067	Potassium Chloride AR (500g)	48.4575g
SA:C0250	Sodium Cacodylate Trihydrate 98% (100g)	21.4g
FS:H8040	Hydrochloric Acid 37% AR (2.5L(P)) added to mixture to adjust to pH 7.0	

3.1.3.3 pH-cycling process

The pH-cycling process were done as follows:

i. Glass specimen jars (Figure 3.26) containing 40ml of demineralisation that were labelled according the pH cycling groups. 2 specimens were placed in each glass jar. These glass jars were then placed in the incubator (37°Celsius) for 6 hours.

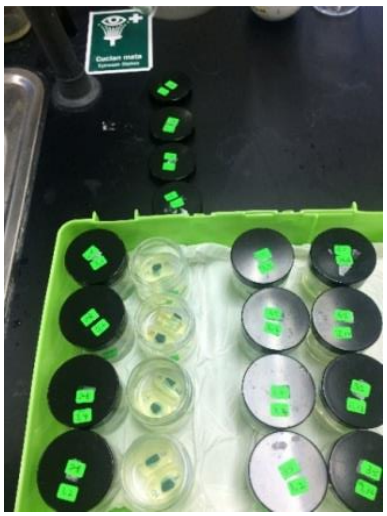

Figure 3.26: Image of specimens in jars containing remineralising solution

Each jar contains 2 specimens (4 test sites).

ii. After 6 hours, the specimens were rinsed with reversed osmosis (R.O) water and then dabbed dry. Specimens were carefully placed in glass jars containing 20 ml of remineralising solutions, 2 specimens per glass jar (Figure 3.27 and Figure 3.28). These specimens were then placed in the incubator (37° Celsius) for 17.5 hours. It is not 18 hours, taking into account the time it takes to process the specimens after each demineralisation cycle.

Figure 3.27: Image of specimen jar containing demineralising solution

Each jar will contain 2 specimens that are carefully removed from the jars containing remineralising solutions.

Figure 3.28: Specimens being placed carefully in the jar

The specimens were rinsed and dried, and placed in demineralising solutions. This process was done carefully in order to protect and not damage the surface of test sites.

iii. This process of remineralisation and demineralisation of the specimens was done daily except on weekends when specimens were soaked in glass jars containing 20mls of remineralisation solution (2 specimens in each jar) placed in the incubator.

iv. This daily cycle of demineralisation and remineralisation will be carried out for 0, 7, 14, 21, 28, 35 days for groups of specimens labelled as GS, G7, G14, G21, G28 and G35 respectively. Remineralisation solutions were changed 3 times a week (Mondays, Wednesdays and Fridays) and demineralisation solutions changed twice a week (Mondays and Thursdays) to avoid saturation.

At the end of the pH cycling process based on the duration needed, specimens were then soaked in R.O. water (40mls) in a glass jar (2 teeth per glass jar and both specimens with the same duration of pH cycling) and placed in the incubator (37° Celsius) until the time the scanning would be carried out which was no longer than 7 days.

3.1.3.4 Scanning using OCT

Specimens were removed from the incubator and dried (air dry for 30 seconds using a hand air blower after blot-dry of surface with a dry paper towel) just before the testing is done. Specimen is mounted unto the platform used with the Thorlabs Swept Source OCT system (OCS 1300SS) (Figure 3.10 and Figure 3.29).

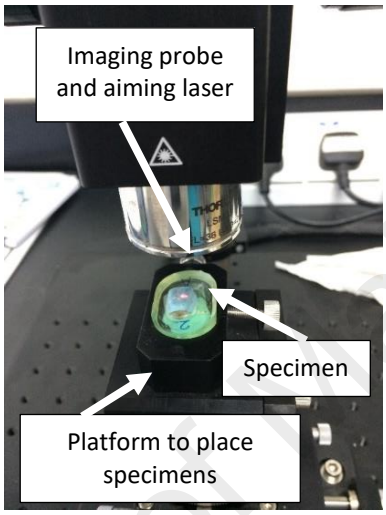

Figure 3.29: Imaging Probe in Probe Adapter Stand

The specimens are placed where the beam is at the centre of test sites.

A 10µL pipette (Eppendorf Research Plus pipette) and Universal 10µl pipette tips (Extragene Inc., Taiwan) and (EGTIP-10-C) from Gene Express PLT (LLP0001852-LGN)) were used to deliver 0.7µl of R.O. water onto test sites.

Adjustments of the position of the specimens were done to ensure that the surface of test sites were as horizontal as possible, and the scanning done were performed at the centre where the diameter of the test sites were at their maximum. To ensure that the specular reflection on droplets were clear, adjustments to the brightness and contrast were done.

Using the ThorLab software (Figure 3.30), a B-scan image of the specimen was taken at every 10 seconds interval for a period of 2 minutes at the centre of the test site. (Length

of frame on OCT is determined at 2.2mm for X-axis (1024 pixels) and 2mm for Y-axis (512 pixels). The experiment was repeated 3 times for each test site and an average height was taken at each time point. Figures 3.31 to 3.33 are examples of images taken before, during and after the drop is placed. The difference in height can be seen between Figures 3.33 and 3.34 which were images taken 30 seconds apart.

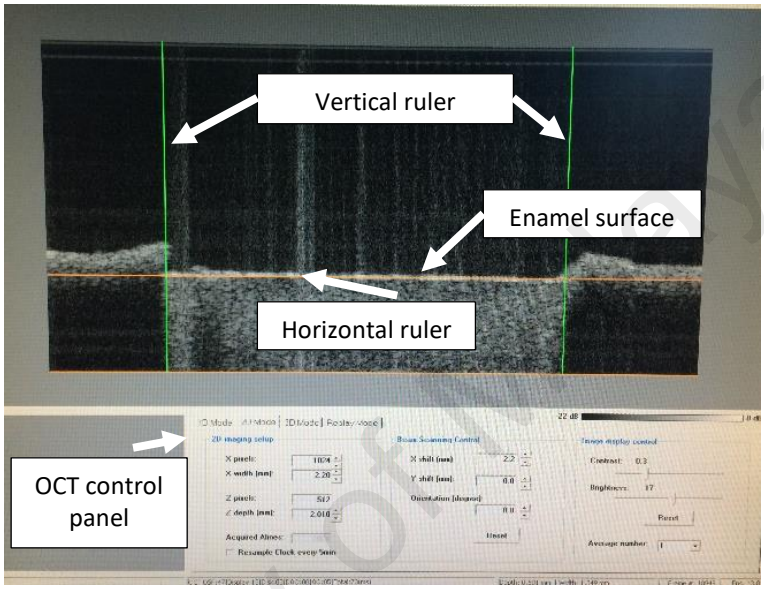

Figure 3.30: ThorLab software screen

The OCT control panel at the bottom of the screen is toggled to ensure that the parameters remain the same throughout the experiment for all the test sites.

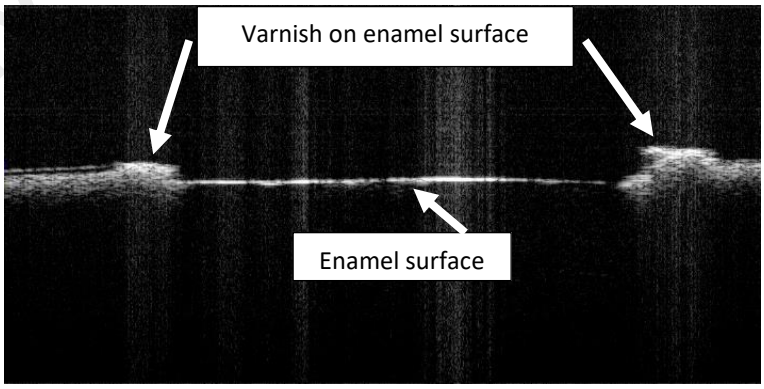

Figure 3.31: Image taken with OCT before droplet of water is placed

This is an image taken with OCT before a drop of water is placed. Varnish can be seen on both sides of the image.

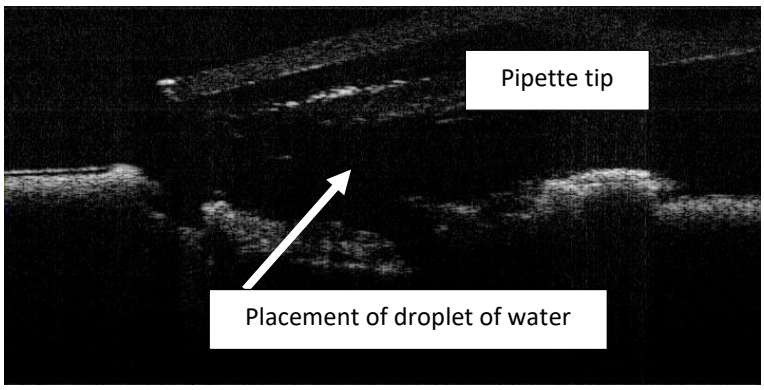

Figure 3.32: Image taken with OCT during the placement of droplet of water

The arrow shows the placement of droplet of water using a micropipette. In this image the pipette tip can be seen.

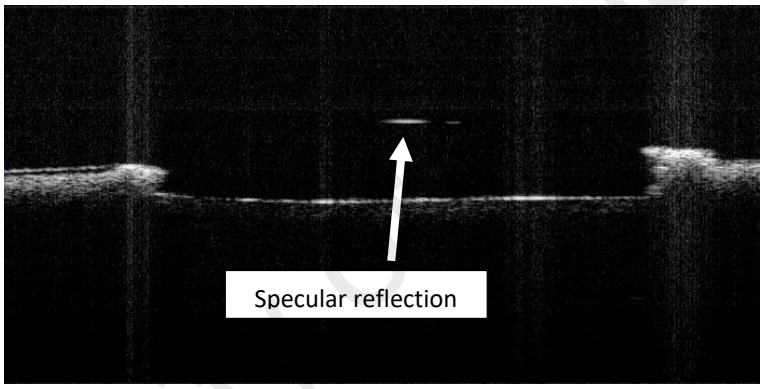

Figure 3.33: Image taken with OCT at 0 second

Droplet of water placed with visible specular reflection at top of droplet.

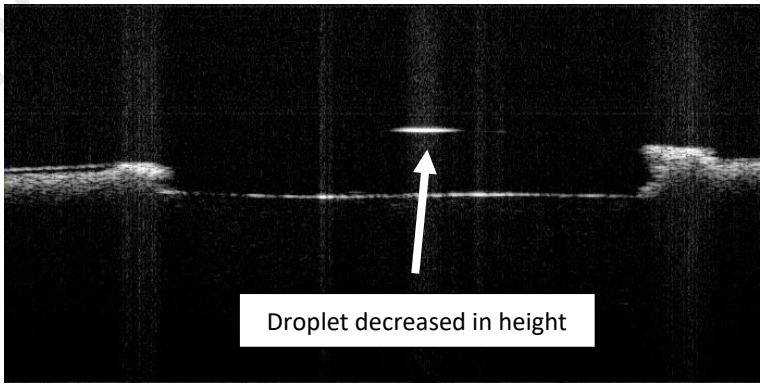

Figure 3.34: Image taken with OCT of droplet of water at 30 seconds

After 30 seconds the height of the drop decreases as seen in this image due to volume loss from sorptivity and evaporation.

The length from edge of screen at the bottom of the image to the enamel surface in every frame is set at 0.601mm for the purpose of standardization. When base of the enamel is distorted due to light refraction, the enamel surface maintains at 0.601mm from edge of screen and height of drop is calculated from this point (yellow line in Figure 3.35).

As noticed during pilot study, the drops on the test site typically goes beyond the boundaries slightly and therefore measurements of the diameter for the drop as well as diameter of the exposed enamel area was taken for each test site on the specimens. Distortion due to refraction of light happens when water drop is on the surface of the test site. When snapshots of 10-second interval frames were viewed at a fast pace, the boundary of where the distortion happen can be clearly seen. That is the edge of the drop on the varnish. Figures 3.35-3.39 below show the measurements that were taken (red arrows on images showing the parameters of the measurements).

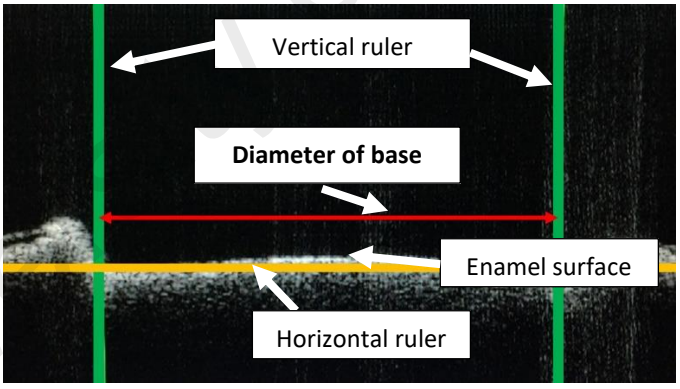

Figure 3.35: Parameters for measurement of diameter of base of test site

This image shows where the diameter of the base of test site is measured from. The 2 vertical electronic rulers are placed at the edge of the test site where the varnish starts and the measurement between the 2 rulers are recorded.

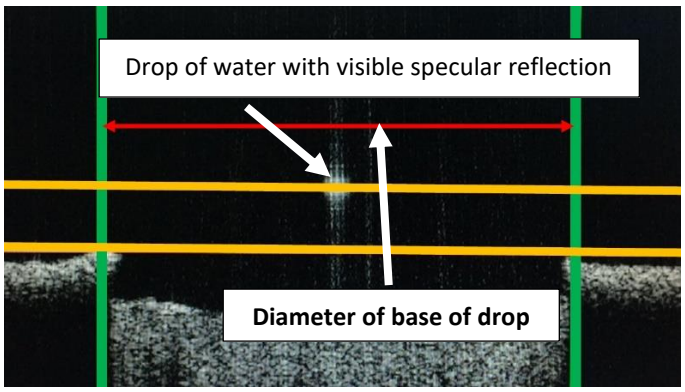

Figure 3.36: Parameters for measurement of diameter of base of drop

The base of the drop is measured in this image with the 2 vertical electronic rulers placed slightly beyond the edge of the test site where the margin of the drop is at. The measurement between the 2 rulers are then recorded.

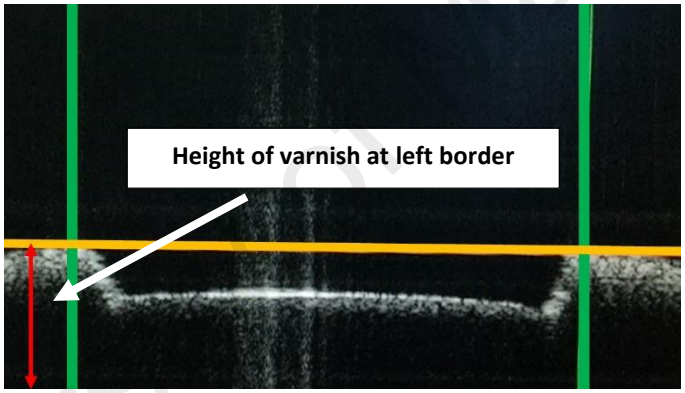

Figure 3.37: Parameters for measurement of height of varnish at left border

Height of the varnish is recorded on both left and right side as both are typically not of the same exact height.

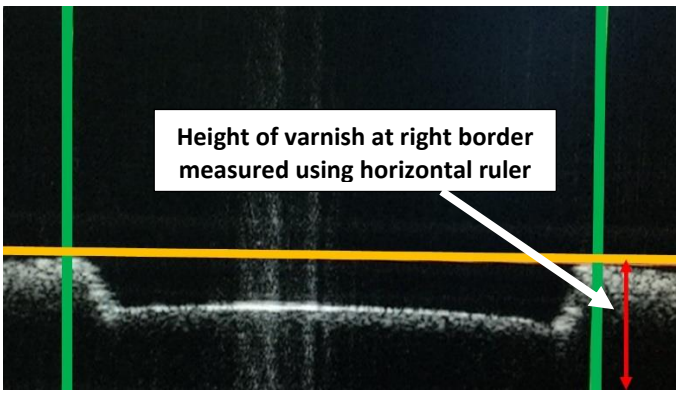

Figure 3.38: Parameters for measurement of height of varnish at right border

Height of the varnish at the right border is recorded. Subsequently, an average is taken and used as the base height where the height of the drop is measured from.

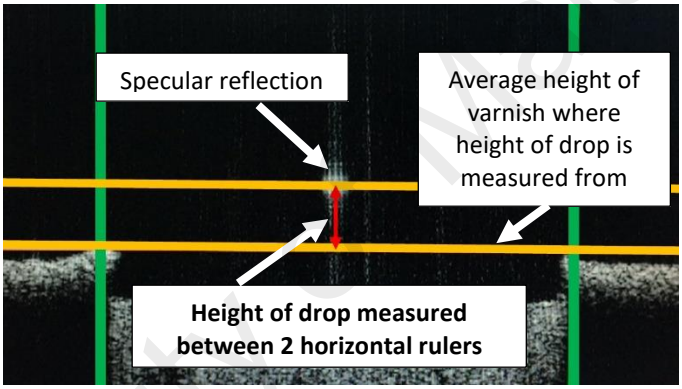

Figure 3.39: Parameters for measurement of height of droplet of water

The height of the drop is measured between the 2 horizontal rulers, one placed at the average height of varnish, the other placed on the specular reflection of the drop of water. Measurements are taken at every 10 second intervals for 2 minutes.

Evaporation rate was calculated with tests done at the beginning of every test day. A flat plastic surface with no absorption capabilities was used for the experiment to calculate the volume loss due to evaporation for all the specimens. The surface was painted with varnish leaving a small circular window similar to the preparations done for the specimens. Also similar to the specimens, the flat surface underwent the procedure 3 times and an average height at each time point was calculated.

3.1.3.5 Flow chart of experiment

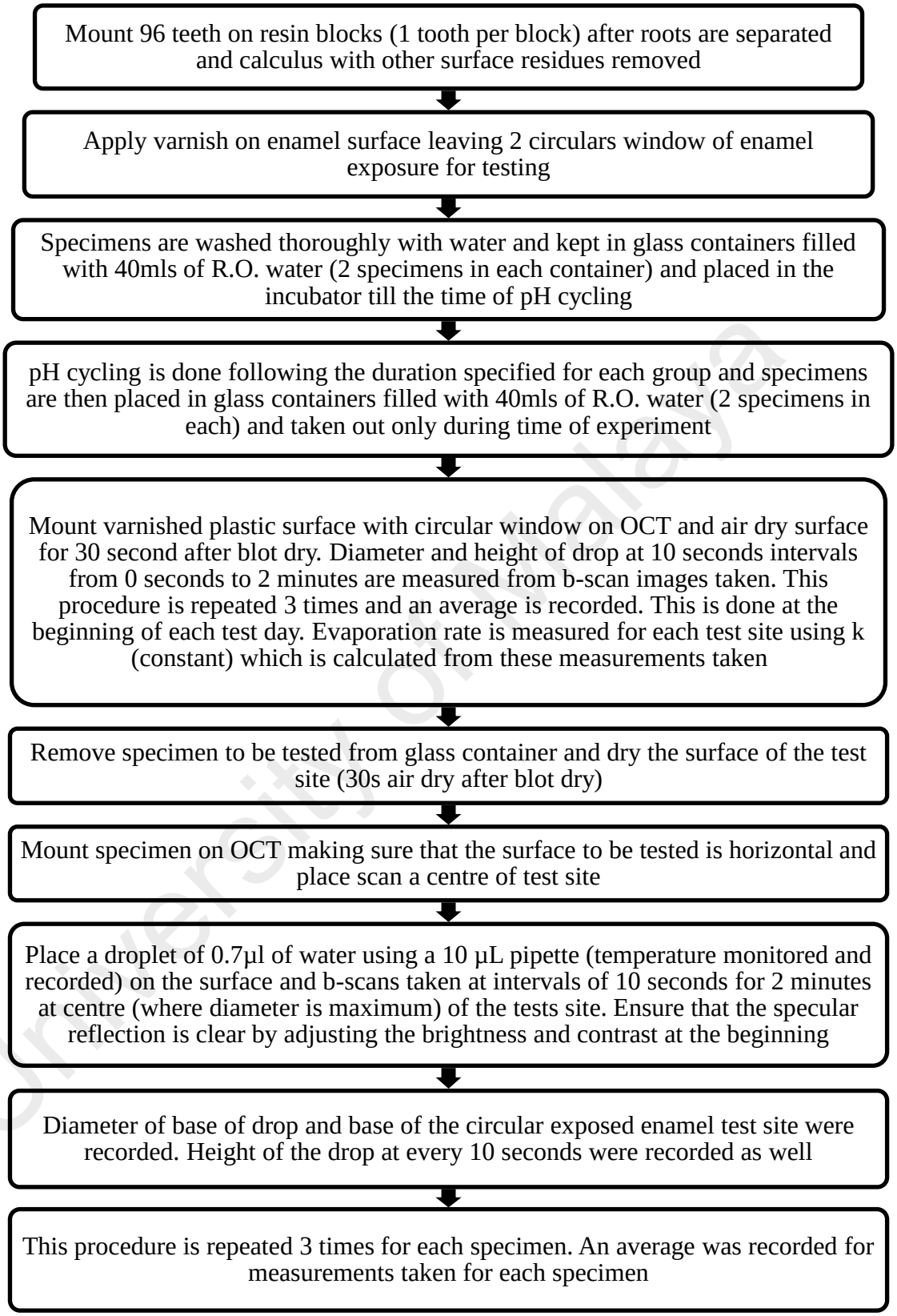

This is a flow chart of the step by step of the experiment. Detailed step by step is attached in Appendix A.

3.1.3.6 Calculations

Calculation for volume loss due to sorptivity uses the same calculations done in the pilot study (Subsection 4.1.2.5). However, measurements taken from the experiment for the calculations done were more accurate (Figures 3.35-3.39). As explained earlier, the droplets were slightly beyond the boundaries of the test sites. Figure 3.40 is an illustration that shows how the measurements were taken. The height of the drop (h3) was measured from the average height of varnish on both sides of the test sites (average of h1 and h2) to the tip of the drop which is marked by the presence of a visible specular reflection. For calculation for volume lost due on evaporation, diameter of the drop, Ddrop, was used. For sorptivity, the diameter used was the diameter of the base (Dbase) where the absorption takes place.

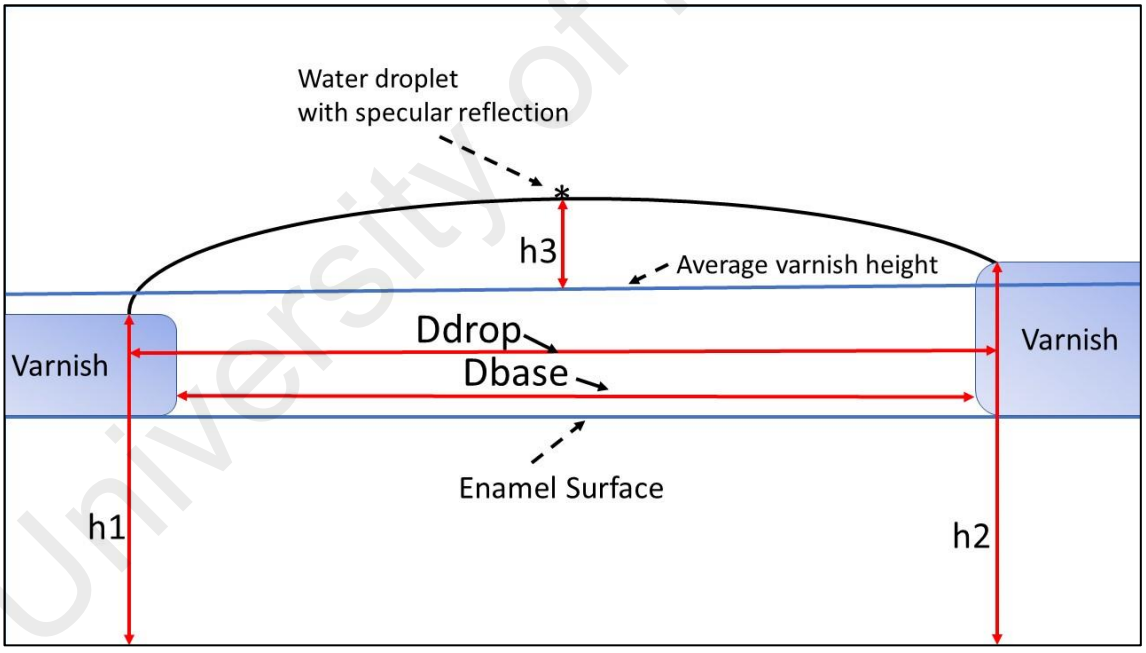

Figure 3.40: Illustration of measurements taken of the droplet

This diagram illustrates the measurements to be taken for calculations.

3.2 Micro-CT Scanning, Image Processing and Data analysis

24 specimens, 4 from groups GS to G35 were chosen and each specimen had 2 test sites. In total, there were 8 test sites per pH cycling group used for scanning.

Scanning of the specimens was performed using microcomputed tomography (Micro-CT) equipment (XT H 225, Nikon Metrology Inc., Brighton, MI, USA) (Figure 3.41). The scanning parameters used were 95kV, 90µA, 708ms of exposure, 720 projections and 4 frames per projection. The total scanning time was approximately 35 minutes for each specimen.

Figure 3.41: Microcomputed tomography equipment

3D reconstructions were done using the software CT Pro 3D (Nikon metrology, Inc., Brighton, MI, USA). Voxel size ranged from 6µm- 9µm, averaging at 7µm. Dicom files were exported using VGStudio MAX 2.1 (Volume Graphics GmbH, Heidelberg, Germany). Images were taken with 16-bit capabilities and measurements at 8-bit. Scans were processed using ImageJ. 3 horizontal sections or scans were chosen near the largest diameter of each test site. From each image, grey scale profile were generated from 3 randomly selected line (data point) across the lesion using the Plot Profile function. A total of 9 line profiles were taken from each test site (Figure 3.42).

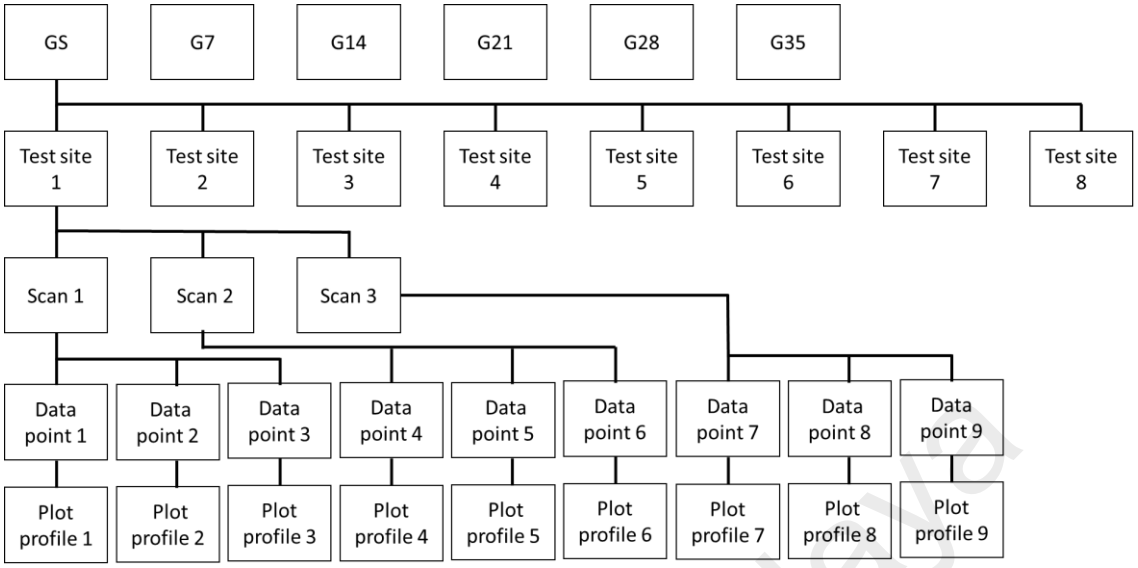

Figure 3.42: Schematic diagram of collection of data points and plot profiles

A schematic diagram showing an example of a test site generating 9 plot profiles

3.2.1 Calculations

Measurements of area under curve (AUC) using the trapezoidal rule ($\frac{y_1+y_2}{2} \times (x_1 - x_2)$) for grey scale values were calculated for 10 µm(0-10µm) as seen in example of graph in Figure 3.43, 20 µm (10-20 µm), 30 µm (20-30 µm), 40 µm (30-40 µm) and 50 µm (40-50µm) from each plot profile. The mean values at 10- 50 µm (MeanAUC10-MeanAUC50) were then calculated from AUC measurements of 9 data points taken from each test site.

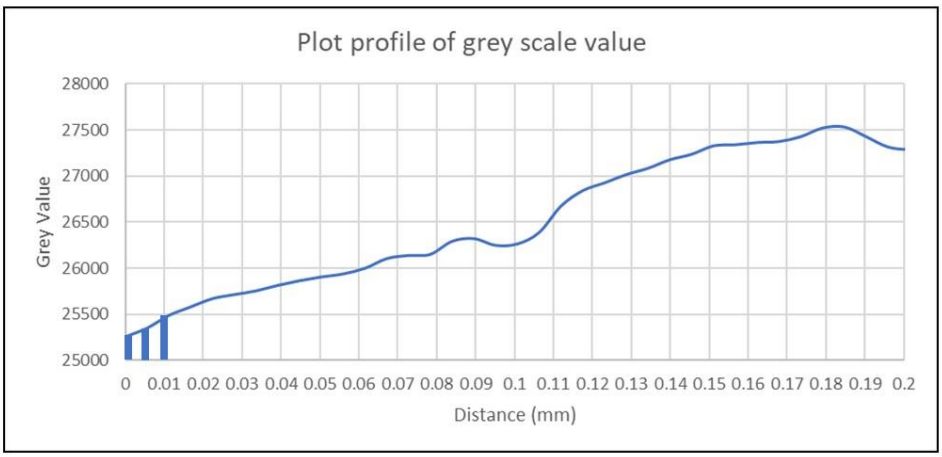

Figure 3.43: Plot profile of grey scale value for calculation of AUC

Blue stripes mark the area where the AUC is calculated for 10µm

Mean Delta Z for 0- 10µm(DZ10), 10-20µm(DZ20), 20-30µm(DZ30), 30 40µm(DZ40), 40-50µm(DZ50) were calculated by deducting mean AUC values at those depths from mean grey scale value measured at 150µm x depth of 10 µm. Grey scale value at 150µm was chosen because at this level, there was no demineralisation seen on all test sites.

Therefore,

DZ10 = (10µm x mean grey scale value at 150µm) – MeanAUC10 (illustration in Figure 3.44)

DZ20 = (10µm x mean grey scale value at 150µm) – MeanAUC20

DZ30 = (10µm x mean grey scale value at 150µm) – MeanAUC30

DZ40 = (10µm x mean grey scale value at 150µm) – MeanAUC40

DZ50 = (10µm x mean grey scale value at 150µm) – MeanAUC50

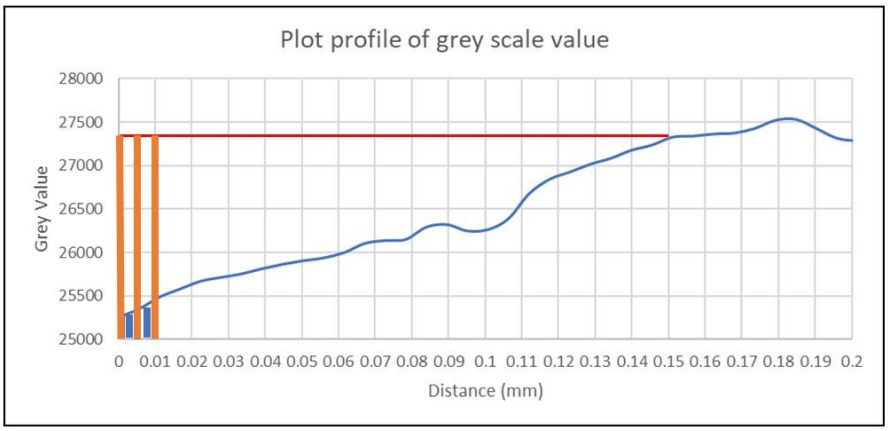

Figure 3.44: Plot profile of grey scale value for calculation of DZ10

DZ10 is calculated from total grey value which is area covered by red stripes minus mean AUC for 10µm

Total DeltaZ (TDZ) was then calculated from the mean DZ data collected. Hence, for every test site,

TDZ10= DZ10

TDZ20= DZ10 + DZ20

TDZ30= DZ10 + DZ20 + DZ30

TDZ 40= DZ10 + DZ20 + DZ30 + DZ40

TDZ50= DZ10 + DZ20 + DZ30 + DZ40 + DZ50 (illustration as shown in Figure 3.45)

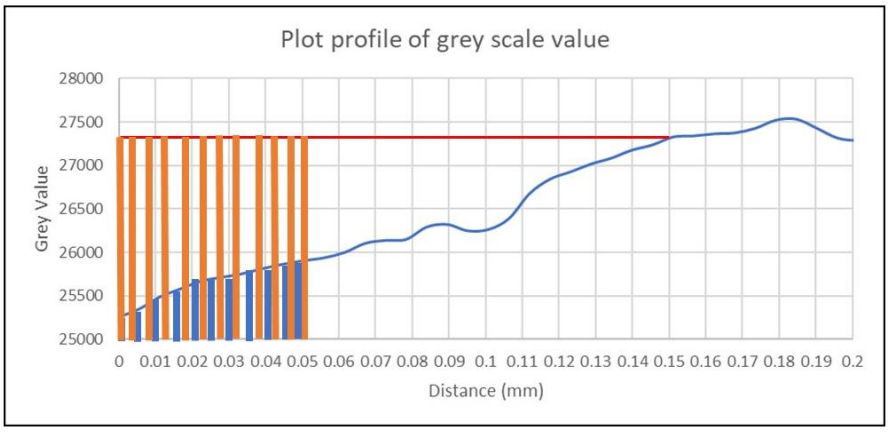

Figure 3.45: Plot profile of grey scale value for calculation of TDZ50

TDZ50 is total area marked by red stripes minus total AUC for 50µm

3.3 Integrated reflectivity from OCT

Test sites were dab dried and then air-dried for 30 seconds with an air blower. B and C-scans were taken of the test sites using the Thorlabs Swept Source OCT system (OCS 1300SS with the following parameters, X-2.2mm (1024 pixels), Y- 1.8mm (512 pixels), Z-2.01mm (512 pixels). Using Matlab, 100 frames from the middle of the region of interest (ROI) were taken using a ruler in the enface view (Figure 3.46).

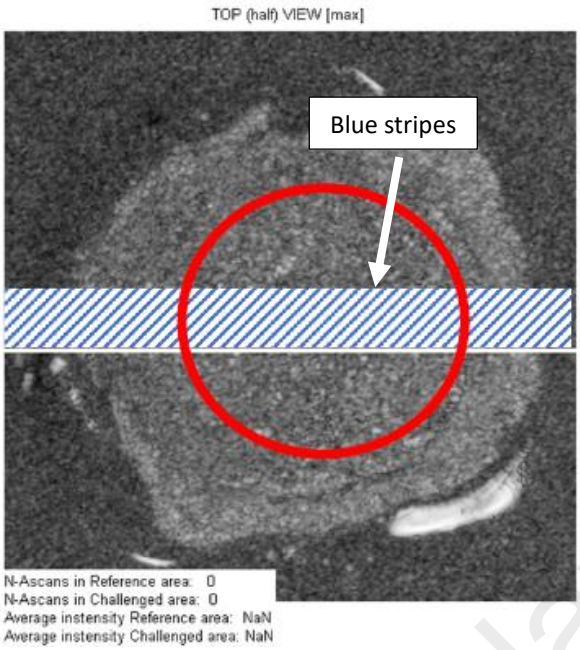

Figure 3.46: Top view of a test site generated using Matlab

Blue stripes in the red circle shows the ROI of which backscatter intensity is measured from on the test site.

From the information generated, backscatter intensity (integrated reflectivity, IR) of A-scans of each lesion were recorded and tabulated using 2D Analytics (Figure 3.47 and Figure 3.48). Parameters were determined and fixed for all samples (details in Table 3.6) except for the algorithm filter which was toggled to provide best results.

Table 3.6: Parameters used in measurement of IR

A-Scan Parameters		
ROI Settings	Width	300
Surface Finding Settings	Left Limit	1
	Top Limit	10
	Bottom Limit	300
	Right Limit	1024
Aligning Settings	Upper Margin	15
	Depth	300

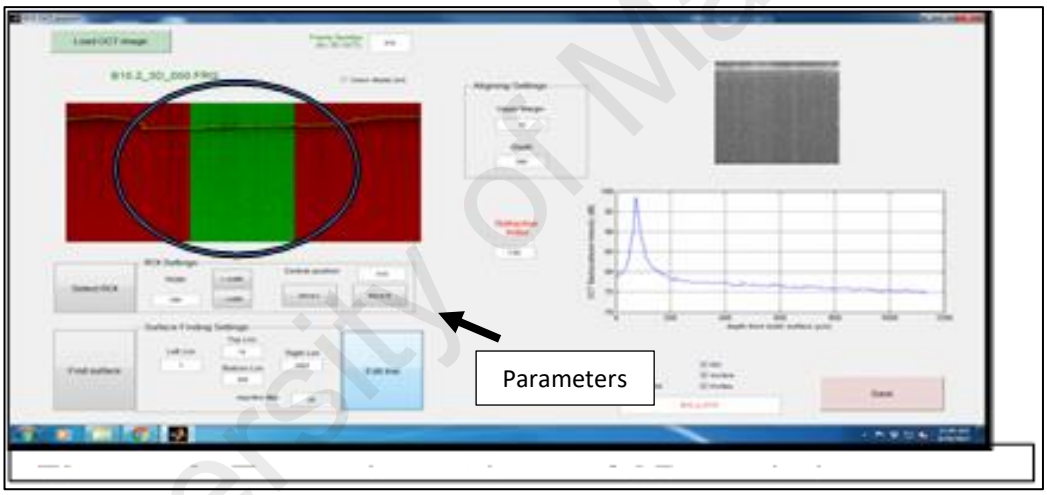

Figure 3.47: Screenshot of 2D analytics

The parameters can be set at the bottom left side of the screen in 2D analytics.

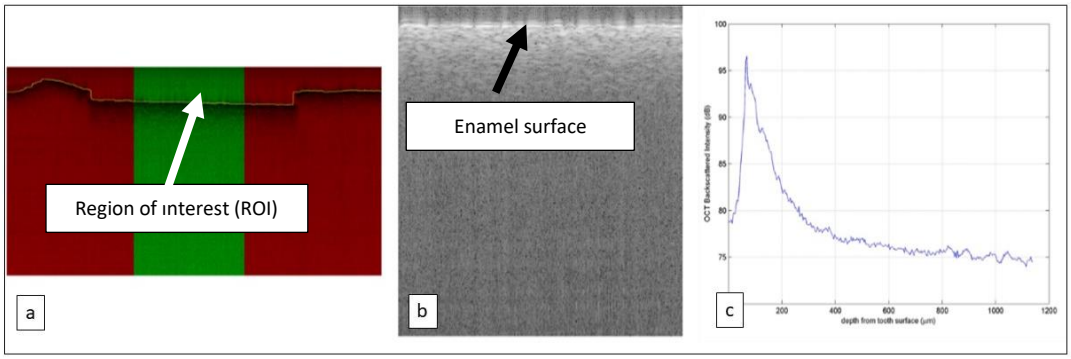

Figure 3.48: Details in screenshot of 2D analytics

(a) shows the ROI of lesion highlighted in green. (b) is the image of surface of enamel of ROI and (c) is the graph generated of backscattered intensity which is used to calculated integrated reflectivity.

3.3.1 Calculations

Value calculated from the descending slope of the area under curve (AUC) of A-scans represents the integrated reflectivity of each regions of interest (ROI) sites. Steps for calculation of AUC for each A-scans were repeated and mean values were used in the calculations. Total value of AUC for 5 A-scans (each scan are 10 frames apart) represents the total integrated reflectivity for each test site in this study. AUC of subsurface area between 0 to 10**µ**m in depth (IR10), 0 to 20µm (IR20), 0-30µm (IR30), 0-40µm (IR40) and 0 to 50µm (IR 50) were then calculated.

Therefore, the calculation for IR 10 to IR 50 are as follows:

i. Mean of A-scans at physical depth from test sites ranging from -14.5**µ**m to 300**µ**m was generated. Figure 3.49 is an example of the graph generated of the backscattered intensity for a sample test site.

ii. Area under curve (AUC) was calculated using the Trapezoidal Rule $(\frac{y_1+y_2}{2} \times (x_1 - x_2))$ for A-scans at depth of 0 to 51µm

iii. Steps were repeated for all A-scans of each sample to obtain a mean AUC for each test site.

iv. AUC values of 5 A-scans from each test site were summed up

v. IR10, IR 20, IR 30, IR 40, IR 50 were then calculated.

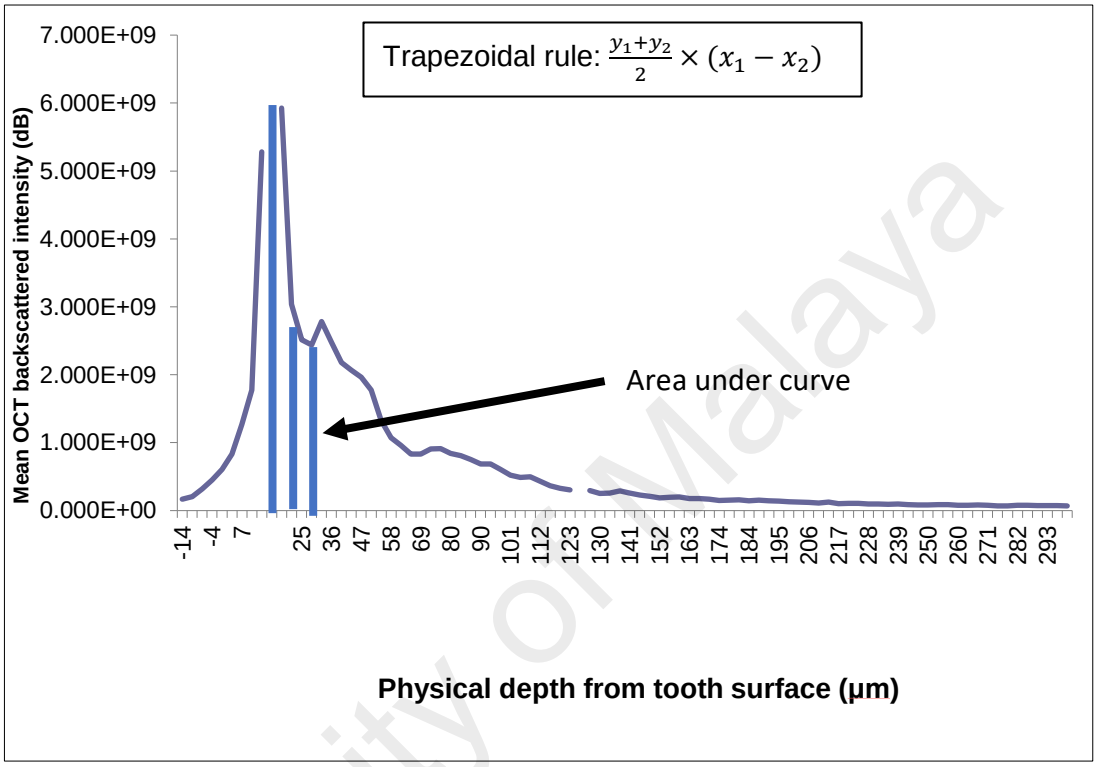

Figure 3.49: Graph showing backscatter intensity

Blue stripes indicated the area under curve (AUC) that is measured for measurement of integrated reflectivity.

3.4 Scanning Electron Microscope (SEM)

5 test sites per group (GS-G35) were chosen. The test sites were cut at the centre and perpendicular to the surface of the test sites using a low speed precision cutting instrument. Ultrasonication was done for 1 minute on the test sites to remove smear layer in order to have a clear visual of the surface. SEM magnification of 500x, 1000x, 2000x were taken using SEM (Quanta FEG 250, Holland) (Figure 3.50) with processing software, INCA, for qualitative analysis as well as to understand further the surface characteristics of each group tested. To qualitatively evaluate the SEM images obtained

from the test sites, characteristics namely loss of enamel surface, surface porosity and remineralised enamel surface were noted.

Figure 3.50: SEM Equipment

3.5 Qualitative assessment of Micro-CT Images

Images from Micro-CT taken of 8 test sites per group were examined. Observations were made to determine the presence of visible demineralisation of enamel surface, loss of surface enamel and presence of a surface layer.

3.6 Photographic Images

Photographic images were taken with a resolution of 12 megapixel to observe clinical appearance of 5 specimens (2 test sites per specimen) for each group. All test sites were air dried for 10 seconds before images were taken. The presence of white spot lesions was observed. The prominence of the white spot lesions, whether they were mild or very prominent were noted.

3.7 Stereo microscope Images

Images were taken using stereo microscope (Olympus SZX7-S4-Gel) (Figure 3.51) of 5 specimens (10 test sites) from each group at 1.25x and 5.6x. Cell D was the software

used to process these images. Varnish was removed from the surface and cleaned. It was then air dried for 10 seconds before the images were taken.

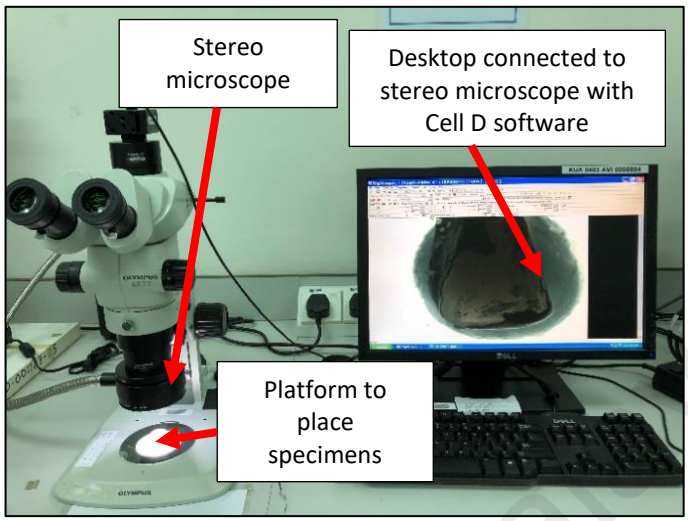

Figure 3.51: Stereo microscope equipment

Images for 1.25x were assessed based on whether the test sites were visible after varnish had been removed. The presence of a visible test site indicated the presence of a demineralised lesion. For the 5.6 x images, observations were made on whether there's visible striae on the surface of the test sites and whether a surface layer was visible on the enamel surface. The purpose of observing the presence of striae is to monitor the presence of demineralisation. As demineralisation progresses the presence of striae become more prominent. It is noted that the description of a surface layer here describes a smooth surface seen on the enamel surface which could either be an existing enamel surface or the formation of a surface layer after pH cycling.

3.8 Statistics

For Statistical Analysis, SPSS 25(IBM) was used to analyse the outcome parameter for Sorptivity, TDZ10 to TDZ50 and IR10 to IR 50. For test of normality, Shapiro-Wilk, Q-Q plots and Box-plots were used to test if the distribution was normal. Parametric tests were used as the data satisfied the criteria for normal distribution. Levene's test was used

to look at homogeneity of variances. One-way ANOVA was used to compare between groups and Post-hoc Tukey was employed if the distribution was normal and homogeneity of variance can be assumed. If homogeneity cannot be assumed, then, Post-Hoc Dunnett's T3 was used. To compare between 2 variables, Bivariate (Pearson) correlation was used. For correlation analysis, apart from looking at overall correlations and within individual groups, correlations were also explored within the following groupings:

i. GS-G7-G14- Results from test sites in GS, G7 and G14
ii. GS-G7-G14-G21- Results from test site in GS, G7, G14, G21
iii. G21-G2-G35- Results from test sites in G21, G28, G35
iv. GpHCycling- Results from test sites in G7, G14, G21, G28 G35

CHAPTER 4: RESULTS

4.1 Sorptivity

A total of 96 teeth (specimens) were selected and used in this study. The specimens were divided into 6 groups with 16 teeth per group. Each tooth was varnished leaving 2 round exposed enamel surface providing 32 test sites per group. All the groups except the control group (GS) underwent pH cycling for different duration of time per group- 7 days pH cycling group (G7) went through pH cycling for 7 days, 14 days pH cycling group (G14) for 14 days, 21 days pH cycling group (G21) for 21 days, 28 days pH cycling group (G28) for 28 days and 35 days pH cycling group (G35) for 35 days. The value of sorptivity of water is consequent of the equations described in section 3.1.2.5 (b). Figure 4.1 is a graph plotted with volume over area (V_{st}/A) as a function of square root of time, $\sqrt{t}$, for one of the test sites in G14 (C1.2). A linear relationship is observed and sorptivity of water for the test site was derived from the gradient of the line plot and used in subsequent statistical analysis.

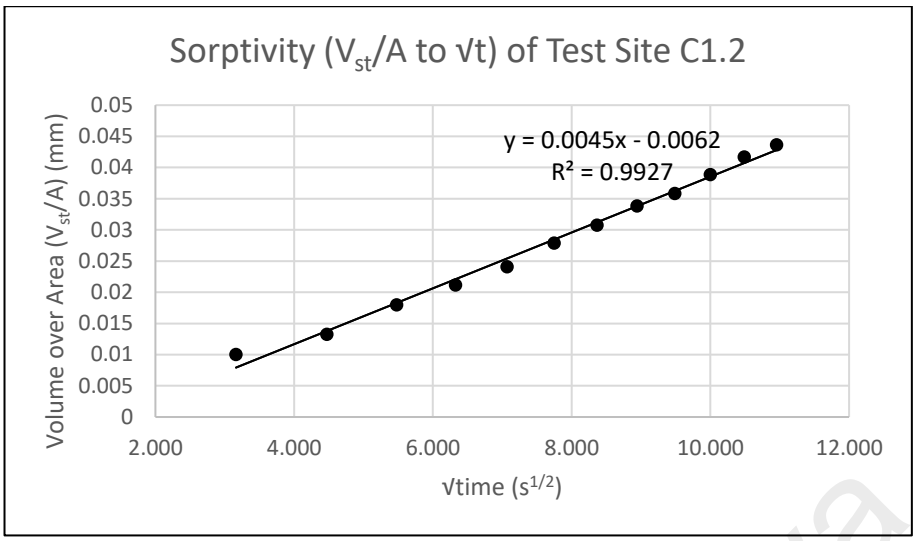

Figure 4.1: Example of a graph plotted with volume over area (V_{st}/A) as a function of square root of time, $\sqrt{t}$, for **a test site**

The gradient of V_{st}/A as function of $\sqrt{t}$, is the sorptivity for this test site. In this particular example, sorptivity is 0.0045, as seen in the equation in the graph.

Figure 4.2-4.7 provides an overview of the line plots of V_{st}/A as function of $\sqrt{t}$ for all the test sites from GS to G35 respectively. There is a general linear upward trend for all the test sites in the various groups, showing the linear relationship between V_{st}/A and $\sqrt{t}$ over the period of 2 minutes.

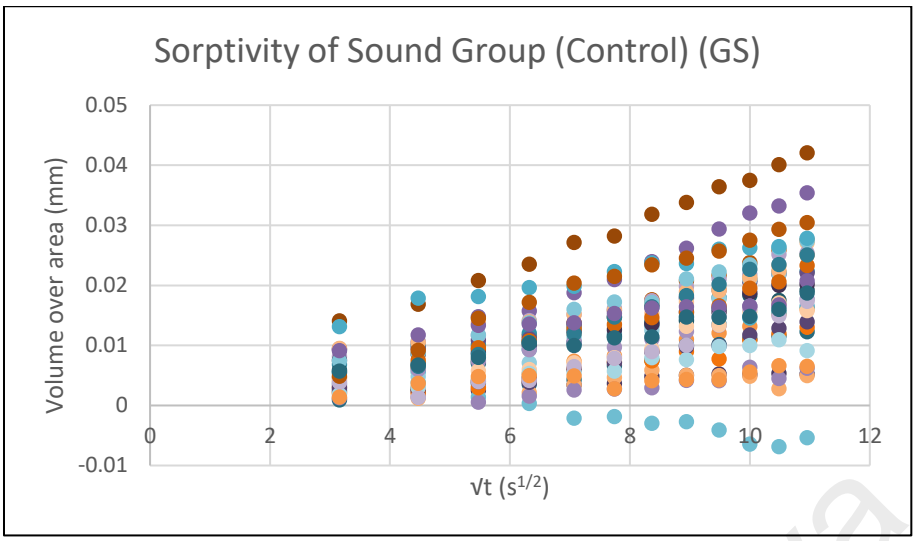

Figure 4.2: Graph of volume over area (V_{st}/A) as a function of square root of time, $\sqrt{t}$, for GS

There is a linear relationship between V_{st}/A and $\sqrt{t}$ *for many of the test sites. There are also test sites showing a negative linear relationship and some have static* V_{st}/A *over* $\sqrt{t}$ *. Hence, it is noticed that there is a rather wide range of sorptivity values for the test sites in GS. Undetected surface characteristics for instance the presence of fluorapatite and hypermineralised surface layer may cause sorptivity values to be low.*

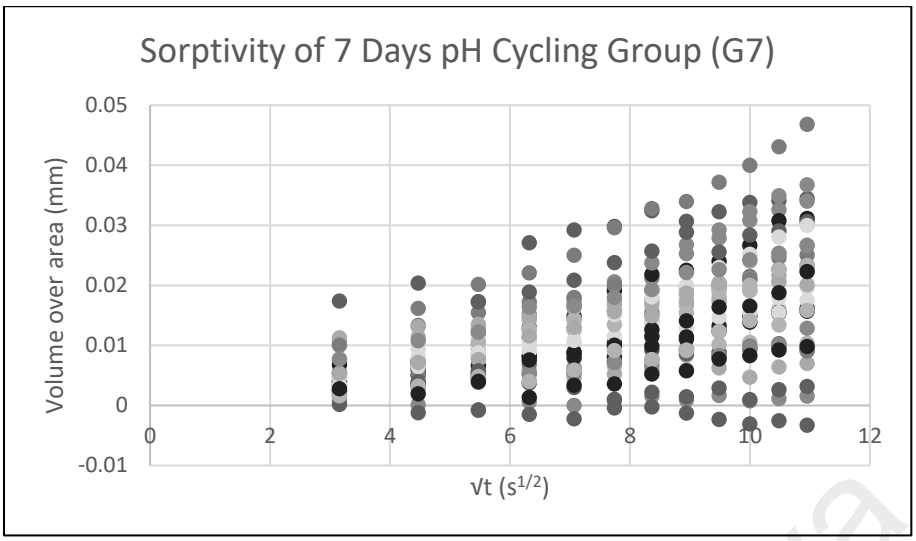

Figure 4.3: Graph of volume over area (V_{st}/A) as a function of square root of time, $\sqrt{t}$, for G7

Based on this graph, sorptivity values seem to vary for different test sites. Most of the test sites show positive linear relationship and some show static V_{st}/A over $\sqrt{t}$. There is no negative linear relationship observed. This could be due to the fact that enamel surfaces react at different speed to pH cycling process and the difference can be detected after 7 days of pH cycling by showing different sorptivity values.

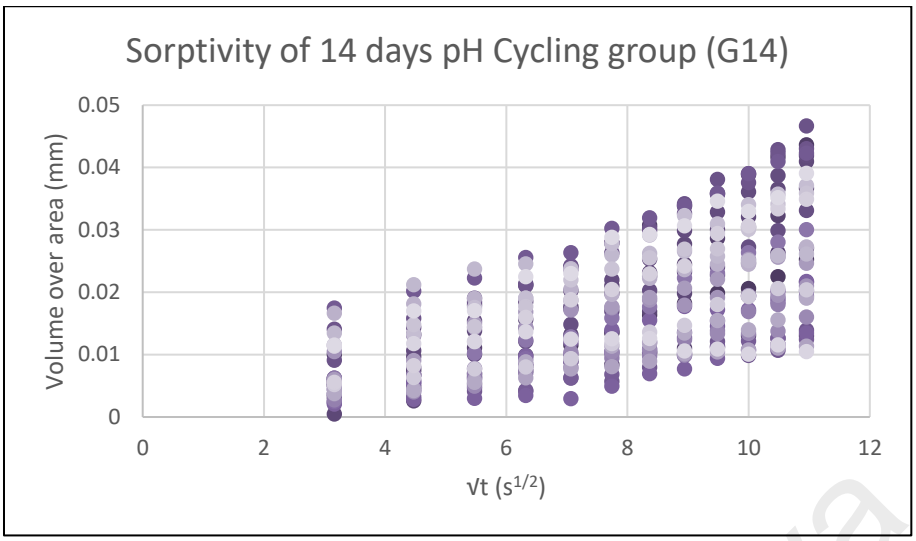

Figure 4.4: Graph of volume over area (V_{st}/A) as a function of square root of time, $\sqrt{t}$, for G14

Sorptivity values for test sites in G14 showed uniformly positive linear relationship between V_{st}/A and $\sqrt{t}$ with *steeper gradient than G7, indicating high sorptivity levels.*

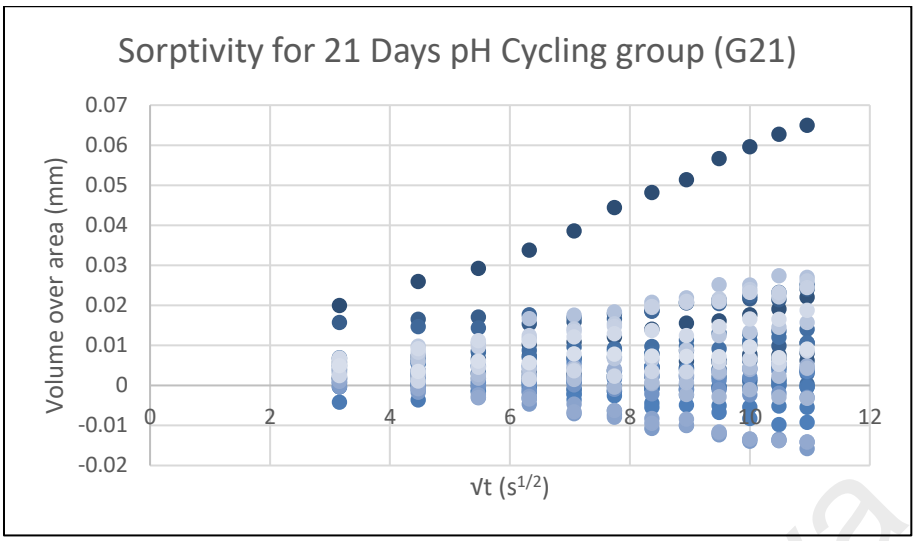

Figure 4.5: Graph of volume over area (V_{st}/A) as a function of square root of time, $\sqrt{t}$, for G21

V_{st}/A did not increase with increasing $\sqrt{t}$ *in all test sites in G21, except for one, indicating low sorptivity values. The one exception test site is seen to demonstrate a steep positive relationship between* V_{st}/A and $\sqrt{t}$. *Upon a closer observation, it was found that the varnish on this test site had debonded and therefore there was a leakage. Hence it was deemed an outliner and later removed and not included in the statistical analysis.*

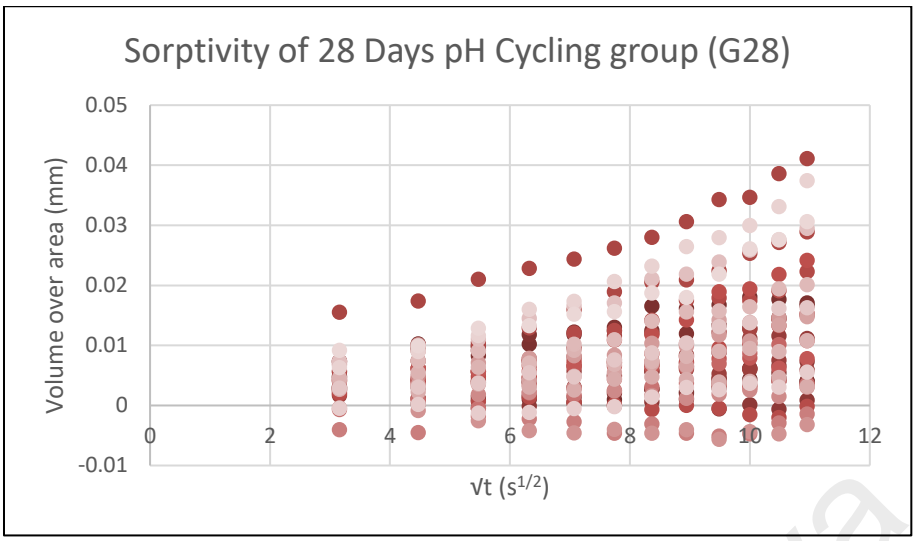

Figure 4.6: Graph of volume over area (V_{st}/A) as a function of square root of time, $\sqrt{t}$, for G28

Test sites in G28 seem to show a wide range of sorptivity values with most showing a positive linear relationship and some, a static V_{st}/A to $\sqrt{t}$.

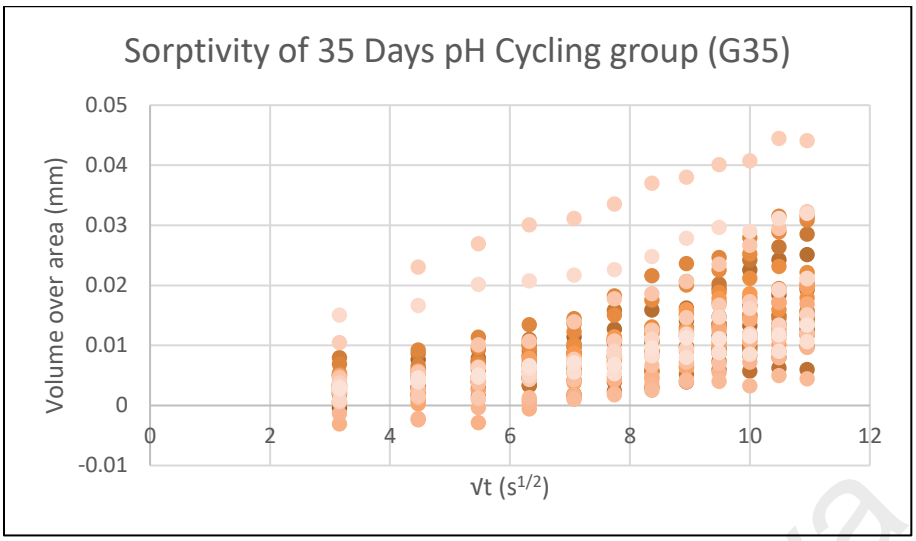

Figure 4.7: Graph of volume over area (V_{st}/A) as a function of square root of time, $\sqrt{t}$, for G35

Sorptivity values for test sites in G35 showed uniformly positive linear relationship between V_{st}/A and $\sqrt{t}$ with an increase overall sorptivity value compared with G28.

Statistical analysis was done using IBM SPSS Software Version 25 for all groups. Four outliers from GS and one from G21 were removed due to high discrepancy in data compared to the other test sites in the group. GS is the control group with sound enamel test sites. However, the OCT integrated reflectivity data for 4 test sites from GS were 10 times higher than the others in the group. Inspection of these test sites at the end of the study with a stereomicroscope revealed opaque area of demineralisation. It was concluded that there could have been pre-existing demineralisation that were undetected during the initial screening and storage of the samples in R.O. water may have caused these 'un-sound' test sites to demineralise further. This is because in its natural state in the environment, R.O water has a slightly acidic pH due to absorption of carbon dioxide from the atmosphere. The acidic pH can cause the demineralisation to occur. Therefore, the results from these test sites were removed. One of the test sites in G21 was removed as it was considered an outlier within its group during initial descriptive statistical analysis. In Figure 4.5, it is also clear that one of the test sites had a much higher sorptivity rate than

the rest in its group. Consequently, the number of test sites (n) used in statistical analysis for the various groups were 28, 32, 32, 31, 32 and 32 for GS to G35 respectively.

Figure 4.8 shows the mean Sorptivity of the various groups. Detailed values of means are provided in the descriptive portion of statistical analysis (Table 4.1). There is an increase in mean values from GS to G14 followed by a drop to G21. Thereafter, the mean sorptivity values increase at G28 and G35.

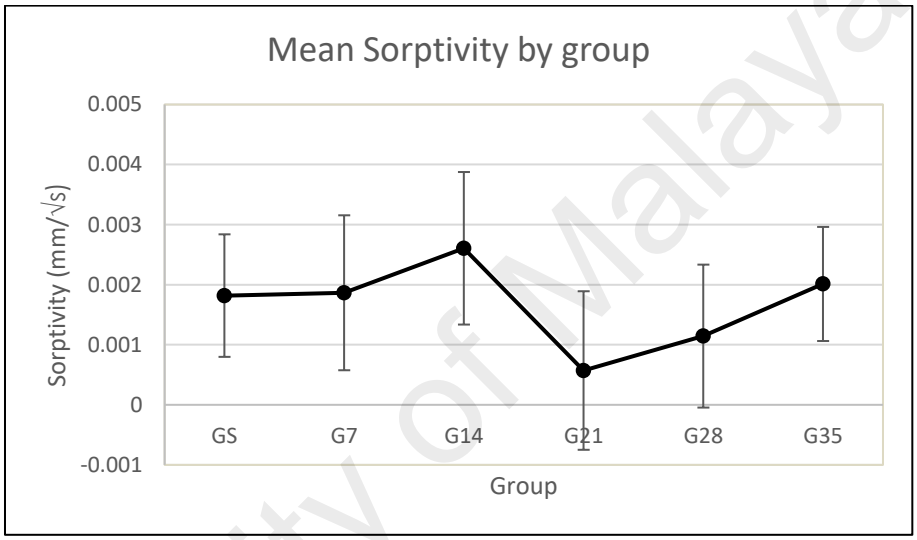

Figure 4.8: Graph of mean sorptivity by group

Mean sorptivity by group shows the progress of sorptivity with increasing state of demineralisation. There is an increase from GS to G14 with a drop in G21 to a level below that of GS. Thereafter, mean sorptivity increased again with increasing demineralisation.

.

Table 4.1: Descriptive statistics of sorptivity by groups

Groups	Mean	Standard deviation	95% CI (lower bound)	95% CI (upper bound)	Range	Standard Error
GS	0.00171	0.00102	0.00132	0.00211	0.00510	0.00019
G7	0.00187	0.00129	0.00140	0.00233	0.00480	0.00023
G14	0.00261	0.00127	0.00215	0.00307	0.00490	0.00023
G21	0.00039	0.00132	-0.00009	0.00088	0.00520	0.00024
G28	0.00114	0.00119	0.00072	0.00157	0.00390	0.00021
G35	0.00201	0.00095	0.00167	0.00236	0.00350	0.00017

For test of normality, Shapiro-Wilk Test of Normality was used (typically used for n<50) and results show normal distribution for all groups (p-value of more than 0.05). Box plot shows a few outliers in GS and G21. However, results from Shapiro-Wilk test of normality and QQ plot show normal distribution. It was therefore concluded that the distribution of the data was normal and parametric tests were used for further investigations. Levene's test of homogeneity of variance shows the p-value of 0.188 which is more than 0.05 and thus, homogeneity of variance can be assumed. One-way ANOVA shows a p-value of less than 0.05 ($p=6.33x10^{-11}$). A conclusion can be made based on this outcome that there is at least one pair in the groups showing significant difference. Post-hoc Tukey test was further performed to determine where the significant difference lies. Statistically significant differences were detected between GS with G14 (p= 0.046) and G21 (p= 0.00043), G7 with G21 (p=0.000027), G14 with G21 ($p=6.75x10^{-11}$) and G28 (p=0.000026), G35 with G21(p=0.000003) and G28 (p=0.043). Details of statistical analysis can be found in Appendix B.

As mentioned above, mean sorptivity for GS is 0.00171, G7 is 0.00187, G14 is 0.00261, G21 is 0.000394, G28 is 0.00144 and G35 is 0.00201. Sorptivity of GS is significantly different from G14 whereby sorptivity is 1.5 times more in G14. Sorptivity of GS is also significantly different from G21 whereby sorptivity for GS is 3 times more

than G21. When comparing between groups that had undergone pH cycling, mean sorptivity of the maximum seen in G14 is significantly higher by 6.6 times than the minimum sorptivity value seen in G21. G7 is also significantly higher than G21 by 4.7 times and G35 is 5 times higher than G21. Details of the statistical analysis can be found in Appendix B.

4.2 Total Delta Z (TDZ)

Image analysis of the Micro-CT scans taken for the test sites were done using the Plot Profile function in ImageJ. Below is an example of an image taken with Micro-CT (Figure 4.9) of a test site. Plot profile was configured to plot the grey value from the enamel surface to 200 microns subsurface (white line in Figure 4.9) and a graph is generated as shown in Figure 4.10 for the computation of AUC. Each test site had 9 randomly chosen points/locations and mean AUC was computed.

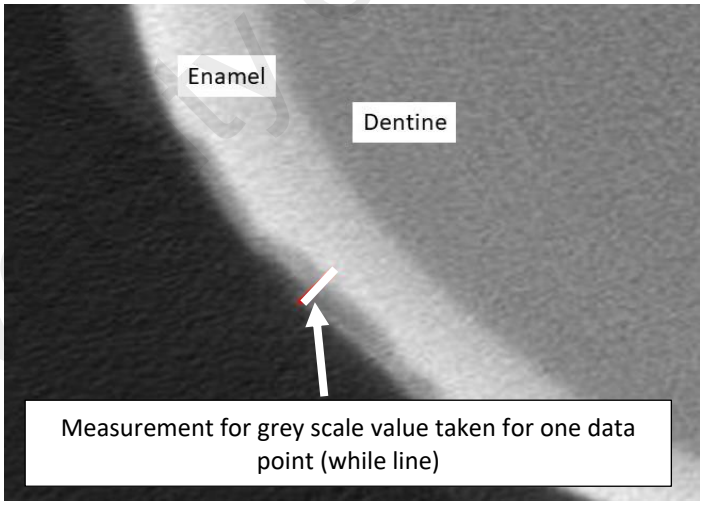

Figure 4.9: Image taken with Micro-CT (Test site E8.2 from G28)

Plot profile is used to measure grey scale value at each chosen point/location as seen in the image above where the white line is drawn.

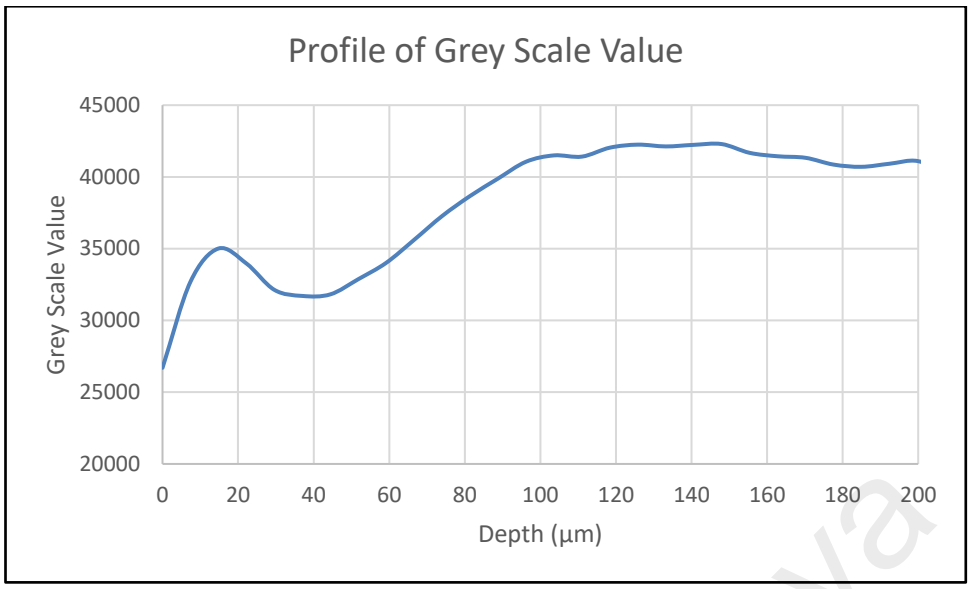

Figure 4.10: Profile of grey scale value at 1 location of test site E8.2 (G28)

The graph above shows the profile of grey scale value of a particular chosen point from which area under curve (AUC) is measured.

Total delta Z (TDZ) for 10 µm (TDZ10), 20 µm (TDZ20), 30 µm (TDZ30), 40 µm (TDZ40) and 50 µm (TDZ50) depth from surface for 8 test sites (4 teeth) per group were then calculated (as described in Section 4.2.1). Table 4.2 and Figure 4.11 below shows mean results for TDZ by thickness of enamel surface and pH cycling groups. Mean TDZ10 by group in Figure 4.12 shows an incline from GS to G14 followed by a decrease to G21 and then again, an incline from G21 to G35.

Mean Total Delta Z for TDZ20, TDZ30, TDZ40 and TDZ50 (Figure 4.13 to Figure 4.16) shows a general incline from GS to 35 with a slight deep at G21 as well though less obvious as the thickness increases. Negative values are seen in GS for all groups except TDZ10 due to beam hardening which is typically seen at 20 to 50 microns thickness. Beam hardening causes the grey scale values at 20 to 50 microns to be higher (when there is no demineralisation) than at 150 microns. Because of the higher levels, when the value of grey scale at 150 microns is used as a reference point, calculations show negative

values for GS at 20 to 50 microns. This phenomenon does not affect the results because beam hardening is an effect seen in all the images taken with Micro-CT.

Table 4.2 : Mean total Delta Z by group

	GS		G7		G14		G21		G28		G35	
	Mean	SD	Mean	SD	Mean	SD	Mean	SD	Mean	SD	Mean	SD
TDZ10	50.21	11.65	79.90	10.50	89.46	7.74	44.34	30.42	81.78	10.89	88.53	16.72
TDZ20	-3.60	37.98	149.12	30.40	179.39	47.37	79.86	72.26	173.31	39.12	208.30	45.93
TDZ30	-50.75	48.88	159.49	45.09	190.32	73.38	85.04	82.50	197.80	60.63	250.40	60.04
TDZ40	-92.12	56.31	155.94	56.40	192.60	94.67	75.98	81.91	215.05	86.62	283.40	76.77
TDZ50	-122.94	60.06	143.40	64.12	185.59	109.46	63.68	79.64	220.25	111.89	299.34	90.46

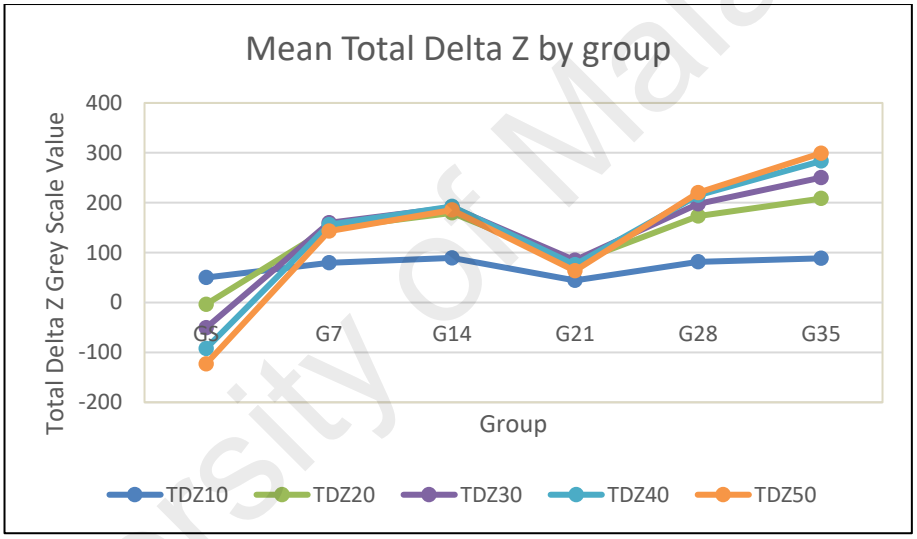

Figure 4.11: Graph of mean Total Delta Z (TDZ) by group

Mean TDZ10 does not show much difference between groups compared to TDZ20 to TDZ50. The difference in mean TDZ by group become more prominent as the surface layer becomes thicker. This is to be expected because as the thickness increases, more data is captured and the difference in grey value increases.

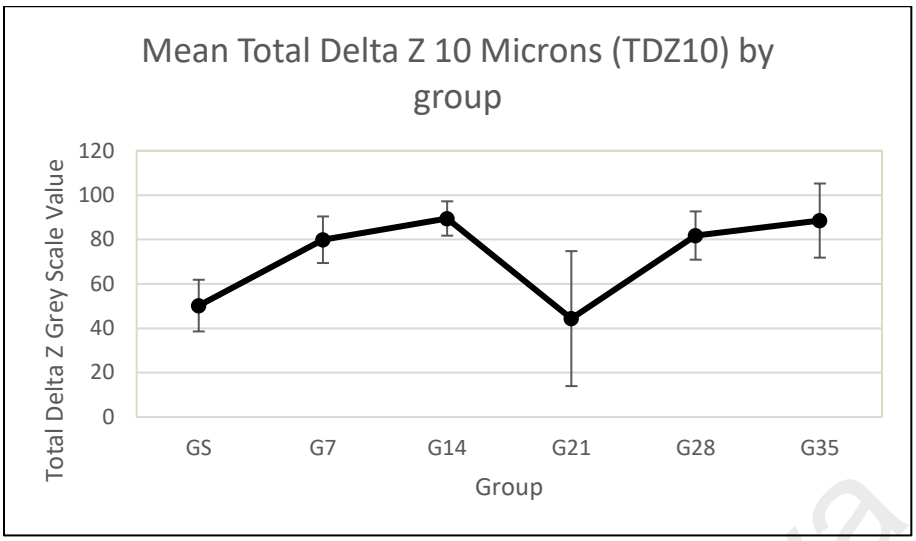

Figure 4.12: Graph of mean TDZ10 by group

In the graph above, mean TDZ 10 by group shows an increase from GS to G14 followed by a drop in G21 which is the lowest point in the graph. Thereafter, an increase from G21 to G35 is seen. This pattern is also seen in mean sorptivity values by group.

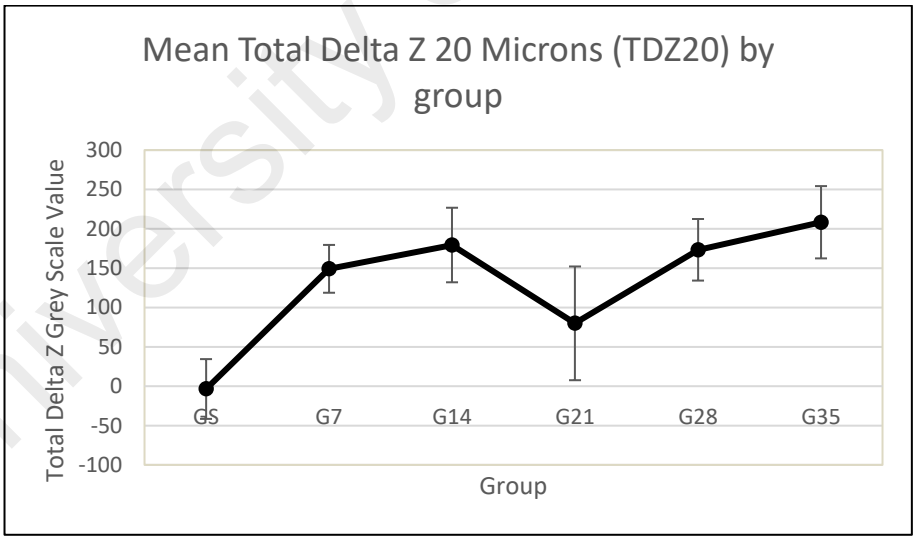

Figure 4.13: Mean TDZ20 by group

Mean TDZ20 by group shows a similar trend as mean sorptivity by group. There is an increase from GS to G14 followed by a drop in G21 and thereafter, an increase to G35. In general, there is an upward trend from GS to G35.

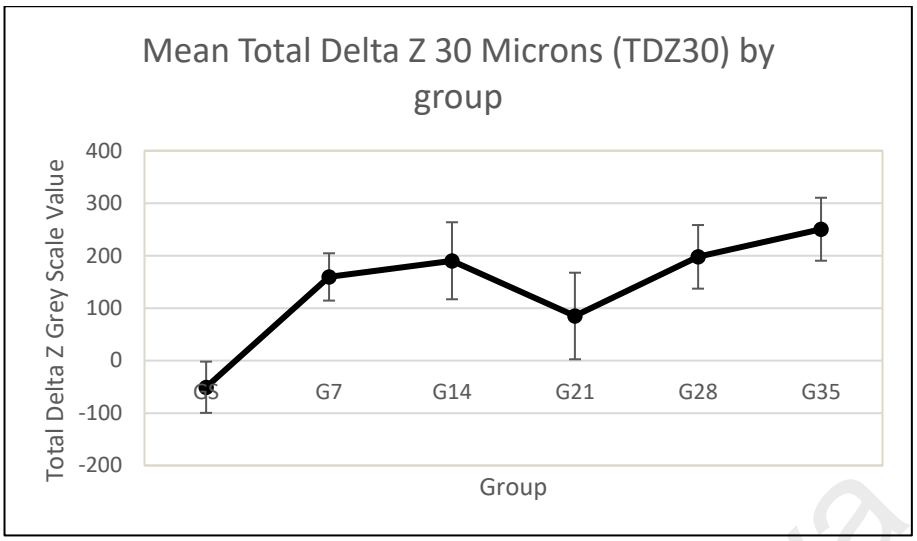

Figure 4.14: Mean TDZ30 by group

Mean TDZ30 by group shows an uptrend. There is an increase from GS to G14 followed by a slight drop in G21 and then an increase again to G35. It is noted that G21 has a higher mean TDZ value than GS showing a reduction in mineral density at this enamel surface thickness.

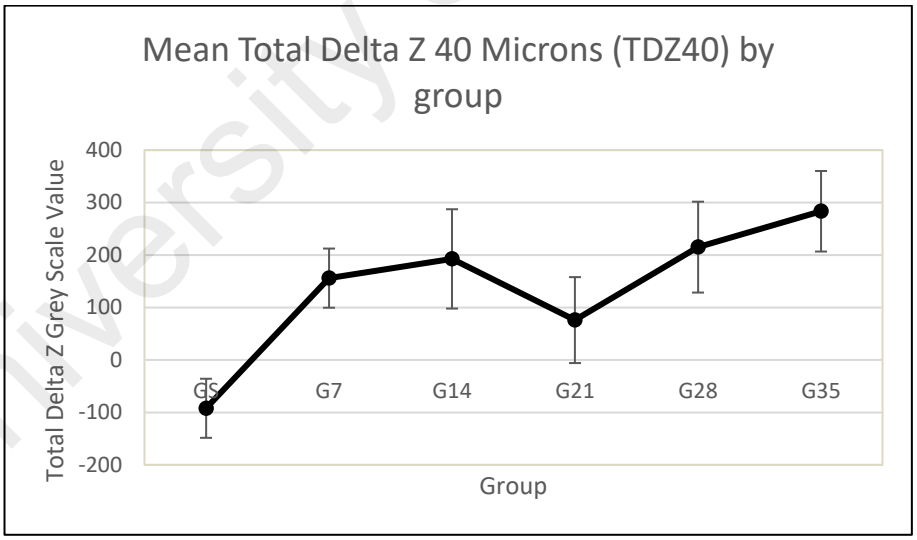

Figure 4.15: Mean TDZ40 by group

Mean TDZ40 by group shows a steeper uptrend than TDZ 30. There is an increase from GS to G14 followed by a slight drop in G21 and then an increase to G35. G7 to G35 have significantly higher mean TDZ value than GS showing loss of mineral density.

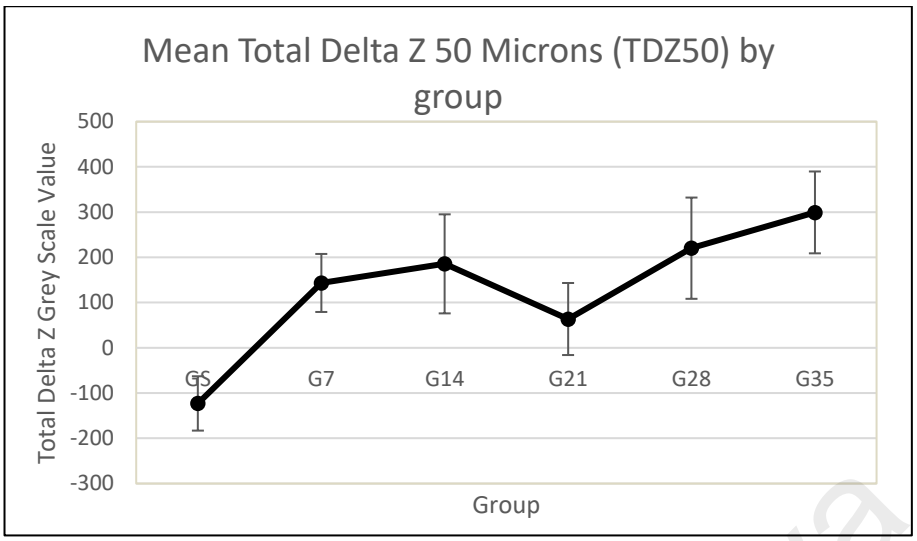

Figure 4.16: Mean TDZ 50 by group

Mean TDZ50 by group shows the steepest uptrend compared to TDZ10 to TDZ40. There is an increase from GS to G14 followed by a slight drop in G21 and then an increase to G35. G7 to G35 have significantly higher mean TDZ value than GS showing loss of mineral density.

Statistical analysis was done on results for Total Delta Z (TDZ) of different enamel surface thickness namely TDZ10, TDZ20, TDZ30, TDZ40, TDZ50 using IBM SSPS Version 25 Software for all the pH cycling groups including the control group that did not undergo any pH cycling.

4.2.1 TDZ10

Shapiro-Wilk Test of Normality was used (typically used for n<50) and results show normal distribution for all groups (p-value of more than 0.05). Based on the results from Shapiro-Wilk test of normality, Q-Q plots and box plot, it was concluded that the distribution of the data is normal. Levene's test of homogeneity of variance shows the p-value of 0.000001 which is less than 0.05 and thus, homogeneity of variance cannot be assumed. Parametric tests and post-hoc Dunnett's T3 were used for further investigations. One-way ANOVA shows a p-value of 4.31×10^{-7} which is less than 0.05 and therefore

there is statistically significant difference between groups. Post-hoc Dunnett's T3 shows significant differences between GS with G7(p=0.001), G14(p=0.000052), G28 (p=0.001), G35 (p=0.002) as well as G14 with G21 (p= 0.041). There is no significant difference detected between GS and G21. Bivariate (Pearson) Correlations for TDZ10 and sorptivity show significant correlation with Pearson Correlation coefficient of 0.461 (p=0.001). There are no correlations detected with sorptivity within groups as well as when GS, G7, G14 (GS-G7-G14) were groups together. However, when GS, G7, G14 and G21 (GS-G7-G14-G21) were grouped together, there is significant correlation with sorptivity detected with Pearson correlation coefficient of 0.535 (p=0.002). Significant correlation is detected as well when G21, G28 and G35 (G21-G28-G35) were grouped together with Pearson correlation coefficient of 0.606 (p= 0.002). Finally, when G7, G14, G21, G28 and G35 (GpHCycling) were grouped together, there is significant correlation detected with Pearson correlation coefficient of 0.548 (p=0.000254).

4.2.2 TDZ20

Shapiro-Wilk Test of Normality was used (typically used for n<50) and results show normal distribution for all groups (p-value of more than 0.05). Based on the results from Shapiro-Wilk test of normality, QQ plot and box plot, it was concluded that the distribution of the data is normal. Levene's test of homogeneity of variance shows the p-value of 0.019 which is less than 0.05 and thus, homogeneity of variance cannot be assumed. Parametric tests and post-hoc Dunnett's T3 were used for further investigations. One-way ANOVA shows a p-value of 8.06×10^{-11} which is less than 0.05 and therefore there is statistically significant difference between groups. Post-hoc Dunnett's T3 shows significant differences between GS and G7(p=0.000008), G14(p=0.000013), G28 (p=0.000004) as well as G35 (p=0.000002). There is no significant difference detected between GS and G21 but significant difference is also detected for G21 with G35 (p=0.015). Bivariate (Pearson) Correlations for TDZ20 and sorptivity show no significant

correlations. There are no correlations detected with sorptivity within the pH cycling groups as well as with GS-G7-G14 and GS-G7-G14-G21. Significant moderate correlation is found in G21-G28-G35 group with Pearson correlation coefficient of 0.585 (p= 0.003). In GpHCycling group, there is a weak correlation detected as well with Pearson correlation coefficient of 0.396 (p=0.011).

4.2.3 TDZ30

Shapiro-Wilk Test of Normality was used (typically used for n<50) and results show normal distribution for all groups (p-value of more than 0.05). Based on the results from Shapiro-Wilk test of normality, QQ plot and box plot, it was concluded that the distribution of the data is normal. Levene's test of homogeneity of variance shows the p-value of 0.266 which is more than 0.05 and thus, homogeneity of variance can be assumed. Parametric tests and post-hoc Tukey were used for further investigations. One-way ANOVA shows a p-value of $4.1x10^{-11}$ which is less than 0.05 and therefore there is statistically significant difference between groups. Post-hoc Tukey shows significant differences between GS and all groups; G7($p=6.42x10^{-7}$), G14($p=2.63x10^{-8}$), G21 (p=0.001), G28 ($p=1.22x10^{-8}$), G35 ($p=6.63x10^{-11}$). Significant differences are also detected for G21 with G14 (p=0.021), G28 (p= 0.011) and G35 (p=0.000068). Bivariate (Pearson) Correlations for TDZ30 and sorptivity show no significant correlations. When compared within the groups, significant correlation is detected in G35 with Pearson correlations coefficient of 0.762 (p=0.028). GS-G7-G14 and GS-G7-G14-G21 did not show any significant correlations with sorptivity. Significant correlation is found in G21-G28-G35 group with Pearson correlation coefficient of 0.596 (p= 0.002). In GpHCycling group, there is also weak correlation detected with Pearson correlation coefficient 0.347 (p=0.028).

4.2.4 TDZ40

Shapiro-Wilk Test of Normality was used (typically used for n<50) and results show normal distribution for all groups (p-value of more than 0.05). Based on the results from Shapiro-Wilk test of normality, QQ plot and box plot, it was concluded that the distribution of the data is normal. Levene's test of homogeneity of variance shows the p-value of 0.598 which is more than 0.05 and thus, homogeneity of variance can be assumed. Parametric tests and post-hoc Tukey were used for further investigations. One-way ANOVA shows a p-value of $3.19x10^{-11}$ which is less than 0.05 and therefore there is statistically significant difference between groups. Post-hoc Tukey shows significant differences between GS and all groups; G7(p=0.000001), G14($p=5.53x10^{-8}$), G21 (p=0.001), G28 ($p=8.36x10^{-9}$), G35 ($p=3.33x10^{-11}$). Significant differences are also detected for G7 and G35 (p=0.022), G21 with G14 (p=0.044), G28 (p= 0.010) and G35 (p=0.000041). Bivariate (Pearson) Correlations for TDZ40 and sorptivity show no significant correlations. When compared within the groups, significant correlation is detected in G35 with Pearson correlations coefficient of 0.816 (p=0.013). GS-G7-G14 group and GS-G7-G14-G21 did not show any significant correlations with sorptivity. Significant correlation is found in G21-G28-G35 group with Pearson correlation coefficient of 0.616 (p= 0.001). In GpHCycling group, there is also weak correlation detected with Pearson correlation coefficient of 0.331 (p=0.037).

4.2.5 TDZ50

Shapiro-Wilk Test of Normality was used (typically used for n<50) and results show normal distribution for all groups (p-value of more than 0.05). Based on the results from Shapiro-Wilk test of normality, QQ plot and box plot, it was concluded that the distribution of the data is normal. Levene's test of homogeneity of variance shows the p-value of 0.617 which is more than 0.05 and thus, homogeneity of variance can be assumed. Parametric tests and post-hoc Tukey were used for further investigations. One-

way ANOVA shows a p-value of $7.73x10^{-11}$ which is less than 0.05 and therefore there is statistically significant difference between groups. Post-hoc Tukey shows significant differences between GS and all groups; G7(p=0.000005), G14($p=2.19x10^{-7}$), G21 (p= 0.002), G28 ($p=1.69x10^{-8}$), G35 ($p=6.17x10^{-11}$). Significant differences are also detected for G7 and G35 (p= 0.012), G21 with G28 (p= 0.012) and G35 (p=0.000049). Bivariate (Pearson) Correlations for TDZ50 and sorptivity show no significant correlations. When compared within the groups, significant correlation is detected in G35 with Pearson correlation coefficient of 0.830 (p=0.011). GS-G7-G14 group and GS-G7-G14-G21 did not show any significant correlations with Sorptivity. Significant correlation is found in G21-G28-G35 group with Pearson correlation coefficient of 0.63 (p= 0.001). In GpHCycling group, there is also weak correlation detected with Pearson correlation coefficient of 0.323 (p=0.042).

4.2.6 Correlations

TDZ10 is the only layer that shows correlations with sorptivity when all test site measurements were used. This reflects that Sorptivity is closely related to a thin layer on the surface. Correlations with sorptivity are detected in pHCycling and G21-G28-G35 groups for TDZ10 to TDZ50 while no correlation is detected in GS-G7-G14 groups.

Details of the statistical analysis can be found in Appendix C.

4.3 Integrated reflectivity (IR)

Analysis done on the result for Integrated Reflectivity (IR) at 0-10µm (IR10), 0-21µm (IR20), 0-29µm (IR30), 0-40µm (IR40) and 0-51µm (IR50). Overall mean IR by surface layer thickness and pH cycling group is tabulated in Table 4.3. Figure 4.17 shows mean A-scans for integrated reflectivity (AUC) for all groups from -3.6microns to 123 microns. Overall, at a glance, most of the groups peaked and levelled out at about the same depth except for GS which seem to drop faster than the other groups. This was to be expected

as GS is the control group and therefore shows less intensity at all levels as compared to the other groups which are demineralised. Images with high specular reflection that cause skewing of results were removed. Of the 32 test site images per group that were taken, the total number of images taken and measured were 21 for GS, 13 for G7, 20 for G14, 18 for G21, 27 for G28 and 26 for G35.

Table 4.3: Mean integrated reflectivity by group

	GS		G7		G14	
	Mean	SD	Mean	SD	Mean	SD
IR10	9.29×10^{9}	4.27×10^{9}	9.94×10^{9}	3.38×10^{9}	1.31×10^{10}	4.43×10^{9}
IR20	3.91×10^{10}	1.71×10^{10}	4.42×10^{10}	9.77×10^{9}	5.42×10^{10}	9.95×10^{9}
IR30	4.58×10^{10}	1.89×10^{10}	7.16×10^{10}	1.07×10^{10}	7.73×10^{10}	1.10×10^{10}
IR40	4.99×10^{10}	1.99×10^{10}	9.52×10^{10}	1.38×10^{10}	9.59×10^{10}	1.52×10^{10}
IR50	5.25×10^{10}	2.03×10^{10}	1.06×10^{11}	1.60×10^{10}	1.05×10^{11}	1.83×10^{10}
	G21		G28		G35	
	Mean	SD	Mean	SD	Mean	SD
IR10	9.15×10^{9}	2.63×10^{9}	9.13×10^{9}	3.32×10^{9}	1.03×10^{10}	5.07×10^{9}
IR20	4.57×10^{10}	1.02×10^{10}	4.25×10^{10}	1.45×10^{10}	4.30×10^{10}	1.80×10^{10}
IR30	6.96×10^{10}	1.30×10^{10}	6.89×10^{10}	1.93×10^{10}	6.53×10^{10}	2.41×10^{10}
IR40	9.21×10^{10}	1.69×10^{10}	9.34×10^{10}	2.42×10^{10}	8.60×10^{10}	3.00×10^{10}
IR50	1.03×10^{11}	1.91×10^{10}	1.06×10^{11}	2.74×10^{10}	9.72×10^{10}	3.32×10^{10}

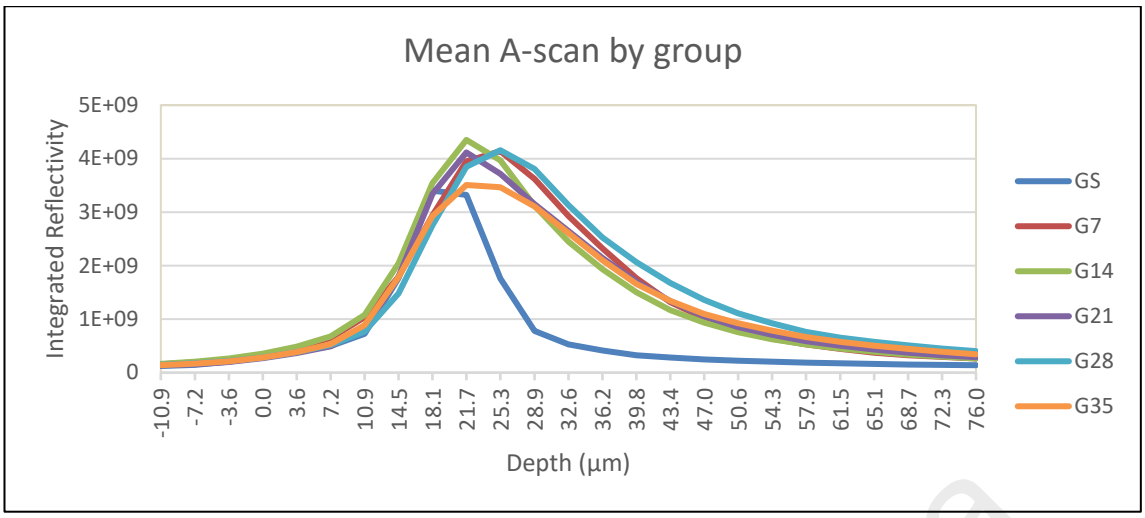

Figure 4.17: Mean A-scan by group

The slopes in this graph of Mean-A scan by group show a similar trend in all groups except for GS. GS has a steeper drop after the highest point which is also the lowest value compared to the other groups. This is expected as GS does not have surface demineralisation and therefore has lower integrated reflectivity values because sound teeth do not reflect near infra-red light as much as demineralised surface.

Mean IR 10 (Figure 4.18) shows a steady increase from GS to G14 and a decrease at G21 and G28 followed by a slight increase in G35. For IR 20 (Figure 4.19), there is a sharp increase from GS to G14 followed by a decline from G14 to G35. There is a significant increase seen for mean of GS to the other groups for IR30, IR40 and IR 50 (Figure 4.20- 4.22) while the mean of G7, G14, G21, G28 and G35 are quite similar one to the other and are not significantly different.

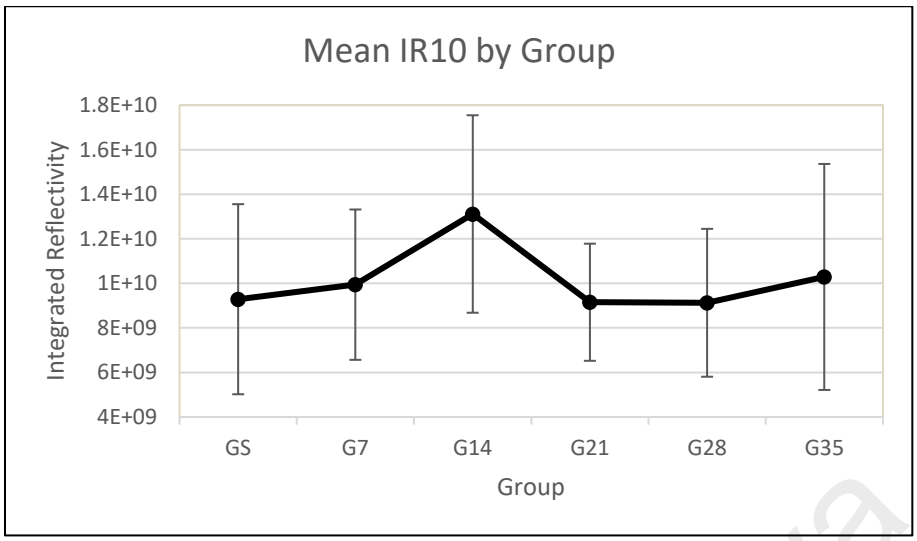

Figure 4.18: Mean IR10 by group

This graph of mean IR10 by group shows an increase from GS to G14 followed by a drop in G21 and then an increase again to G35. This trend is similar with mean sorptivity by group.

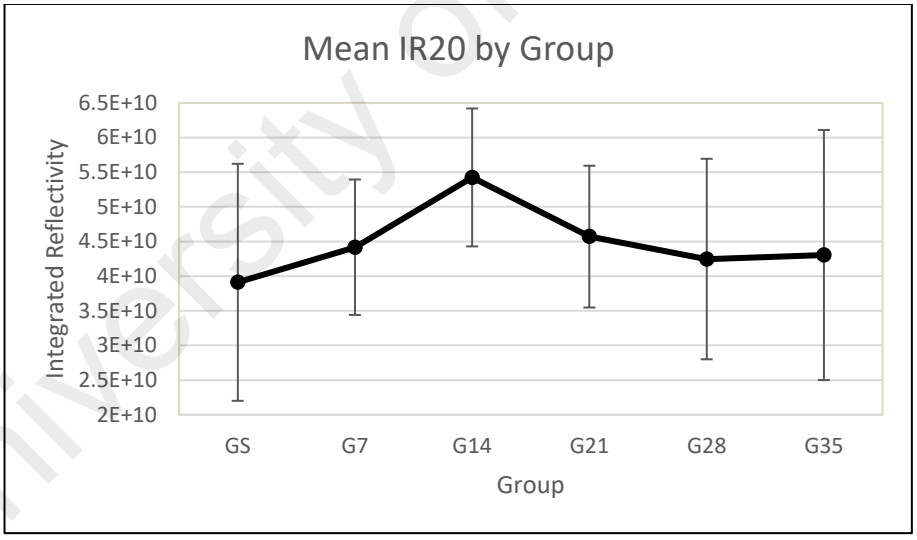

Figure 4.19: Mean IR20 by group

Mean IR20 by group shows an increase from GS to G14 and then decreasing from G14 to G35. The increase from GS to G14 and then the drop at G21 is also seen in mean sorptivity by group.

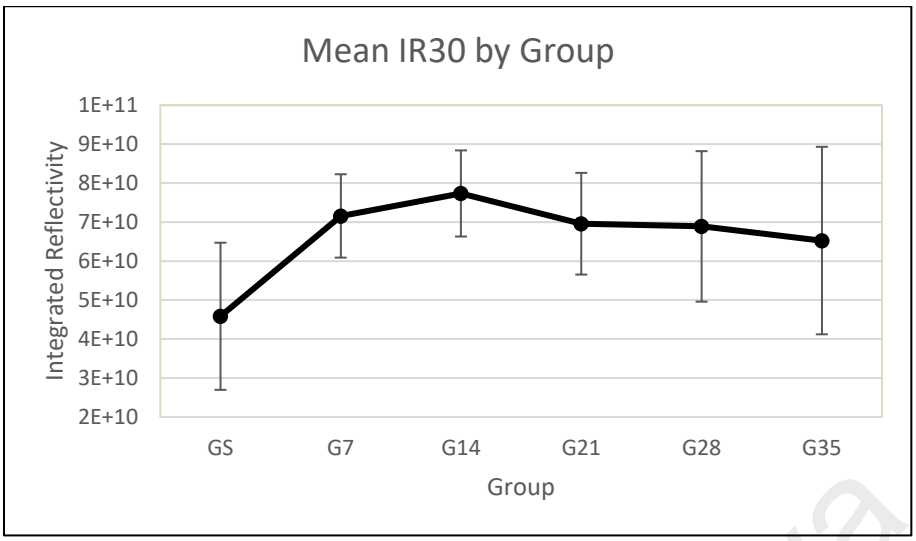

Figure 4.20: Mean IR30 by group

Mean IR30 by group shows a sharp increase from GS to G7. From G7 to G35, mean IR are almost similar one to the other. There is a similar uptrend from GS to G14 for mean IR30 by group with mean sorptivity by group.

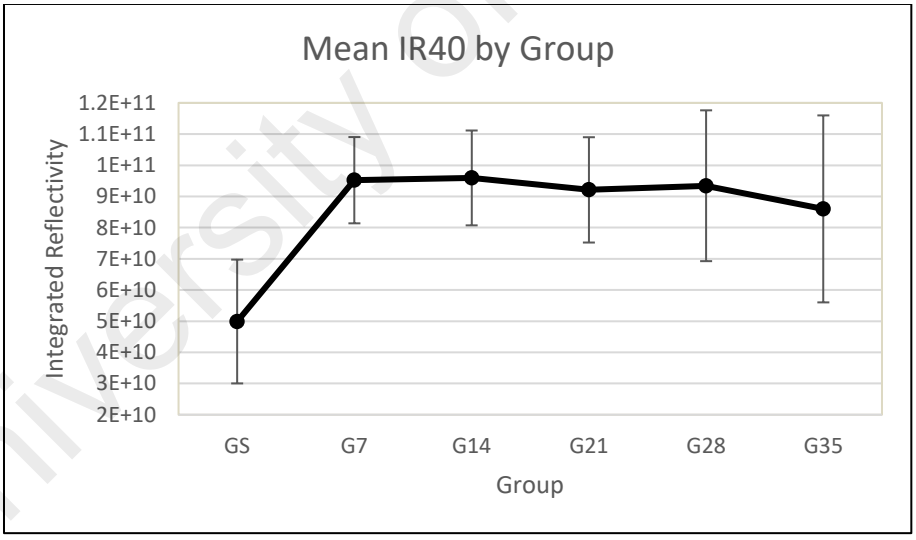

Figure 4.21: Mean IR 40 by group

Mean IR40 by group shows GS significantly lower than all the other groups. There is a sharp increase from GS to G7. G7 to G35 show almost similar IR values. The only similarity with mean sorptivity by group is the increase from GS to G7.

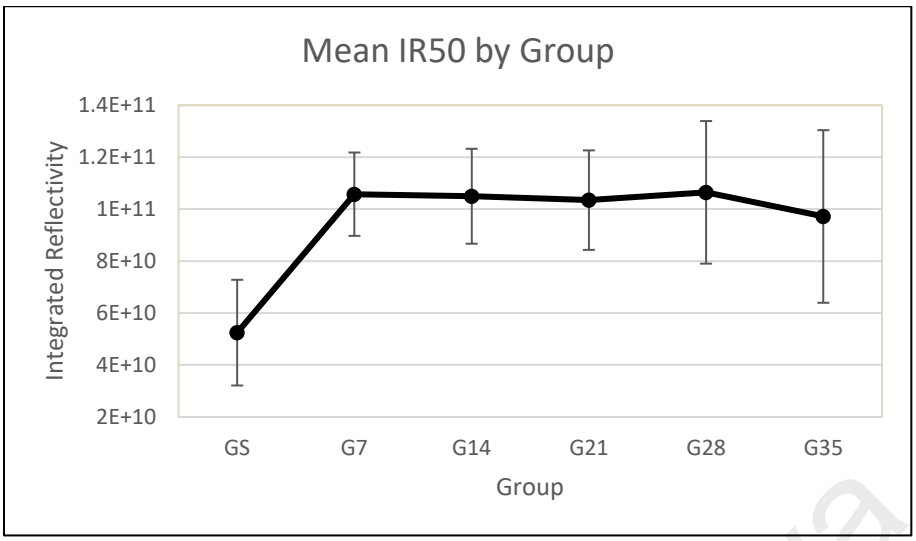

Figure 4.22: Mean IR50 by group

Mean IR50 by group shows GS significantly lower than all other groups. There is a sharp increase from GS to G7. G7 to G35 show almost similar IR values. The only similarity here with mean sorptivity by group is the increase from GS to G7. This result is expected because of the nature of data capturing of OCT. The near infra-red light is reflected from the demineralised enamel surface. And at thicker layers, the cumulative IR calculated makes it difficult to differentiate between groups.

Statistical analysis was done on results for Integrated Reflectivity (IR) of different enamel surface thickness namely IR10, IR20, IR30, IR40 and IR50 using IBM SSPS Version 25 Software for all the pH cycling groups including the control group that did not undergo any pH cycling.

4.3.1 IR10

Shapiro-Wilk Test of Normality (typically used for n<50) shows normal distribution for 5 of 6 groups (>0.05) in IR10. Based on the results from Shapiro-Wilk test of normality, QQ plot and box plot, it was concluded that the data has a normal distribution for all groups. Levene's test of homogeneity has a p-value of 0.093 which is more than 0.05 and therefore, homogeneity of variance can be assumed. Parametric tests were used

for further investigations. For IR 10, One-way ANOVA shows a p-value of 0.015. Therefore, there is statistically significant difference between groups. Post-hoc Tukey shows significant difference between GS and G14 with a p-value of 0.033. G14 is significantly different from G21 (p=0.034) and G28 (p=0.013). There is no significant difference detected between GS and G21. Bivariate (Pearson) Correlations between sorptivity and IR 10 show no significant correlations but a correlation is detected within group G28 with a Pearson correlation coefficient of -0.463 (p= 0.015). Correlations are detected for GS-G7-G14 and GS-G7-G14-G21 with Pearson correlation coefficient of 0.277(p=0.043) and 0.275 (p=0.019 respectively. No correlations are detected with G21-G28-G35 and GpHCycling.

4.3.2 IR20

Shapiro-Wilk Test of Normality (typically used for n<50) shows normal distribution for all results (>0.05) in IR20. Based on the results from Shapiro-Wilk test of normality, QQ plot and box plot, it was concluded that the distribution of the data has a normal distribution for all groups. Levene's test of homogeneity has a p-value of 0.006 which is less than 0.05 and therefore, homogeneity of variance cannot be assumed. Parametric tests were used for further investigations. For IR 20, One-way ANOVA shows a p-value of 0.026. Therefore, there is significant difference between the groups. Post-hoc Dunnett's T3 shows significant differences between GS and G14 (p=0.021) and G14 with G28 (p=0.027). No significant difference found between the other groups. Bivariate (Pearson) Correlations between Sorptivity and IR 20 shows no overall correlations but correlation is detected within G28 with a Pearson correlation coefficient of -0.411 (p=0.016). Correlation detected for GS-G7-G14 has a Pearson correlation coefficient of 0.326 (p=0.016). There are no correlations detected in G21-G28-G35, GS-G7-G14-G21 as well as GpHCycling group.

4.3.3 IR30

Shapiro-Wilk Test of Normality (typically used for n<50) shows normal distribution for 5 of 6 groups (>0.05) in IR 30. Based on the results from Shapiro-Wilk test of normality, QQ plot and box plot, it was concluded that the data has a normal distribution. Levene's test of homogeneity has a p-value of 0.02 which is less than 0.05 and therefore, homogeneity of variance cannot be assumed. Parametric tests were used for further investigations. For IR 30, One-way ANOVA shows a p-value of 0.000004 (lower than 0.05). Thus, there is a significant difference between pH cycling groups. Post-hoc Dunnett's T3 shows significant differences between GS with G7 (p=0.000243), G14 (p=0.00003), G21 (p=0.001), G28 (p=0.002201) and G35 (p=0.047). There is no significant difference seen between the other groups. Bivariate (Pearson) Correlations between sorptivity and IR 30 as well as within groups show no overall correlations. For GS-G7-G14, a correlation is detected with a Pearson correlation coefficient of 0.331 (p=0.014). No correlation is found in G21-G28-G35, GS-G7-G14-G21 group as well as GpHCycling group.

4.3.4 IR40

Shapiro-Wilk Test of Normality (typically used for n<50) shows normal distribution for 5 of the 6 groups (>0.05) in IR 40. Based on the results from Shapiro-Wilk test of normality, QQ plot and box plot, it was concluded that the data has a normal distribution. Levene's test of homogeneity has a p-value of 0.022 which is less than 0.05 and therefore, homogeneity of variance cannot be assumed. Parametric tests were used for further investigations. For IR 40, One-way ANOVA shows a p-value of 1.87×10^{-10} (lower than 0.05). Therefore, there is a significant difference between pH cycling groups. Post-hoc Dunnett's T3 shows significant differences between GS and G7 ($p=1.05 \times 10^{-7}$), G14 ($p= 6.69 \times 10^{-9}$), G21 ($p= 2.49 \times 10^{-7}$), G28 ($p= 2.36 \times 10^{-7}$) and G35 (p= 0.000177). There is no significant difference seen between all the other groups. Bivariate (Pearson) Correlations

between Sorptivity and IR40 shows no overall correlations and no correlations within groups. However, correlation is detected for GS-G7-G14 with Pearson correlation coefficient of 0.331(p=0.015). There are no correlations detected for G21-G28-G35, GS-G7-G14-G21 and GpHCycling groups.

4.3.5 IR50

Shapiro-Wilk Test of Normality (typically used for n<50) shows normal distribution for 5 of 6 groups (>0.05) in IR 50. Based on the results from Shapiro-Wilk test of normality, QQ plot and box plot, it was concluded that the data has a normal distribution. Levene's test of homogeneity has a p-value of 0.039 which is less than 0.05 and therefore, homogeneity of variance cannot be assumed. Parametric tests were used for further investigations. For IR 50, One-way ANOVA shows a p-value of $9.43x10^{-12}$ (lower than 0.05). Thus, there is a significant difference between pH cycling groups. Post-hoc Dunnett's T3 shows significant differences between GS and G7 ($p=2.77x10^{-8}$), G14 ($p=1.74Ex10^{-9}$), G21 ($p= 1.87x10^{-8}$), G28 ($p= 8.04x10^{-9}$) and G35 (p=0.000017). There is no significant difference seen between all the other groups. Bivariate (Pearson) Correlations between sorptivity and IR50 shows no overall correlations and no correlations within groups. However, there is correlation detected for GS-G7-G14 with Pearson correlation coefficient of 0.341(p=0.012). There is no correlation detected for G21-G28-G35, GS-G7-G14-G21 and GpHCycling groups.

4.3.6 Correlations

There are no correlations detected for all layers in IR when test site measurements from all groups are selected. However, there are correlations with sorptivity detected for IR10 to IR50 for GS-G7-G14. Also noted is a mild correlation detected in GS-G7-G14-G21 group for IR10 only.

Details of the statistical analysis can be found in Appendix D.

4.4 Qualitative Analysis

4.4.1 SEM Images

To qualitatively evaluate the SEM images obtained from the test sites (5 test sites per group), these characteristics were observed:

i. Loss of enamel surface- This category measures the ability to visually see the loss of surface enamel forming craters on the surface of the test sites in the 500x images as seen in Figure 4.23.

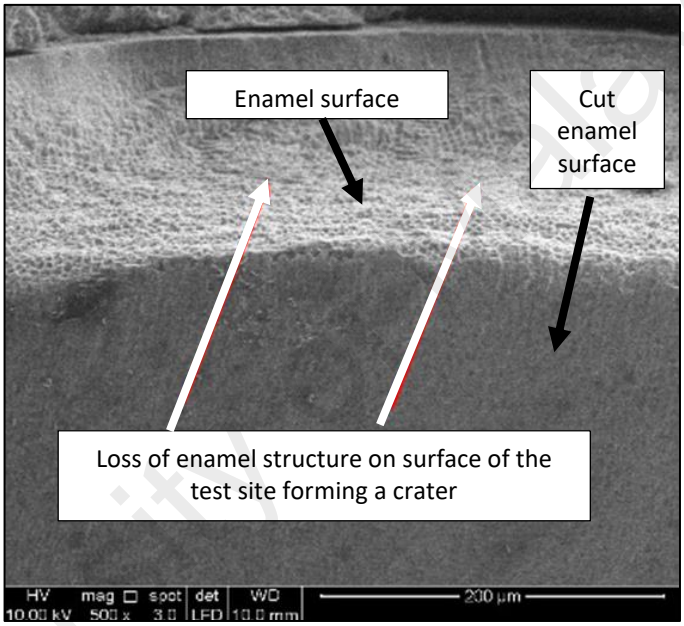

Figure 4.23: SEM image at 500x of test site B15.2 from G7

This SEM image shows loss of enamel on surface forming a crater.

ii. Demineralisation and porosity- This category looks into the presence of structural changes in the anatomy of the enamel surface and rods in the 1000x images as in Figure 4.24 and honeycomb-like pattern caused by microporosity and pore like structure formation on surface enamel in the 2000x images as seen in the example shown in Figure 4.25. Demineralised enamel surface that appeared to have remineralised were also recorded as seen in Figure 4.26.

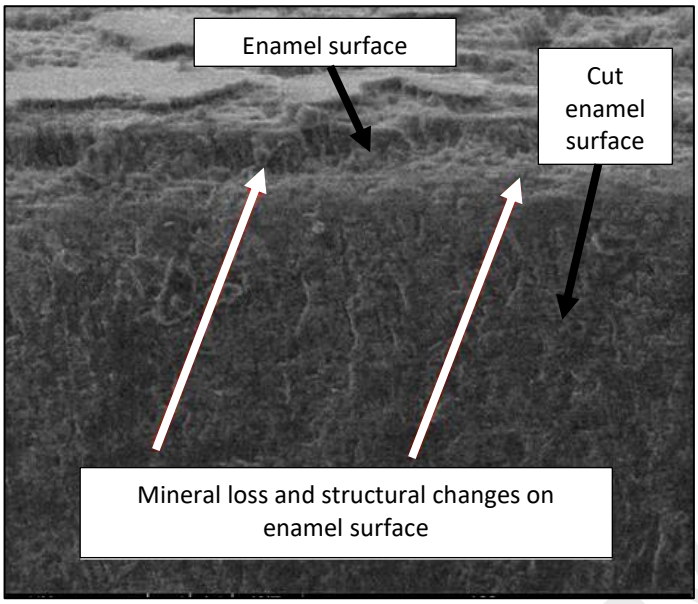

Figure 4.24: SEM image at 1000x of test site C3.2 from G14

This SEM image show mineral loss and structural changes on enamel surface.

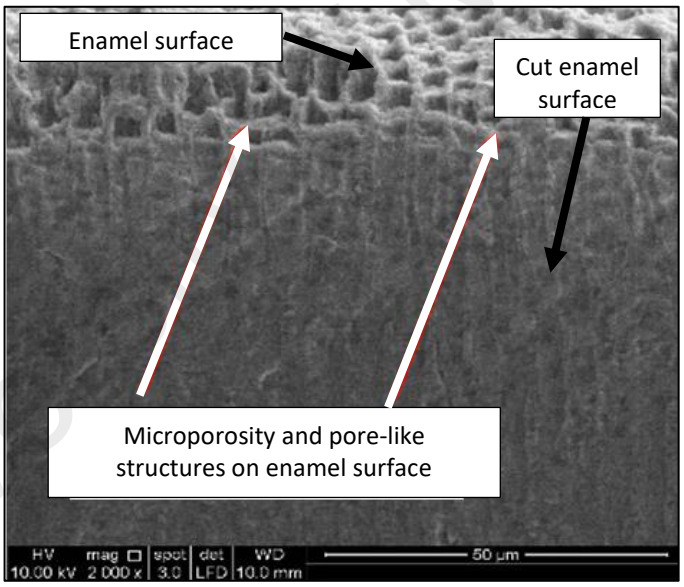

Figure 4.25: SEM image at 2000x of test site B14.2 from G7

Microporosity and pore-like structures on enamel surface are seen on this SEM image.

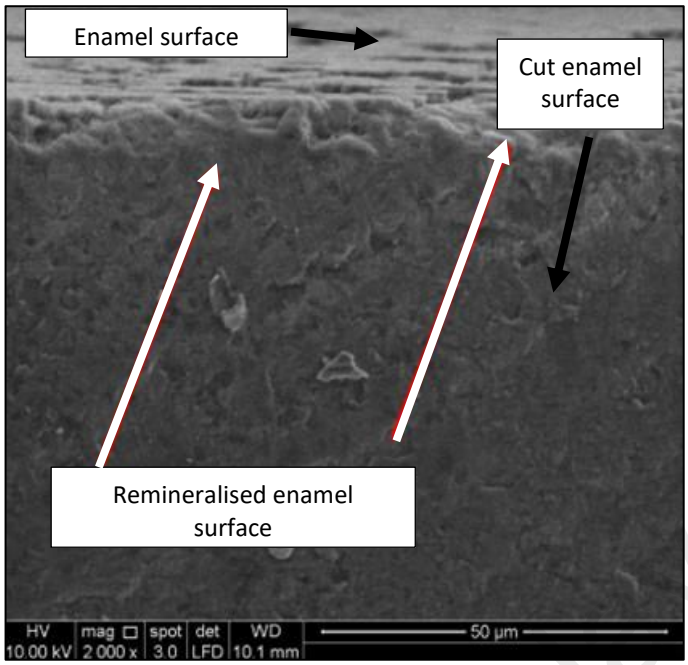

Figure 4.26: SEM image at 2000x of test site D9.1 from G21

Remineralisation on the enamel surface is seen in this SEM image. Pore-like structures due to demineralisation seem to have remineralised and have occluded.

Table 4.4 shows the tabulation of the results by group.

Table 4.4: Qualitative analysis of SEM images by group

Group	Loss of enamel surface	Demineralisation	Microporosity
GS	None	None	None
G7	3 of 5	4 of 5	4 of 5
G14	4 of 5	5 of 5	5 of 5 and 1 remineralised
G21	2 of 5	4 of 5	5 of 5 and 3 remineralised
G28	4 of 5	5 of 5	5 of 5
G35	5 of 5	5 of 5	5 of 5

5 test sites per group were analysed.

SEM images for GS appear to be normal and without demineralisation. There are no microporosity and no finger-like extensions seen which is typically seen on enamel

surface that had undergone demineralisation. Surface appear smooth on all samples of various magnifications.

Ultrasonication that was done to remove smear layer may cause the loss of enamel surface due to weakness of surface integrity on test sites in groups that underwent pH cycling. Therefore, in group G7, some of the test sites show loss of enamel surface and honeycomb-like microporosity can be seen penetrating from the surface to the subsurface region.

G14 shows more surface porosity with most surfaces showing enamel loss as compared to test sites from G7. Microporous surface is visible on most of the test sites.

There are mixed results for G21 with some test sites with only a few showing signs of surface loss. Demineralisation is seen in most test sites and microporosity in all test sites in G21 but it is well noted that many of the test sites in G21 show signs of remineralisation.

Most of the test sites in G28 show signs of further decay with severe loss of surface enamel as well as subsurface demineralisation. It is interesting to note that 1 of the images of a test site showed an intact enamel surface but a hollow sub surface area. Demineralisation has occurred subsurface and the pore structures that form in demineralised enamel has coalesced to form a hollow ‘cave-like’ area in the subsurface region. Enamel surfaces on all test sites in G35 show surface loss with surface microporosity. Figures in Appendix E are SEMs of 5 test site for each group at 500x, 1000x and 2000x whereby specimens from GS are identified as A, G7 as B, G14 as C, G21 as D, G28 as E and G35 as F with identification numbers for specific test sites.

4.4.2 Micro CT Images

Images from Micro-CT taken of 8 test sites per group were examined. Observations were made to determine the presence of visible demineralisation of enamel surface, loss of surface enamel and presence of a surface layer as shown in examples below (Figures 4.27 to 4.29). Test sites were then quantified based on these criteria.

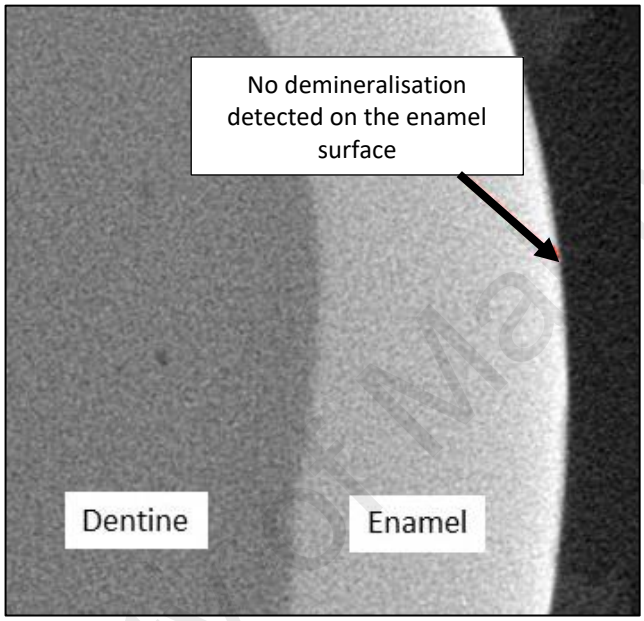

Figure 4.27: Micro-CT scan of A12.2 test site from GS

No demineralisation is seen on the enamel surface in this Micro-CT scan.

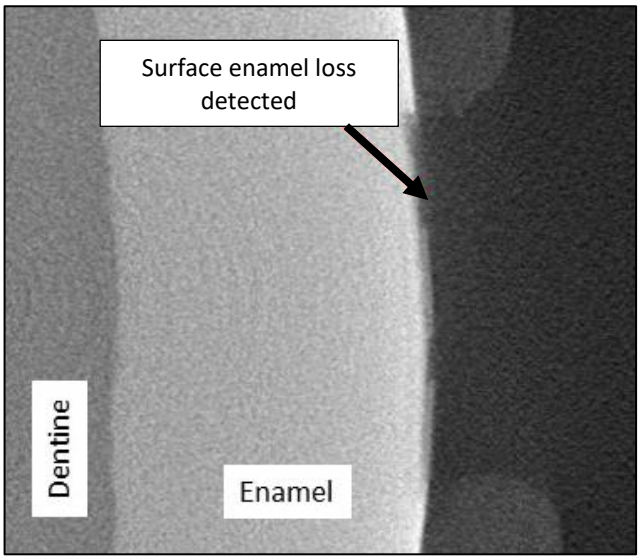

Figure 4.28: Micro-CT scan of D7.1 test site from G21

Demineralisation is seen in the Micro-CT scan with visible loss of enamel surface structure.

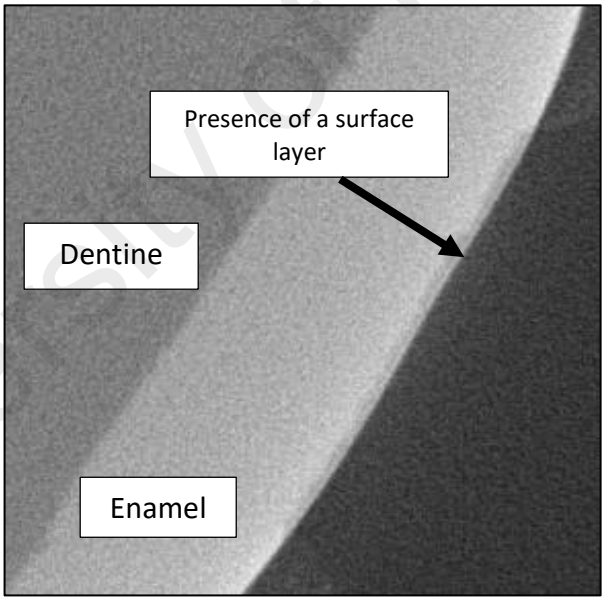

Figure 4.29: Micro-CT scan of D10.2 test site from G21

A surface layer is detected in this image and a demineralised subsurface region.

Table 4.5 shows the tabulation of the results by group.

Table 4.5: Tabulation of surface enamel loss and presence of a surface layer seen on Micro-CT images

	No demineralisation seen	Surface enamel loss	Presence of a surface layer
GS	8	0	0
G7	1	5	2
G14	1	5	2
G21	1	4	3
G28	1	5	2
G35	0	5	3

8 test sites per group per group were analysed.

There are no visible signs of demineralisation on the surface of test sites for Micro-CT images taken for GS. In G7, 5 of the test sites show loss of enamel surface while no demineralisation is seen in 1 test site. 5 of the test sites in G14 show loss of enamel surface and no demineralisation detected in 1 test site. For G21, 4 of the test sites show loss of surface enamel and 1 of the test sites did not show any no demineralisation. 5 test sites in G28 and G35 exhibit a more severe loss of surface enamel particularly at the centre of the lesions. Overall, there is a general increase in the severity of demineralisation from G7 to G35 shown by a steady increase in severity of surface enamel loss as well as subsurface demineralisation. Many test sites in all groups except for GS showing the presence of a surface layer with subsurface demineralisation of different severity. Figures in Appendix F are images taken near the centre of the test sites with Micro-CT which have been cropped for ease of reporting. Specimens from GS are identified as A, G7 as B, G14 as C, G21 as D, G28 as E and G35 as F with identification numbers for specific test sites.

4.4.3 Photographic images

Photographic images of 5 specimens (2 test sites per specimen) for each group were examined. The presence of white spot lesions was observed. The prominence of the white

spot lesions, whether they were mild or very prominent were also noted. Observations for criteria mentioned are shown in examples below (Figures 4.30 to 4.32).

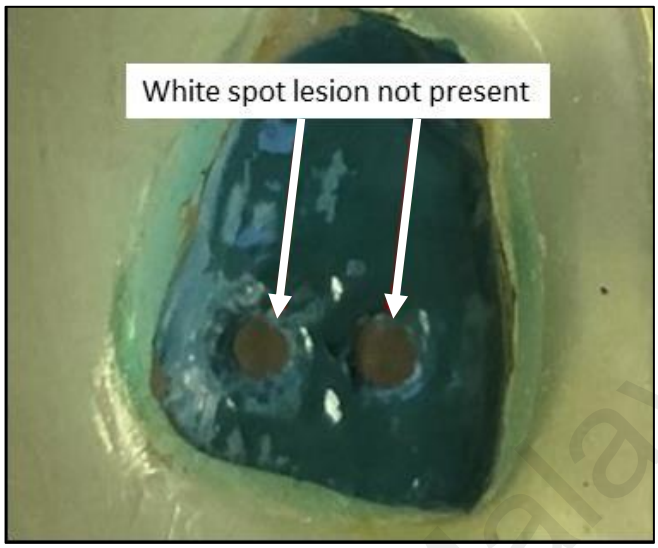

Figure 4.30: Photographic image of test sites on D3 from G21

This image shows that white spot lesion is not present and the surface of the enamel does not have a chalky appearance.

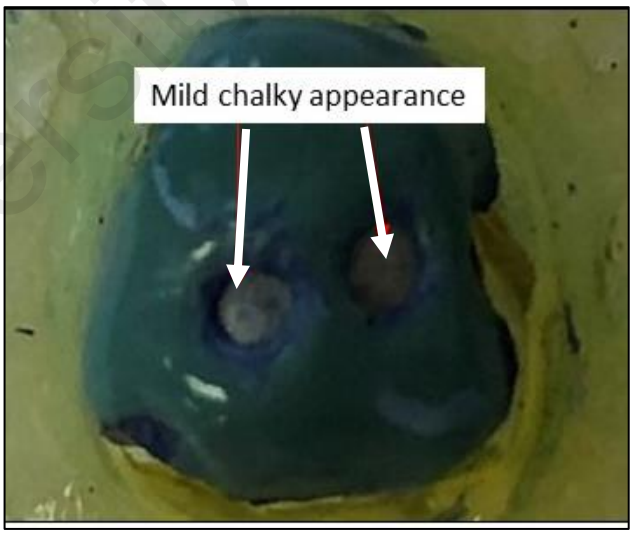

Figure 4.31: Photographic image of test sites on C8 from G14

White spot lesions with a mild chalky appearance are seen on the test sites in this image.

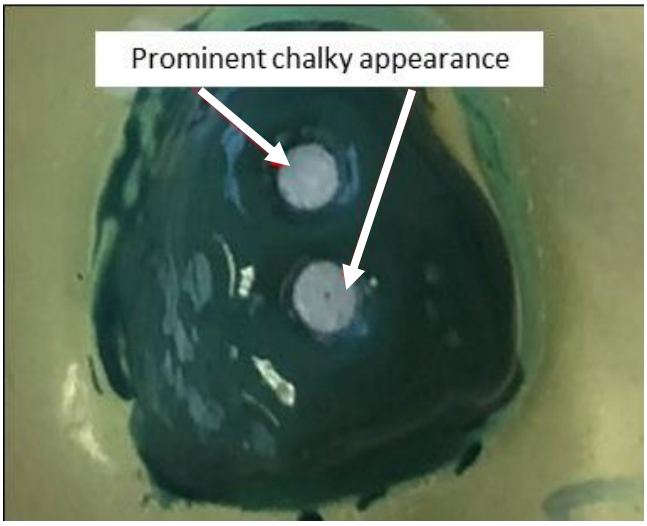

Figure 4.32: Photographic image of test sites on D15 from G21

Image shows white spot lesions on test sites with prominent chalky appearance.

Table 4.6 shows the tabulation of the results by group.

Table 4.6: Tabulation of presence of white spot lesions

	White spot lesions with mild chalky appearance	White spot lesions with prominent chalky appearance	No visible white spot lesion
GS	2	0	8
G7	6	4	0
G14	2	8	0
G21	2	6	2
G28	2	8	0
G35	0	10	0

10 test sites per group were analysed.

All images taken for GS except 2 showed a typical sound enamel surface gloss. The chalky appearance may be due to demineralisation of the enamel due to prolonged soaking in R.O water before the images were taken. Most of the G7 test sites have white spots while most test sites in G14 also have white spots which appear to be more prominent compared to G7. Many of the test sites in G21 appear to have chalky surface too but it was noted that some of the test sites did not have visible white spot lesions on

them. Most of the test sites in G28 and all of G35 had very prominent white spots lesions. Overall, most of the samples in G7 to G35 appear to be white spot lesions of various intensity, progressively appearing chalkier. G21 had some test sites which appear sound and did not have a chalky appearance. Figures in Appendix G are the photographic images. Specimens from GS is identified as A, G7 as B, G14 as C, G21 as D, G28 as E and G35 as F with identification numbers for specific specimens. Same specimens were used for clinical and stereo microscope images.

4.4.4 Stereo microscope images

Results were tabulated from 5 specimens (10 test sites) for each group. For images taken with 1.25x magnification, the visibility of the test sites was the criteria. Figure 4.33 below is an example of a visible test site.

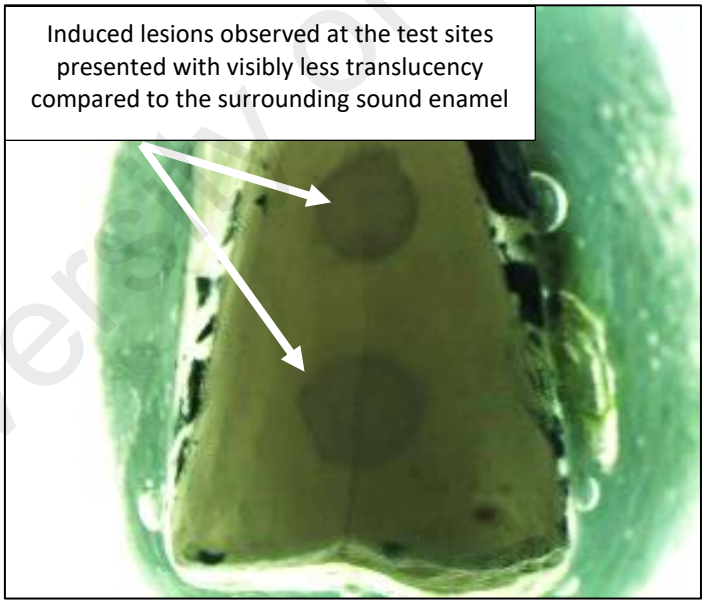

Figure 4.33: Image taken using stereo microscope at 1.25x of test sites on B5 from G7

Image shows visible test sites with less translucency indicating the presence of white spot lesions.

For images taken at 5.6x magnification, observations were made on whether there's visible striae on the surface of the test sites and whether a surface layer was visible on the enamel surface. Figure 4.34 is an example of the presence of a visible striae and Figure 4.35 is an example of the presence of a surface layer.

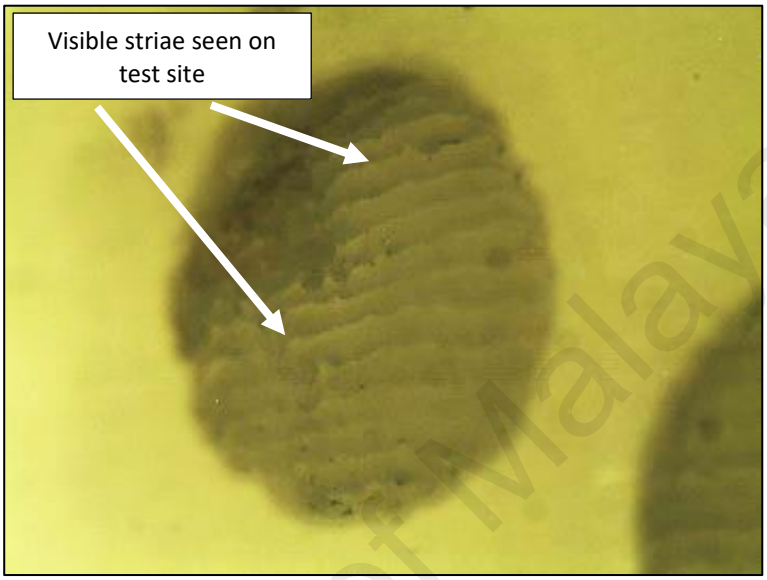

Figure 4.34: Image taken using stereo microscope at 5.6x of test site E16.1 from G28

Image showing visible striae on test site indicating that the surface is demineralised.

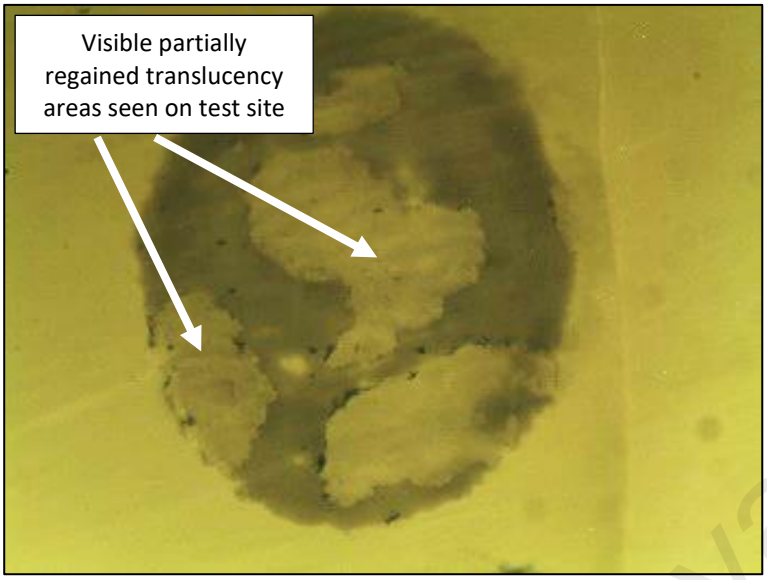

Figure 4.35: Image taken using stereo microscope at 5.6x of test site D13.1 from G21

Image shows visible partially regained translucency areas indicating the presence of a surface layer.

Table 4.7 and 4.8 show the tabulation of the results by group for images taken at 1.25x and 5.6x.

Table 4.7: Tabulation of results of test site visibility at 1.25x using stereo microscope

1.25X	Visible
GS	1
G7	9
G14	8
G21	6
G28	10
G35	10

10 test sites per group were analysed.

Table 4.8: Tabulation of results of presence of striae and/or a surface layer on test sites at 5.6x using stereo microscope

5.6x	Visible	Striae	Presence of a surface layer
GS	6	2	0
G7	10	7	6
G14	8	7	4
G21	8	2	8
G28	10	8	3
G35	10	7	1

10 test sites per group were analysed.

Exposed enamel test sites on specimens in GS are hardly visible at 1.25x. At 5.6x, many of the test sites are visible but not obvious. Lesions in G7 are visible at 1.25x as well as at 5.6x. Many of the surfaces appear intact with the appearance of a surface layer with striae fairly visible in most test sites. Lesions in G14 are also visible at 1.25x as well as at 5.6x. The surfaces appear to be less intact with striae more visible in most test sites with a surface layer visible on some of the surfaces. Surfaces appear somewhat intact for most samples in G21 with striae less visible as compared to G7, G14, G28 and G35. There appears to be formation of a surface layer for most lesions in G21. Most of the test sites in G28 have surfaces that are less intact and striae much more visible. A surface layer is not visible on many of the lesions. All of the surfaces on test sites in G35 are less intact and striae is visible with hardly any surface layer visible for all lesions. Overall, lesion progressed from G7 to G35 with a surface layer more noticeable in many of the test sites in G21. Figures in Appendix H are images taken of the test sites both in 1.25x and 5.6x. Specimens from GS are identified as A, G7 as B, G14 as C, G21 as D, G28 as E and G35 as F with identification numbers for specific test sites. Same specimens were used for clinical and stereo microscope images.

CHAPTER 5: DISCUSSION

5.1 Sorptivity

Demineralisation of tooth surface causes porosity. It is a known fact that porosity causes the surface to absorb liquid from its surrounding but thus far, little has been done to correlate rate of sorption to the level of porosity on the tooth surface. The aim of this study was to look for a correlation between sorptivity and porosity or density of the tooth surface. Using the modified Featherstone model, 6 groups of specimens including a control group underwent the experiment with the assumption that each group will exhibit a certain porosity level and therefore a certain sorptivity rate. To quantify the results, calculations were done at 10, 20, 30, 40 and 50 microns depths using Total Delta Z measurements on grey scale values from Micro-CT as well as Integrated Reflectivity measured from area under the curve of A-scans generated from OCT.

Sorptivity looks at absorption of water on the enamel surface using capillary action. At the same time, Washburn's equation (Washburn, 1921) relates sorptivity to pore diameter which in turn relates to porosity and therefore to density of the surface and material. At a certain degree of porosity and density of enamel surface, the sorptivity rate is constant.

In general, the test sites in the various pH cycling groups exhibit a range of response to acid attack and therefore a range in sorptivity measurements. However, One-way ANOVA shows significant difference between the groups for sorptivity. When individual groups were compared, there were significant differences detected between certain groups including GS with G14 as well as G21 with all groups except G28. This significant difference shows that sorptivity levels can potentially be categorized for use in future clinical diagnosis of enamel surface porosity.

An initial climb was seen for mean sorptivity rate from GS through to G14 but then a sudden drop is seen at G21 and then a steady climb again to G35. This is an interesting observation as from this graph alone (Figure 5.1), one can see that sorptivity levels can be cyclical, similar to the dynamics of caries progression.

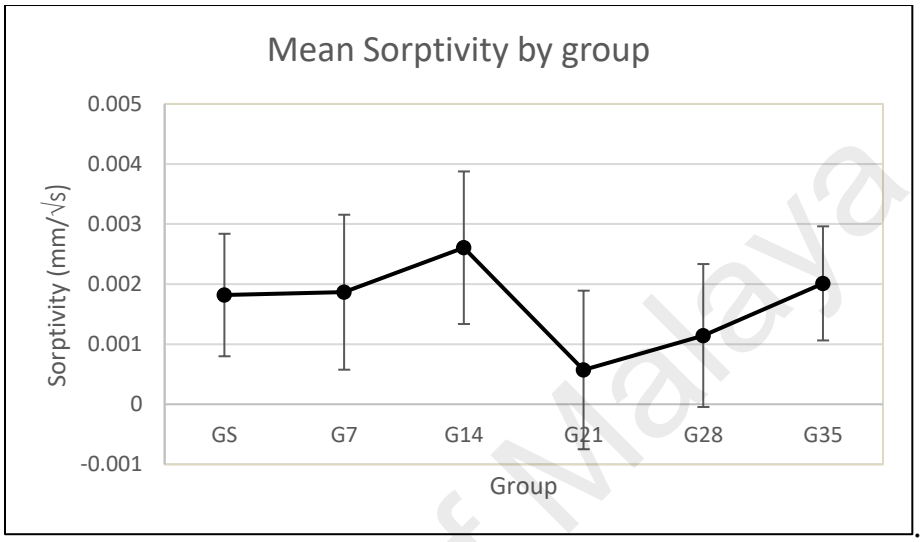

Figure 5.1: Graph of mean sorptivity by group

Mean sorptivity by group shows that the sorptivity measured follows the cycle of demineralisation and remineralisation. The highly mineralised surface layer that is formed has very low porosity on the surface.

It is a known fact that a surface protective layer is formed when the tooth surface undergoes continuous demineralisation threats and is part of the pathophysiology of caries formation (Featherstone et al., 1978). The GS-G14 climb suggests that the initial loss of mineral causes the surface to be porous and sorptivity levels to rise. However, when a surface layer is formed for G21, the level of sorptivity goes down to below the level of sorptivity in sound teeth. Over time, when the demineralisation assault continues, the protective layer is destroyed and a deeper demineralisation with increased porosity and loss of tooth surface occurs (Ole Kejerskov, 2008). This phenomenon is captured and measured by the increase in sorptivity from G21 to G35. This in an interesting finding

because it shows that due to the formation of a surface layer on most of the test sites in G21, sorptivity level is significantly lower than that of sound enamel. The presence of a surface layer on teeth that causes low porosity which is undetected in remineralisation studies may be the reason why there is still a lack of evidence in its success as seen in systematic reviews done by Paula and Sonesson M (Paula et al., 2017; Sonesson et al., 2017).

Sorptivity of GS is significantly different than G14 whereby sorptivity of G14 is 1.5 times more than GS. Sorptivity of GS is also significantly different from G21 whereby sorptivity for G21 is 3 time less than GS. Therefore, a white spot lesion with sorptivity of more than 1.5 times of sound enamel of the same tooth does not have a surface layer while white spot lesion with sorptivity of 3 times less than sound enamel shows the presence of an intact surface layer.

When comparing between results from groups that had undergone pH cycling, the difference in mean sorptivity of the maximum value seen in G14 and minimum in G21 is 6.6 times. This result suggests that surface remineralisation has occurred in most test sites with the formation of a surface layer in G21. Clinically, sorptivity values can be used to determine the efficacy of a remineralisation solutions. After undergoing remineralisation therapy, a reduction in sorptivity values for a white spot lesion of 3 to 6 times may indicate 2 things. First, that surface mineralisation has occurred and that a highly mineralised surface layer is present. Secondly, remineralisation solutions may not penetrate into the sub-surface region in subsequent treatment provided and therefore, visible appearance of the white spot lesion will remain. Hence, other measures need to be taken to remove or reduce the appearance of the white spot lesion.

To further understand the pathophysiology of the induced lesions and given that there is a drop in sorptivity from G14 to G21, a study can be done with shortened interval

between G14 and G21 to understand the details of the change. Also, a study can be done to look at the connection between sorptivity and groups that undergo pH cycling process of more than 35 days to further understand the connection between sorptivity and caries progression.

5.2 TDZ

Mean TDZ10 by group shows a similar pattern as mean sorptivity. An increase in mean TDZ can be seen from GS to G14 and then a decrease in G21 followed by an incline again to G35 (Figure 5.2). The increase in GS to G14 is expected as demineralisation increases steadily. Mean TDZ10 for G21 is lowest compared to the other groups but has a rather high standard deviation. During the duration of 0-21 days, demineralisation occurs and dissolved minerals move to the surface from subsurface levels (Nicola X. West, 2014; Robinson C, 2000). The concentration of minerals on the surface forms a highly mineralized surface layer, which acts as a protective barrier against further demineralisation causing a decrease in porosity which is reflected in low sorptivity levels and mean TDZ10 for G21. The continued increase in sorptivity from G21- G35 is observed as demineralisation continues with the breakdown of surface layer and loss of enamel surface. This phenomenon is also reflected in the increase in mean TDZ10. Therefore, an increase in mean TDZ10 by group which translates to a decrease in mineral density as seen in GS to G14 and G21 to G35 coincides with the increase in sorptivity. The decrease in sorptivity at G21 after G14 corresponds to the decrease in TDZ which means an increase in mineral density. Significant difference can be seen between GS and G14 in both TDZ10 and mean sorptivity. This significant difference shows that sorptivity can potentially be used to measure enamel surface density. There is also significant difference between G14 and G21 in TDZ10 as is also seen in mean sorptivity further confirming that sorptivity measurements can be used to determine the presence of a

surface layer on white spot lesions after a period of observation or remineralisation therapy.

For mean TDZ 20 by groups, significant differences are also detected between GS and G14 but no significant difference detected between GS with G21, and G14 with G21 (Figure 5.3). Mean TDZ20 is higher in all other groups compared to GS.

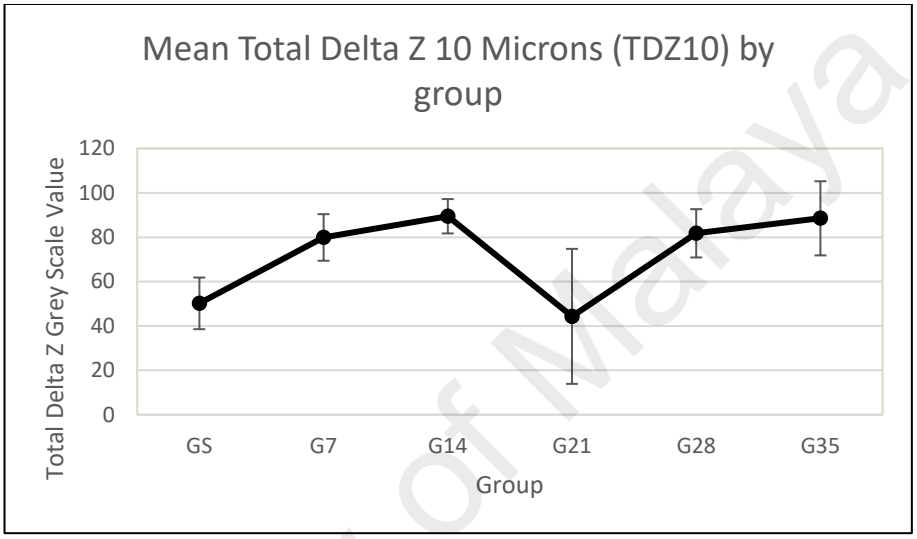

Figure 5.2: Graph of mean TDZ 10 by group

Mean TDZ10 by group follows the same correlation between groups as seen in mean sorptivity by group

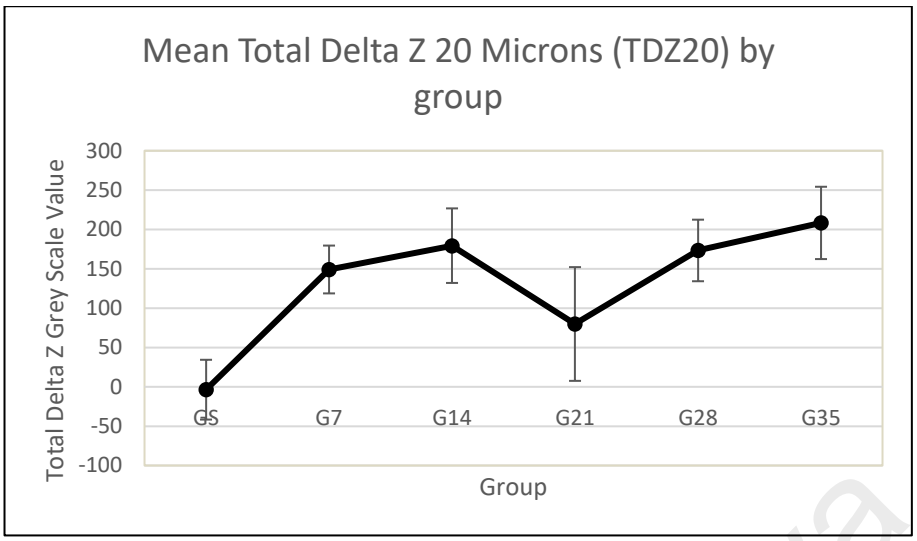

Figure 5.3: Graph of mean TDZ 20 by group

Mean TDZ 20 by group has a similar correlation between groups as seen in mean sorptivity by group but in general, it shows an upward trend. G21 is seen here to be higher than GS.

Further into the subsurface region, at TDZ 30, TDZ40 and TDZ50, there are significant differences detected between mean TDZ of GS and all the other groups which have higher mean values compared to GS. This is to be expected because as demineralisation progress over time, minerals migrate from subsurface levels to the surface and therefore significant differences is detected between GS and all the other groups which reflects not only mineral density on the surface but also the subsurface region. Comparing means of TDZ of pH cycling groups, there is still a slight decrease in G21 suggesting that mineral density in G21 is still noticeably lower.

Correlation is detected between Sorptivity and TDZ10 when all results of test sites were used. This suggests that rate of absorption is most closely related to surface characteristics and porosity at TDZ 10 and therefore can be explored as a clinical diagnostic tool to determine surface porosity and the presence of a surface layer. At deeper levels, from TDZ20 to TDZ50, no correlations were detected.

However, when test sites from pH cycling groups were compared (GpHCycling), correlations were detected from TDZ10 to TDZ50 with TDZ10 showing highest correlations. This shows that the correlation between the degree of porosity and sorptivity can be detected at all levels for demineralised enamel surface often clinically visible as white spot lesions. Hence, this results further confirms that sorptivity can be used to measure porosity levels and detect presence of a surface layer on white spot lesions before and after a period of observation or remineralisation therapy.

The wide range of sorptivity levels measured for specimens in Group GS could be due to undetected surface enamel characteristics such as sclerosed enamel, highly fluoridated or highly calcified surface which affects its density or porosity. At the same time, these characteristics cannot be significantly quantified using Micro-CT. This phenomenon could be the confounding factor causing correlations between sorptivity and TDZ to be undetectable in GS-G7-G14 group. More research can be done to look at pre-existing conditions of sound enamel using methods such as chemical analysis of the surface to further understand the correlation of sound enamel with sorptivity.

It is well noted that with the addition of G21 results to the GS-G7-G14 group, GS-G7-G14-G21, showed correlations between sorptivity and TDZ10. This result suggests that as the lesion matures, correlations between surface density detected with micro-CT and sorptivity increases. Therefore, correlation is seen even with the presence of GS.

G21-G28-G35 shows correlations at all levels with TDZ10 showing the strongest correlation. These results are seen because demineralisation has gone to deeper levels and is more uniformly coupled with destruction of the surface layer. Also noted are the strong correlations within G35 for TDZ30 to TDZ50 suggesting that prolonged pH cycling causes the difference in degree of change in the test sites within the group to be significant enough to be detected and correlation to be seen at deeper levels. This

suggests that further studies can be done to provide a better understanding of the correlations between more mature and pronounced demineralised lesions and sorptivity. Also, research can be done to determine whether sorptivity levels can be used to quantify the threshold of which a demineralised lesion can no longer be restored with remineralisation therapy and a restorative procedure is needed.

5.3 IR

Integrated reflectivity (IR) measurements obtained from OCT images shows encouraging results as well. For mean IR 10 by groups, there is significant difference detected between GS and G14 as well as G14 with G21. These significant differences were also reported in mean sorptivity and mean TDZ10. Figure 5.4 which shows mean IR10 results for all groups exhibits similar progression as mean sorptivity and TDZ. There is an initial climb from GS to G14 showing an increase in demineralisation followed by a drop in G21 and then another climb to G35, though not a steep one. The enamel surface, while progressively being demineralised, remains largely intact for most test sites from GS to G14. A highly mineralized surface layer is seen in most test sites in G21 causing mean IR 10 to decline after which the surface progressively breaks down and loses surface integrity from G21-G35. A possible reason that G21 to G35 did not show a sharp increase as seen in mean sorptivity and TDZ10 is due to the algorithm used in MatLab, which is the software that is being used to generate A-scans for calculation of integrated reflectivity in this study. In order for the software to generate A-scans efficiently, a flattening out effect is applied on the enamel surface making the surface flat and smooth in this program. In G21 to G35, the surfaces of the test sites start be breakdown and become uneven. Therefore, because of the flattening out effect on the enamel surface, the software does not take into account the demineralised and missing surface area. With this reason, G28 and G35 did not exhibit the type of incline expected in a highly demineralised enamel region.

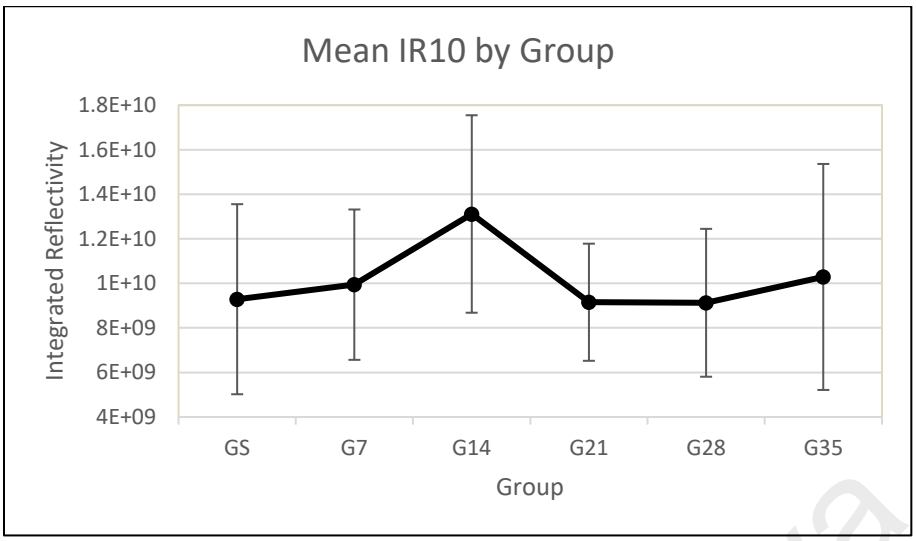

Figure 5.4: Graph of mean IR10 by group

Mean IR10 by group shows a similar correlation between groups as seen in mean sorptivity by group with the increase from GS to G14 followed by a drop at G21 and then an increase to G35.

Mean results for IR 20 shows significant difference between GS and G14 but no significant difference between G14 and G21 (Figure 5.5). There is the initial climb from GS to G14 and then it starts to decline from G14 to G21 and G28 followed by a slight increase for G35. The trend between mean is similar from GS to G21 but from G21 to G35, there is no increase as seen in G21-G35 of sorptivity and TDZ20 due to the limitations of the software used. Also, mean for G21 is higher that GS for IR 20.

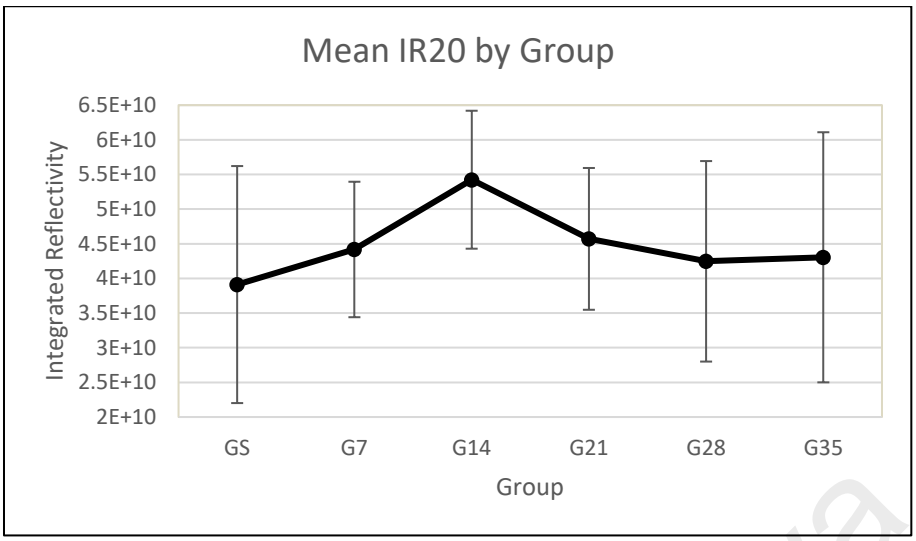

Figure 5.5: Graph of mean IR20 by group

Mean IR20 by group does not show a similar correlation between all the groups as seen in mean sorptivity by group but it is well noted that the climb from GS to G14 and then a drop to G21 is also seen in mean sorptivity and mean TDZ10.

IR30, IR40 and IR50 show statistical significance between GS and all the other groups but no significant difference is found amongst the other groups. G7, G14, G21, G28 and G35 is significantly higher than GS and mean between groups does not show the same trend as seen in mean sorptivity, TDZ10 and IR 10. This is due to the mechanism of data capturing for OCT whereby the extend and intensity of the near infra-red beam reaching a certain distance is dependent on the surface quality of enamel. The higher the reflection and deflection of beam on the surface due to surface demineralisation, the less it penetrates into the subsurface region. Mean IR 30 to IR 50 measurements show the presence of demineralisation in G7 to G35 but differentiation between groups could not be detected.

Correlation is seen in GS-G7-G14 of all IR groups which is very encouraging. Given the limitations of OCT, a correlation can still be detected between sorptivity and IR suggesting that sorptivity can be used to quantify surface porosity. No correlation is seen

when groups with more matured and highly demineralised test sites were compared with sorptivity measurements due to the mechanism of data capturing in OCT and processing of information in MatLab. As the lesion becomes highly demineralised, the difference in IR measurements between lesions become undetectable and therefore no correlations with sorptivity is detected. It is well noted that correlation is seen in GS-G7-G14-G21 between IR10 and sorptivity which is also seen between TDZ10 and sorptivity.

5.4 Qualitative Analysis

From the study of images taken with SEM, there is a steady climb in the number of test sites with demineralised and loss of surface enamel from GS to G14 with the increased presence of microporosity in enamel rods. A remineralisation phenomenon is seen on some of the test sites in G21 as well as a reduction in the number of test sites with surface enamel lost. Severe loss of enamel surface and demineralisation is seen in most test sites in G28 and G35 with increased visibility of microporosity. Based on these observations, a similar trend is seen in mean sorptivity by group. When overall increase of surface porosity is noticed in SEM from GS to G14 and G21 to G35, mean sorptivity by group also increased and the decrease in mean sorptivity in G21 is reflected in the remineralisation of enamel rods seen in many of the test sites in this group.

From images taken from Micro-CT scans, one can also see the correlation between sorptivity and enamel surface loss. There is a gradual deterioration from GS to G14 with demineralisation seen as radiolucency on images of enamel surface progressively becoming more severe from G7 to G14. This coincides with the increase in sorptivity in GS to G14. Many test sites in G21 shows the presence of a surface layer that is still intact and highly mineralized. Some show a breakdown of enamel surface altogether with subsurface layer replacing the missing layer while one of the test sites did not show signs of demineralisation. Further loss of surface enamel and mineral density becomes

progressively more obvious in test sites from G28 to G35. This trend is mirrored in the drop in mean sorptivity in G21 and then the progressive increase to G28 and G35.

Clinical images of test sites showed that it was fairly difficult to ascertain the severity of the demineralisation as most of the lesions in G7 to G35 were clinically considered as white spot lesions emphasizing the need for another way to diagnose the severity of such lesions as well as determining the presence of a surface layer. However, there are some subtle differences noticed when comparing one group with another. In general, the test sites in GS did not have white spot lesions. Many lesions in G14, G28 and G35 were particularly white and had a prominent chalky appearance. Lesion in G21 were white spot lesions too but there were less test sites with prominent chalky in appearance compared to G14, G28 and G35. These findings suggest a correlation between clinical images observed and mean sorptivity in groups.

Stereo microscope images also coincide with mean sorptivity results. In general, the lesions on test sites seem to progressively worsen from G7 to G35 with visible surface layer observed in most lesions in G21. The number of lesions visible on images taken with 1.25x magnification of test sites that had undergone pH cycling is lowest in G21. Images taken with 5.6x magnification show that G21 had the highest number of test sites showing the presence of a surface layer. This too coincides with the mean sorptivity of G21 being the lowest amongst the groups.

Overall, there is a clear trend seen between pH cycling groups whereby the increase in demineralisation on surface enamel can be seen from GS to G14 and then a decline in G21 with the presence of a surface layer followed by a continued progress in demineralisation in G28 and G35. This trend is seen in mean sorptivity measurements which is echoed by results from mean TDZ10 and IR10 as well as qualitative analysis with SEM images, Micro-CT images, clinical and stereo microscope images. The

relationship seen between Sorptivity and TDZ 10 as well as IR 10 shows that there is indeed a correlation between surface mineral density or porosity and the rate of absorption of water on the surface. Qualitative analysis via images taken show a general increase in demineralisation on enamel surface except for in G21 whereby the formation of a surface layer is seen in many of the test sites.

5.5 Confounding factors

One of the main challenges of this research was the method used. As there are no predecessors for this study, the method used was modified from previous studies done for measuring other aspects of the tooth. The varnish used on the surface was known to provide a good barrier between tooth and water. It was therefore assumed that during the experiment, no water had seeped underneath the varnish surface due to varnish expansion in water, degradation and delamination. Another assumption taken during the study is that there is no or negligible destruction of teeth surface after repeated testing is done. R.O. water, where the specimens are kept in while waiting for the tests to be done, is also assumed to not cause noticeable degradation or demineralisation of surface of the test sites.

Evaporation rates were taken at the beginning of each test day and an assumption was made that the rate did not change or that the change is negligible throughout the day of the experiment.

According to Washburn's equation, the temperature of water can affect the rate of absorption due to capillary action. Therefore, the temperature of water droplets was kept at a certain range and it is of the assumption that this range does not confound the results significantly.

CHAPTER 6: CONCLUSION

Sorptivity of water on surface of enamel which looks at the rate of absorption is a novel idea and has not previously been investigated. The purpose of looking at sorptivity of water on enamel surface is to determine whether there is a correlation between sorptivity and porosity or state of mineralisation. This study has shown that sorptivity is linearly and inversely correlated to the state of mineralisation of the enamel surface with results backed by both quantitative analysis with TDZ and IR as well as qualitative analysis using micro-CT images, SEM images, clinical as well as stereo microscope images. In clinical diagnosis, sorptivity can be used to determine the presence of a surface layer. If sorptivity level of a demineralised enamel surface can be used to determine surface porosity, then, a customized treatment plan can be done with the use of proper materials and procedures. Progress in remineralisation can also be determined. This will increase the success rate of remineralisation therapy and reduce waste. OCT as an instrument for purpose of measuring sorptivity clinically can be further explored as it is a non-invasive method for determining surface porosity and presence of a surface layer.

6.1 Recommendations

Here are some recommendations for future research:

i. Studies can be done on sorptivity levels of various types of pre-existing surface lesions on teeth such as white spot lesions, fluorotic lesions, hypomineralised enamel and sclerosed enamel.
ii. Studies can be done to associate sorptivity with efficacy of various fluoride and calcium compounds used in remineralisation of demineralised enamel surface.
iii. Translation of the use of sorptivity to clinical setting can be done by looking at ways to measure it in patient non- invasively.

iv. More studies can be done to look at using sorptivity to measure the threshold of irreversibility of demineralised tooth surface.

REFERENCES

Adair, S. M., Bowen, W. H., Burt, B. A., Kumar, J. V., Levy, S. M., Pendrys, D. G., . . . Whitford, G. M. (2001). Recommendations for using fluoride to prevent and control dental caries in the United States. Centers for Disease Control and Prevention. *MMWR Recomm Rep, 50*(Rr-14), 1-42.

Afonso, R. L., Pessan, J. P., Igreja, B. B., Cantagallo, C. F., Danelon, M., & Delbem, A. C. B. (2013). In situ protocol for the determination of dose-response effect of low-fluoride dentifrices on enamel remineralization. *J Appl Oral Sci, 21*(6), 525-532. doi:10.1590/1679-775720130309

Algarni, A., Kang, H., Fried, D., Eckert, G. J., & Hara, A. T. (2016). Enamel Thickness Determination by Optical Coherence Tomography: In vitro Validation. *Caries Res, 50*(4), 400-406. doi:10.1159/000446779

Amaechi, B. T. (2015). Remineralization Therapies for Initial Caries Lesions. *Curr Oral Health Rep, 2*(2), 95-101.

Ando, M., Stookey, G. K., & Zero, D. T. (2006). Ability of quantitative light-induced fluorescence (QLF) to assess the activity of white spot lesions during dehydration. *Am J Dent, 19*(1), 15-18.

Angker, L., Nockolds, C., Swain, M. V., & Kilpatrick, N. (2004). Quantitative analysis of the mineral content of sound and carious primary dentine using BSE imaging. *Arch Oral Biol, 49*(2), 99-107.

Arends J, C. J. (1986). The nature of early caries lesions in enamel. . *J Dent Res., 65*(1), 2-11.

Arends J, J. W., Ogaard B, Rölla G. (1987). SEM and microradiographic investigation of initial enamel caries. *Scand J Dent Res., 95*(3), 193-201.

Attin T, W. F. (2014). Methods for assessment of dental erosion. . *Monogr Oral Sci., 25*, 123-142.

Bakhos, Y., & Brudevold, F. (1982). Effect of initial demineralization on the permeability of human tooth enamel to iodide. *Arch Oral Biol, 27*(3), 193-196.

Benic, G. I., Elmasry, M., & Hammerle, C. H. (2015). Novel digital imaging techniques to assess the outcome in oral rehabilitation with dental implants: a narrative review. *Clin Oral Implants Res, 26 Suppl 11*, 86-96. doi:10.1111/clr.12616

Bertacci, A., Lucchese, A., Taddei, P., Gherlone, E. F., & Chersoni, S. (2014). Enamel structural changes induced by hydrochloric and phosphoric acid treatment. *J Appl Biomater Funct Mater, 12*(3), 240-247. doi:10.5301/jabfm.5000179

Brannstrom, M., Linden, L.-A. k., & Johnson, G. (1968). Movement of Dentinal and Pulpal Fluid Caused by Clinical Procedures. *Journal of Dental Research, 47*(5), 679-682. doi:10.1177/00220345680470050201

Brudevold, F., Tehrani, A., & Cruz, R. (1982). The Relationship Among the Permeability to Iodide, Pore Volume, and Intraoral Mineralization of Abraded Enamel. *Journal of Dental Research, 61*(5), 645-648. doi:10.1177/00220345820610050501

Cara, A. C., Zezell, D. M., Ana, P. A., Maldonado, E. P., & Freitas, A. Z. (2014). Evaluation of two quantitative analysis methods of optical coherence tomography for detection of enamel demineralization and comparison with microhardness. *Lasers Surg Med, 46*(9), 666-671. doi:10.1002/lsm.22292

Chan, K. H., Chan, A. C., Fried, W. A., Simon, J. C., Darling, C. L., & Fried, D. (2015). Use of 2D images of depth and integrated reflectivity to represent the severity of demineralization in cross-polarization optical coherence tomography. *J Biophotonics, 8*(0), 36-45. doi:10.1002/jbio.201300137

Chang, N.-Y. N., Jew, J. M., & Fried, D. (2018). *Lesion dehydration rate changes with the surface layer thickness during enamel remineralization.* Paper presented at the SPIE BiOS.

Chersoni, S., Bertacci, A., Pashley, D. H., Tay, F. R., Montebugnoli, L., & Prati, C. (2011). In vivo effects of fluoride on enamel permeability. *Clin Oral Investig, 15*(4), 443-449. doi:10.1007/s00784-010-0406-x

Chu CH, C. A., Lo EC, . (2013). Current and future research in diagnostic criteria and evaluation of caries detection methods. *Oral Health Prev Dent., 11*(2), 181-189.

Clarkson, D. M. (2014). An update on optical coherence tomography in dentistry. *Dent Update, 41*(2), 174-176, 179-180. doi:10.12968/denu.2014.41.2.174

Cochrane, N. J., Anderson, P., Davis, G. R., Adams, G. G., Stacey, M. A., & Reynolds, E. C. (2012). An X-ray Microtomographic Study of Natural White-spot Enamel Lesions. *Journal of Dental Research, 91*(2), 185-191. doi:10.1177/0022034511429570

Colston, B., Sathyam, U., Dasilva, L., Everett, M., Stroeve, P., & Otis, L. (1998). Dental OCT. *Opt Express, 3*(6), 230-238.

De Souza, C. C., Cury, J. L., Coutinho, T. C., Da Silva, E. M., & Tostes, M. A. (2014). Effect of different application frequencies of CPP-ACP and fluoride dentifrice on demineralized enamel: a laboratory study. *Am J Dent, 27*(4), 215-219.

Demian, D., Duma, V. F., Sinescu, C., Negrutiu, M. L., Cernat, R., Topala, F. I., . . . Podoleanu, A. G. (2014). Design and testing of prototype handheld scanning probes for optical coherence tomography. *Proc Inst Mech Eng H, 228*(8), 743-753. doi:10.1177/0954411914543963

E.I.F. Pearce, D. G. A. N. (1989). Microstructural Features of Carious Human Enamel Imaged with Back-scattered Electrons. *Journal of Dental Research, 68*(2), 113-118.

Ekambaram M, M. S. S., Yiu CKY. . (2017). A Review of Enamel Remineralisation Potential of Calcium- and Phosphate-based Remineralisation Systems. *Oral Health Prev Dent., 15*(5), 415-420.

Espigares, J., Sadr, A., Hamba, H., Shimada, Y., Otsuki, M., Tagami, J., & Sumi, Y. (2015). Assessment of natural enamel lesions with optical coherence tomography in comparison with microfocus x-ray computed tomography. *J Med Imaging (Bellingham), 2*(1). doi:10.1117/1.jmi.2.1.014001

Featherstone JD, D. J., Cutress TW. ., . (1979). A mechanism for dental caries based on chemical processes and diffusion phenomena during in-vitro caries simulation on human tooth enamel. *Arch Oral Biol., 24*(2), 101-112.

Featherstone, J. D., Duncan, J. F., & Cutress, T. W. (1978). Surface layer phenomena in in-vitro early caries-like lesions of human tooth enamel. *Arch Oral Biol, 23*(5), 397-404.

Featherstone, J. D., Stookey, G. K., Kaminski, M. A., & Faller, R. V. (2011). Recommendation for a non-animal alternative to rat caries testing. *Am J Dent, 24*(5), 289-294.

Fercher, A. F., Drexler, W., Hitzenberger, C. K., & Lasser, T. (2003). Optical coherence tomography - principles and applications. *Reports on Progress in Physics, 66*(2), 239.

Field, J., Waterhouse, P., & German, M. (2010). Quantifying and qualifying surface changes on dental hard tissues in vitro. *J Dent, 38*(3), 182-190. doi:10.1016/j.jdent.2010.01.002

Frank, R. M. (1990). Structural events in the caries process in enamel, cementum, and dentin. *J Dent Res, 69 Spec No*, 559-566; discussion 634-556. doi:10.1177/00220345900690s112

Galil KA, W. G. (1979). Acid etching patterns on buccal surfaces of permanent teeth. *Pediatric Dentistry, Dec 1*(4), 230-234.

Gomez, J. (2015). Detection and diagnosis of the early caries lesion. *BMC Oral Health, 15*(Suppl 1), S3-S3. doi:10.1186/1472-6831-15-S1-S3

Hall, C. H., William D (2012). *Water transport in brick, stone and concrete, 2nd edn.* (Vol. London and New York: Taylor and Francis).

Hara AT, Z. D. (2014). The potential of saliva in protecting against dental erosion. *Monogr Oral Sci., 25*, 197-205.

He, B., Huang, S., Jing, J., & Hao, Y. (2010). Measurement of hydroxyapatite density and Knoop hardness in sound human enamel and a correlational analysis between them. *Arch Oral Biol, 55*(2), 134-141. doi:10.1016/j.archoralbio.2009.12.005

Hoppenbrouwers, P. M., Scholberg, H. P., & Borggreven, J. M. (1986). Measurement of the permeability of dental enamel and its variation with depth using an electrochemical method. *J Dent Res, 65*(2), 154-157. doi:10.1177/00220345860650021301

Horie, K., Shimada, Y., Matin, K., Ikeda, M., Sadr, A., Sumi, Y., & Tagami, J. (2016). *Monitoring of cariogenic demineralization at the enamel–composite interface using swept-source optical coherence tomography* (Vol. 32).

Huang, T. T., Jones, A. S., He, L. H., Darendeliler, M. A., & Swain, M. V. (2007). Characterisation of enamel white spot lesions using X-ray micro-tomography. *J Dent, 35*(9), 737-743. doi:10.1016/j.jdent.2007.06.001

Inoue, T., Saito, M., Yamamoto, M., Debari, K., Kou, K., Nishimura, F., & Miyazaki, T. (2009). Comparison of nanohardness between coronal and radicular intertubular dentin. *Dent Mater J, 28*(3), 295-300.

Inoue, T., Saito, M., Yamamoto, M., Nishimura, F., & Miyazaki, T. (2013). Mineral Density of Coronal and Radicular Dentin. *Dental Medicine Research, 33*(3), 248-251. doi:10.7881/dentalmedres.33.248

Ismail, A. I., Pitts, N. B., & Tellez, M. (2015). The International Caries Classification and Management System (ICCMS™) An Example of a Caries Management Pathway. *BMC Oral Health, 15*(1), S9. doi:10.1186/1472-6831-15-s1-s9

JS, W. (1990). Effects of fluoride on caries development and progression using intra-oral models. *J Dent Res., 69*(Spec No: 626-33), 634-636.

Karlinsey, R. L., Mackey, A. C., Schwandt, C. S., & Walker, T. J. (2011). SEM evaluation of demineralized dentin treated with professional-strength NaF topical pastes. *Am J Dent, 24*(6), 357-362.

Karlinsey RL, P. A. (2012). Fluoride plus functionalized β-TCP: a promising combination for robust remineralization. *Adv Dent Res., 24*(2), 48-52.

Kidd EA, F. O. (2004). What constitutes dental caries? Histopathology of carious enamel and dentin related to the action of cariogenic biofilms. *J Dent Res., 83*(Spec No C), C35-38.

Kuhar, M., Cevc, P., Schara, M., & Funduk, N. (1997). Enhanced permeability of acid-etched or ground dental enamel. *J Prosthet Dent, 77*(6), 578-582.

Le, M. H., Darling, C. L., & Fried, D. (2010). Automated analysis of lesion depth and integrated reflectivity in PS-OCT scans of tooth demineralization. *Lasers Surg Med, 42*(1), 62-68. doi:10.1002/lsm.20862

Lee, R. C., Darling, C. L., & Fried, D. (2015). Assessment of remineralization via measurement of dehydration rates with thermal and near-IR reflectance imaging. *J Dent, 43*(8), 1032-1042. doi:10.1016/j.jdent.2015.03.005

Lenander-Lumikari, M., & Loimaranta, V. (2000). Saliva and dental caries. *Adv Dent Res, 14*, 40-47. doi:10.1177/08959374000140010601

Li, X., Wang, J., Joiner, A., & Chang, J. (2014). The remineralisation of enamel: a review of the literature. *Journal of Dentistry, 42*, S12-S20. doi:https://doi.org/10.1016/S0300-5712(14)50003-6

Lin, C. L., Kuo, W. C., Chang, Y. H., Yu, J. J., & Lin, Y. C. (2014). Examination of ceramic/enamel interfacial debonding using acoustic emission and optical coherence tomography. *Dent Mater, 30*(8), 910-916. doi:10.1016/j.dental.2014.05.023

Lynch RJ, S. S. (2012). Remineralization agents - new and effective or just marketing hype? *Adv Dent Res., 24*(2), 63-67.

Machoy, M., Seeliger, J., Szyszka-Sommerfeld, L., Koprowski, R., Gedrange, T., & Wozniak, K. (2017). The Use of Optical Coherence Tomography in Dental Diagnostics: A State-of-the-Art Review. *J Healthc Eng, 2017*, 7560645. doi:10.1155/2017/7560645

Mahdian, M., Salehi, H. S., Lurie, A. G., Yadav, S., & Tadinada, A. (2016). Tissue characterization using optical coherence tomography and cone beam computed tomography: a comparative pilot study. *Oral Surg Oral Med Oral Pathol Oral Radiol, 122*(1), 98-103. doi:10.1016/j.oooo.2016.03.021

Meira, K. R., de Mattos Brito, C. S., & de Sousa, F. B. (2015). Predicting infiltration of the surface layer of natural enamel caries. *Arch Oral Biol, 60*(6), 883-893. doi:10.1016/j.archoralbio.2015.03.001

Meredith N, S. M., Setchell DJ, Swanson SA (1996). Measurement of the microhardness and Young's modulus of human enamel and dentine using an indentation technique. *Arch Oral Biol., 41*(6), 539-545.

Meyer-Lueckel, H., Paris, S., & Kielbassa, A. M. (2007). Surface layer erosion of natural caries lesions with phosphoric and hydrochloric acid gels in preparation for resin infiltration. *Caries Res, 41*(3), 223-230. doi:10.1159/000099323

Min, J. H., Inaba, D., Kwon, H. K., Chung, J. H., & Kim, B. I. (2015). Evaluation of penetration effect of resin infiltrant using optical coherence tomography. *J Dent, 43*(6), 720-725. doi:10.1016/j.jdent.2015.03.006

Mjör, I. A. (2009). Dentin permeability: the basis for understanding pulp reactions and adhesive technology. *Brazilian Dental Journal, 20*, 3-16.

Mortman, R. E. (2011). Technologic advances in endodontics. *Dent Clin North Am, 55*(3), 461-480, vii-viii. doi:10.1016/j.cden.2011.02.006

Mota, C. C., Fernandes, L. O., Cimoes, R., & Gomes, A. S. (2015). Non-Invasive Periodontal Probing Through Fourier-Domain Optical Coherence Tomography. *J Periodontol, 86*(9), 1087-1094. doi:10.1902/jop.2015.150047

NakataT, K. Y., Sadr A, Nakashima S, Tagami J. (2018). Effect of a calcium phosphate and fluoride paste on prevention of enamel demineralization. *Dent Mater J., 37*(1), 65-70.

Nanci. (2012). *Ten Cate's Oral Histology, 8th Revised Edition*: Elsevier.

Nee, A., Chan, K., Kang, H., Staninec, M., Darling, C. L., & Fried, D. (2014). Longitudinal monitoring of demineralization peripheral to orthodontic brackets

using cross polarization optical coherence tomography. *J Dent, 42*(5), 547-555. doi:10.1016/j.jdent.2014.02.011

Neuhaus, K. W., Schlafer, S., Lussi, A., & Nyvad, B. (2013). Infiltration of natural caries lesions in relation to their activity status and acid pretreatment in vitro. *Caries Res, 47*(3), 203-210. doi:10.1159/000345654

Neves Ade, A., Coutinho, E., Vivan Cardoso, M., Jaecques, S. V., & Van Meerbeek, B. (2010). Micro-CT based quantitative evaluation of caries excavation. *Dent Mater, 26*(6), 579-588. doi:10.1016/j.dental.2010.01.012

Nicola X. West, A. J. (2014). Enamel mineral loss. *Journal of Dentistry, 42*(Supplement 1), s2-s11.

Oguro, R., Nakajima, M., Seki, N., Sadr, A., Tagami, J., & Sumi, Y. (2016). The role of enamel thickness and refractive index on human tooth colour. *J Dent, 51*, 36-44. doi:10.1016/j.jdent.2016.05.010

Ole Kejerskov, E. K. (2008). *Dental caries, the disease and it's clinical management. 2nd Edition*.

Orchardson, R., & Gillam, D. G. (2006). Managing dentin hypersensitivity. *J Am Dent Assoc, 137*(7), 990-998; quiz 1028-1029.

Palo, R. M., Bonetti-Filho, I., Valera, M. C., Camargo, C. H., Camargo, S., Moura-Netto, C., & Pameijer, C. (2012). Quantification of peroxide ion passage in dentin, enamel, and cementum after internal bleaching with hydrogen peroxide. *Oper Dent, 37*(6), 660-664. doi:10.2341/11-334-l

Paris, S., Soviero, V. M., Chatzidakis, A. J., & Meyer-Lueckel, H. (2012). Penetration of Experimental Infiltrants with Different Penetration Coefficients and Ethanol Addition into Natural Caries Lesions in Primary Molars. *Caries Research, 46*(2), 113-117.

Patil, N., Choudhari, S., Kulkarni, S., & Joshi, S. R. (2013). Comparative evaluation of remineralizing potential of three agents on artificially demineralized human enamel: An in vitro study. *J Conserv Dent, 16*(2), 116-120. doi:10.4103/0972-0707.108185

Paula, A. B., Fernandes, A. R., Coelho, A. S., Marto, C. M., Ferreira, M. M., Caramelo, F., . . . Carrilho, E. (2017). Therapies for White Spot Lesions-A Systematic Review. *J Evid Based Dent Pract, 17*(1), 23-38. doi:10.1016/j.jebdp.2016.10.003

Philip, J. R. (1957). The theory of infiltration: 4. Sorptivity and algebraic infiltrations equations. *Soil Science, 84*(3), 257-264.

Pitts NB, E. K. (2013). ICDAS Foundation; International Caries Detection and Assessment System (ICDAS) and its International Caries Classification and Management System (ICCMS) - methods for staging of the caries process and enabling dentists to manage caries. *Community Dent Oral Epidemiol, 4*(1), e41-52.

Pitts NB, Z. D., Marsh PD, Ekstrand K, Weintraub JA, Ramos-Gomez F, Tagami J, Twetman S, Tsakos G, Ismail A, . (2017). Dental caries. *Nat Rev Dis Primers*.

Pizzo G, P. M., Pizzo I, Giuliana G. . (2007). Community water fluoridation and caries prevention: a critical review. *Clin Oral Investig., 11*(3), 189-193.

Poggio, C., Lombardini, M., Dagna, A., Chiesa, M., & Bianchi, S. (2009). Protective effect on enamel demineralization of a CPP-ACP paste: an AFM in vitro study. *J Dent, 37*(12), 949-954. doi:10.1016/j.jdent.2009.07.011

Polyanin, A. D., Manzhirov, A. V. . (2006). *Handbook of Mathematics for Engineers and Scientists,* : CRC Press.

Rajan, R., Krishnan, R., Bhaskaran, B., & Kumar, S. V. (2015). A Polarized Light Microscopic Study to Comparatively evaluate Four Remineralizing Agents on Enamel viz CPP-ACPF, ReminPro, SHY-NM and Colgate Strong Teeth. *Int J Clin Pediatr Dent, 8*(1), 42-47. doi:10.5005/jp-journals-10005-1281

Regar, E., Schaar, J. A., Mont, E., Virmani, R., & Serruys, P. W. (2003). Optical coherence tomography. *Cardiovascular Radiation Medicine, 4*(4), 198-204. doi:10.1016/j.carrad.2003.12.003

Ren, W., Baig, A., & Li, S. K. (2014). Passive and iontophoretic transport of fluorides across enamel in vitro. *J Pharm Sci, 103*(6), 1692-1700. doi:10.1002/jps.23961

Ripandelli, G., Coppé, A. M., Capaldo, A., & Stirpe, M. (1998). Optical Coherence Tomography. *Seminars in Ophthalmology, 13*(4), 199-202. doi:10.3109/08820539809056053

Robertson, M. A., Kau, C. H., English, J. D., Lee, R. P., Powers, J., & Nguyen, J. T. (2011). MI Paste Plus to prevent demineralization in orthodontic patients: a prospective randomized controlled trial. *Am J Orthod Dentofacial Orthop, 140*(5), 660-668. doi:10.1016/j.ajodo.2010.10.025

Robinson C, S. R., Brookes SJ, Strafford S, Wood SR, Kirkham. (2000). The chemistry of enamel caries. *J.Crit Rev Oral Biol Med., 11*(4), 481-495.

Schlueter, N., Hara, A., Shellis, R. P., & Ganss, C. (2011). Methods for the Measurement and Characterization of Erosion in Enamel and Dentine. *Caries Research, 45(suppl 1)*(Suppl. 1), 13-23.

Schwass, D. R., Swain, M. V., Purton, D. G., & Leichter, J. W. (2009). A system of calibrating microtomography for use in caries research. *Caries Res, 43*(4), 314-321. doi:10.1159/000226230

Shen, P., Manton, D. J., Cochrane, N. J., Walker, G. D., Yuan, Y., Reynolds, C., & Reynolds, E. C. (2011). Effect of added calcium phosphate on enamel remineralization by fluoride in a randomized controlled in situ trial. *J Dent, 39*(7), 518-525. doi:10.1016/j.jdent.2011.05.002

Shetty, S., Hegde, M. N., & Bopanna, T. P. (2014). Enamel remineralization assessment after treatment with three different remineralizing agents using surface

microhardness: An in vitro study. *J Conserv Dent, 17*(1), 49-52. doi:10.4103/0972-0707.124136

Shimada, Y., Sadr, A., Sumi, Y., & Tagami, J. (2015). Application of Optical Coherence Tomography (OCT) for Diagnosis of Caries, Cracks, and Defects of Restorations. *Curr Oral Health Rep, 2*(2), 73-80. doi:10.1007/s40496-015-0045-z

Sicca, B., Quartuccio, Nicolò, Cistaro. (2016). Prevention of dental caries: A review of effective treatments. *J Clin Exp Dent., 8*(5), e604-e610.

Silverstone L.M., S. C. A., Dogon I.L., Fejerskov O. . (1975). Variation in the Pattern of Acid Etching of Human Dental Enamel Examined by Scanning Electron Microscopy. *Caries Research, 9*(5), 373-387.

Sonesson, M., Bergstrand, F., Gizani, S., & Twetman, S. (2017). Management of post-orthodontic white spot lesions: an updated systematic review. *Eur J Orthod, 39*(2), 116-121. doi:10.1093/ejo/cjw023

Sowa, M. G., Popescu, D. P., Friesen, J. R., Hewko, M. D., & Choo-Smith, L. P. (2011). A comparison of methods using optical coherence tomography to detect demineralized regions in teeth. *J Biophotonics, 4*(11-12), 814-823. doi:10.1002/jbio.201100014

Stookey, G. K., Featherstone, J. D., Rapozo-Hilo, M., Schemehorn, B. R., Williams, R. A., Baker, R. A., . . . Faller, R. V. (2011). The Featherstone laboratory pH cycling model: a prospective, multi-site validation exercise. *Am J Dent, 24*(5), 322-328.

Swain, M. V., & Xue, J. (2009). State of the art of Micro-CT applications in dental research. *Int J Oral Sci, 1*(4), 177-188. doi:10.4248/ijos09031

Swedish Council on Health Technology, A. (2008). SBU Systematic Review Summaries *Caries - Diagnosis, Risk Assessment and Non-Invasive Treatment: A Systematic Review*. Stockholm: Swedish Council on Health Technology Assessment (SBU) Copyright (c) 2008 by the Swedish Council on Health Technology Assessment.

ten Cate JM, D. P. (1982). Alternating demineralization and remineralization of artificial enamel lesions. *Caries Res., 16*(3), 201-210.

Testoni, P. A. (2007). Optical Coherence Tomography. *TheScientificWorldJOURNAL, 7*. doi:10.1100/tsw.2007.29

Thylstrup A, B. C., Holmen L. (1994). In vivo Caries Models- Mechanisms for caries Initiation and Arrestment. *Advances in Dental Research, 8*(2), 144-157.

Turkistani, A., Nakashima, S., Shimada, Y., Tagami, J., & Sadr, A. (2015). Microgaps and Demineralization Progress around Composite Restorations. *J Dent Res, 94*(8), 1070-1077. doi:10.1177/0022034515589713

Turkistani, A., Sadr, A., Shimada, Y., Nikaido, T., Sumi, Y., & Tagami, J. (2014). Sealing performance of resin cements before and after thermal cycling: evaluation by optical coherence tomography. *Dent Mater, 30*(9), 993-1004. doi:10.1016/j.dental.2014.05.010

Usenik, P., Burmen, M., Fidler, A., Pernus, F., & Likar, B. (2014). Near-infrared hyperspectral imaging of water evaporation dynamics for early detection of incipient caries. *J Dent, 42*(10), 1242-1247. doi:10.1016/j.jdent.2014.08.007

Vanichvatana, S., & Auychai, P. (2013). Efficacy of two calcium phosphate pastes on the remineralization of artificial caries: a randomized controlled double-blind in situ study. *Int J Oral Sci, 5*(4), 224-228. doi:10.1038/ijos.2013.67

Wang, X., Megert, B., Hellwig, E., Neuhaus, K. W., & Lussi, A. (2011). Preventing erosion with novel agents. *J Dent, 39*(2), 163-170. doi:10.1016/j.jdent.2010.11.007

Wang, Z., Sa, Y., Sauro, S., Chen, H., Xing, W., Ma, X., . . . Wang, Y. (2010). Effect of desensitising toothpastes on dentinal tubule occlusion: A dentine permeability measurement and SEM in vitro study. *Journal of Dentistry, 38*(5), 400-410. doi:https://doi.org/10.1016/j.jdent.2010.01.007

Washburn, E. W. (1921). The Dynamics of Capillary Flow. *Physical Review, 17*(3), 273-283.

White DJ, F. J. (1987). A longitudinal microhardness analysis of fluoride dentifrice effects on lesion progression in vitro. *Caries Res., 21*(6), 502-512.

White DJ, F. R., Bowman WD. (1992). Demineralization and remineralization evaluation techniques-added considerations. *J Dent Res. , 71* Spec No: 929-933.

Wong A, S. P., Young DA,. (2017). Dental Caries: An Update on Dental Trends and Therapy. *Adv Pediatr., 64*(1), 307-330.

Xiang, X., Sowa, M. G., Iacopino, A. M., Maev, R. G., Hewko, M. D., Man, A., & Liu, K. Z. (2010). An update on novel non-invasive approaches for periodontal diagnosis. *J Periodontol, 81*(2), 186-198. doi:10.1902/jop.2009.090419

Zakian, C. M., Taylor, A. M., Ellwood, R. P., & Pretty, I. A. (2010). Occlusal caries detection by using thermal imaging. *J Dent, 38*(10), 788-795. doi:10.1016/j.jdent.2010.06.010

Zhou, X. (2015). *Dental Caries: Principles and Management* Springer.